SLAMMING ANALYSIS OF SKIPS IN MINE SHAFTS

THE EFFECT OF SECONDARY STIFFENING IN THE GUIDES

by

A. D'Arcy-Evans

A thesis submitted in partial fulfillment of the requirements for the degree of Master of Science in Engineering

Department of Mechanical Engineering
University of Cape Town
Rondebosch 7700, Cape Town
South Africa

January 1991

DECLARATION

This is to certify that the results, calculations and other work presented in this thesis are essentially my own and that no part of it has been submitted for a degree at this or any other university.

Signed by candidate

Signature Removed

A D'Arcy-Evans

January 1991

ACKNOWLEDGEMENTS

I hereby acknowledge and greatly appreciate the assistance of the following people and organisations:

- Dr Howard Pearce, for his guidance, advice and encouragement in supervising this work and for proof-reading this document.
- Professor John Martin, for his theoretical guidance.
- Dr Malcolm Greenway, for his insight and interest in the problem.
- Mr Tony Pretorius, for valuable discussions.
- My colleages in the FRD/UCT Centre for Research in Computational and Applied Mechanics and Mechanical Engineering Department for their day to day assistance.
- The Department of Mechanical Engineering for their financial assistance.
- The FRD/UCT Centre for Research in Computational and Applied Mechanics for their financial assistance.
- The Foundation for Research and Development (FRD) for their financial assistance.

ABSTRACT

Previous investigations into the dynamics of skips in deep mine shafts have led to the identification of slamming as a phenomenon that results in exceptionally high forces in the shaft steelwork and conveyance. Slamming may occur when the rollers on the skip, that normally act on the guide, fail. Possible damage caused to the shaft steelwork, as a result of slamming, limits the hoisting speed of the skip. This study extends previous work by investigating the effect of secondary stiffening, due to axial tension effects as the guide deforms, on the slamming response of the skip. A mathematical model of a single slamming event is formulated and a numerical solution procedure presented. A number of computer simulations, including parametric studies, are presented. An important conclusion is that previous slamming models were shown to predict a reduced response when low axial compressive forces are present in the guides while predicting an increased response for high (near the buckling load) axial compressive forces. The inclusion of secondary stiffening, due to axial tension effects, thus represents a significant refinement of the slamming model.

TABLE OF CONTENTS

LIST OF FIGURES

LIST OF TABLES

LIST OF SYMBOLS

A	cross sectional area of guide
a_n	Fourier sine coefficient
$\bar{a}_n$	dimensionless Fourier sine coefficient
B_1	force in first bunton
B_2	force in second bunton
$\bar{B}_1$	dimensionless force in first bunton
$\bar{B}_2$	dimensionless force in second bunton
d	displacement coordinate
E	modulus of elasticity
I	area moment of inertia of guide
I_G	mass moment of inertia of skip
K^L	linear stiffness predictor
k_a	axial spring stiffness
k_b	bunton stiffness
k_g	guide midspan stiffness
$\bar{k}$	ratio of axial stiffness of guide to axial spring stiffness
l	length of guide span
l_1	distance of skip center of gravity from top of skip
M	total bending moment in guide
$\bar{M}$	dimensionless bending moment in guide
M_a	bending moment in guide due to axial forces
M_s	bending moment in guide due to skip force
m	mass of skip, number
m_e	effective mass of skip
N	induced axial force in guide
n	number
P	axial compressive force
P_{cr}	critial (Euler) compressive load for guide
p	ratio of axial load to critical load of the guide
r	ratio of bunton stiffness to guide midspan stiffness, number
s	curvilinear variable
T	skip force

$\bar{T}$	dimensionless skip force
t	time
U	strain energy
$\dot{u}_0$	translational impact velocity of skip
$\bar{V}_s$	dimensionless hoisting velocity of skip
v_s	hoisting velocity of skip
W	work
W_E	work done by external forces
W_I	work done by internal forces
x	coordinate
x_0	initial impact position of skip
Y	dimensionless displacement coordinate
y	displacement coordinate
y_g	guide displacement
$\bar{y}_g$	dimensionless guide displacement
y_b	bunton displacement
$\bar{y}_b$	dimensionless bunton displacement

Greek

α	Newmark integration parameter
Δ	change of a function
δ	Newmark integration parameter, variational symbol
ε	strain
$\varepsilon_1, \varepsilon_2$	tolerances
θ	rotation
ξ	dimensionless coordinate
ξ_0	dimensionless initial impact position
Π	total potential energy
σ	stress
τ	dimensionless time
ω	frequency

1 INTRODUCTION TO THE PROBLEM

1.1 INTRODUCTION

Investigations into the dynamics of skips in deep mine shafts have led to the identification of *slamming* as a phenomenon that results in exceptionally high forces in the shaft steelwork and conveyance. A slamming event usually begins when the skip impacts a guide near the midspan, where the guide is relatively flexible and transverse deflections of the guide result. As the skip is hoisted up the shaft, the guide stiffens considerably as the guide support (the bunton) is approached. The rapidly stiffening guide 'catapults' the skip off the guide with an amplified transverse velocity. Consequently this may initiate further slamming events, known as *sustained slamming*, with accompanying damage to the shaft steelwork. Slamming may occur when the guide roller tyres on the skip, that normally act on the guide, fail.

Previous work has numerically modeled a single slamming event and has led to the identification of the parameters that affect its severity. Although previous models neglected the influence of secondary stiffening, due to axial tension effects as the guide deforms, tentative calculations indicated that secondary stiffening could reduce the skip response, the reduction in response being largest when high axial compressive forces were present in the guide. The objective of this thesis is, therefore, to investigate the effect of secondary stiffening on the response of the skip. This is achieved by including the axial effects in a mathematical model of a slamming event. A number of computer simulations are performed and the results presented and discussed.

Chapter One of this thesis introduces the problem by discussing the background of shaft steelwork design and surveying literature on skip dynamics. The mathematical model including the axial tension effects is derived in Chapter Two while the numerical implementation and verification

of the model is the subject of Chapter Three. The effect of an axial compressive load in the guide on the response of the skip and a parametric study are presented in Chapter Four. The results are discussed and compared to those obtained in previous work. Finally, in Chapter Five, conclusions are drawn as to the influence of secondary stiffening, and suggestions for further study are made.

1.2 Background To The Problem

The economics of the South African gold mining industry has, over the years, necessitated larger and deeper mines in order to exploit less accessible ore bodies. When added to ever increasing productivity demands, one of the inevitable results is a trend towards larger mine shafts with higher hoisting capacities. This has necessitated a parallel trend towards larger skip payloads and high hoisting speeds.

The steelwork in a shaft is a lattice structure supporting the various conveyances, pipes and cables along the length of the shaft. The steelwork consists of horizontal *bunton* sets occurring at intervals in the shaft and vertical members between the bunton sets, called *guides*, restraining the conveyances horizontally in the shaft [9]. Conveyances travelling in shafts equipped with steel guides and buntons are subjected to constant dynamic loads and movements. This dynamic behaviour is a function of many variables in the shaft and changes in these variables to accommodate larger capacity skips have sometimes dramatically affected shaft behaviour. One result has been that traditional shaft design methods, which are largely empirical and do not account satisfactorily for dynamic behaviour, have become unreliable. An example of this outdated design philosophy is illustrated in the approach to designing the shaft steelwork for the lateral loads exerted by the conveyances. Traditionally designers assumed that the lateral load acting on the steelwork was a fraction of the total conveyance and payload weight (usually 10%). This approach took no account of the important design parameters such as conveyance speed, guide stiffness, bunton spacing, the presence of guide rollers etc.

Several widespread problems result from the dynamic behaviour of conveyances. These include loosening of bolts, fatigue cracks, difficulty of maintaining guide alignment, excessive wear and unacceptable levels of vibration. In one severe case fatigue and overload failures of buntons necessitated a bunton replacement and guide realignment programme. Such

major failures are fortunately rare, however even the smaller problems require time consuming and expensive repair and maintenance. Compounding the problem is the need for frequent and detailed inspections, even in the absence of damage, because of the high risks involved.

In order to reduce the occurrence of these costly problems a much better understanding of the dynamic behaviour of the shaft system was necessary. The lack of understanding of the dynamic behaviour of the shaft steelwork system was recognised in the early 1960's. The CSIR conducted test and analysis work under contract to the Chamber of Mines (COM) but this did not seem to influence design or operating practice in the mining houses.

As a result of renewed interest on the part of the mining industry, the Chamber of Mines Research Organization (COMRO) has, since 1982 funded research work on the investigation of the dynamic behaviour of shaft steelwork and conveyances. The Structural Dynamics Research Corporation (SDRC), Milford, Ohio, assisted COMRO in formulating the research program and carried out the major part of the research work. The SDRC work [23,24,25,26,27,28] consisted of test, analysis and design stages. The intention of the test stage was to gain a physical understanding of the problem by collecting operating data and performing a modal analysis on the skip and shaft steelwork. The analytical stage consisted of developing two computer models to simulate the response of the skip when excited by the guide misalignment. The third stage was to develop simple design guidelines for the design of shaft steelwork taking into account dynamic effects. A calibration stage was later added to calibrate the design guidelines.

Compressive forces are induced in the shaft steelwork as a result of deformation of the rock following mining operations around the shaft. Excavations take place away from the mine shaft, leaving a pillar surrounding the shaft to support the weight of the rock above the excavations. This leads to an increase in vertical compressive strains in

the walls of the shaft and consequently the distance between the buntons, to which the guides are attached, decreases. The compressive forces induced in the guides result in a decrease in the transverse stiffness of the guides. If the skip has some transverse velocity (due to a previous guide misalignment or aerodynamic effect) the lower transverse stiffness of the guide results in larger guide deflections. This has the potential of increased amplification of the response of the skip. This effect of compressive forces in the guides was the subject of the study by Pretorius [18,19,20,21].

One of the primary assumptions of Pretorius' [18,19,20,21] analysis was that the guide undergoes only small displacements and can be modeled as a simply supported beam. As a result, the guide exhibits no secondary stiffening as a result of axial elongation. It was shown for a specific case that these stiffening effects could reduce the overall forces in the system and it was suggested that this effect be the subject of a more thorough investigation.

1.3 Review of Previous Work

This section provides a brief survey of the literature available on skip dynamics. Particular attention is given to the work by the SDRC [24] and Pretorius [18,19,21]. Pretorius' [18,19,21] work is particularly important as it provides the background and motivation for this particular study.

Redpath and Shaver [22] discuss various aspects of guide design and installation for wood, steel and rope guides. It was stated, without justification, that forces applied to a guide string are directly proportional to the weight being hoisted and to the square of the speed. Thus an increase in hoisting speed is more difficult to design for than an increase in the weight being hoisted. When discussing guide connections it was further stated that when there is an imperfection in the guide string, the force applied to the guide is inversely proportional to the square of the distance over which the imperfection takes place. Thus poor joints between guides are more serious than a change in direction of the guide string. Various methods for calculating the lateral acceleration of conveyances as a function of guide misalignment and conveyance velocity are presented. One of the major assumptions was that the guides do not deform as the conveyance is forced to follow them.

The discussion on guide design states that it is common practice to assume that the magnitude of the static forces acting on a guide is some percentage of the rope end load. Reference is made to a paper by Bently [2] where it is reported that using 10% of the skip weight as a magnitude of the forces acting on the guide is too conservative. In a written discussion of Bently's [2] paper, Backeberg indicates that forces up to 17% of the skip weight have been measured acting on the guides. Reference is also made to Hoischen [10] who reports that guides are designed on the assumption that one-twelfth of the skip weight represents the horizontal thrust force.

Galloway and Tiley [5] reported that forces of up to twice the skip mass have been measured on occasion. They stated that experience had showed that the guide deflection was significant as the conveyance was drawn over them. A numerical model was developed to predict the velocities at which the skip rebounds from the guide. One of their assumptions was that the buntons are rigid. They proposed that the simplest method of avoiding problems arising from large, high-speed skips running on fixed guides was to provide large stiff rollers and sufficient room for them to work. The model was used to analyze the performance of guidance systems in several mine shafts.

Hutton, James and Schwartz [11] discuss the design of deep shaft systems and highlight the effects of ground movement on shaft steelwork. They identify the problem of axial compressive forces in the guides as a result of mining out the column of rock around the shaft (the pillar). They report that it has been found that the buckling of steelwork can be expected when compressive strains exceed 0.4×10^{-3}. Various shaft pillar models were investigated from a rock mechanics point of view as well as various shaft steelwork configurations. Methods of maintaining shaft steelwork integrity during mining of the pillar are discussed.

Krige and Kemp [13,14,15] initiated a research program specifically aimed at gaining a better understanding of the dynamic behaviour of mine shaft steelwork. The work consisted of both theoretical and experimental stages. The theoretical stage involved the development of a computer model to predict conveyance behaviour through a step by step solution of the equations of motion. The model considered the conveyance as three separate rigid bodies and included the effect of bunton flexibility. The experimental stage consisted of measuring the lateral accelerations of the conveyance and the wheel loads in fourteen different mine shafts. On the basis of the measurements and theoretical analysis, design equations were developed for roller and slipper plate contact.

1.3.1 DESCRIPTION OF THE SDRC RESEARCH PROGRAMME

The SDRC were commissioned by COMRO to research the design philosophies of shaft steelwork. The research programme was divided into a test phase, an analysis phase and a design guideline development phase. The aim of the test phase [23] was to gain a physical understanding of the system behaviour in a problematic shaft.

The test phase revealed that the skip behaved as a rigid body moving in rotation and translation, but elastically restrained by the guide rollers and/or the slipper plates bearing on the guides. During slow operation of the skip the guide rollers managed to ride over small irregularities in the guides. When hoisted at full speed the rollers lacked sufficient travel and preload and *bottomed out* in the loading direction and lost contact with the guides in the unloading direction. Measurement showed that roller forces never exceeded 3% of the skip full weight. Direct metal-to-metal contact occurred when the guide rollers bottomed out. If this happened at stiff points on the guide - near the bunton - bunton forces up to 18% of the skip weight resulted. When the guide rollers were rendered ineffective (by backing them off completely) extremely severe impacts occasionally occurred between the skip and the guide giving rise to bunton forces as high as 46% of the skip weight. Practically this can occur when a guide roller fails in service; a situation that is common for heavy skips with a high tyre preload. Prior to these tests some engineers had observed the direct metal-to-metal impacts of the skip onto the guides and had termed this behaviour *slamming*.

The slamming phenomenon and the high forces that result can be understood with the help of Figure 1.1. This figure shows the trajectory of the top corner of a skip as it negotiates its way past a stiff bunton. It is assumed that the corner of the skip impacts the guide close to the midspan (point A) of the guide but, because of guide flexibility, initially there is very little resistance to the lateral motion of the skip. As the skip

approaches the bunton the guide gets stiffer and stiffer at a rapid rate and at a point (B) the lateral motion of the skip is arrested. After this point the skip is forced back into the opening between the two stiff buntons (C and C^1) a fraction of a second later. The forces needed to induce this rapid lateral acceleration are often very large and cause significant deflection of the buntons. A force of 71 kN was measured at the President Steyn Gold Mine, Number 4 Shaft.

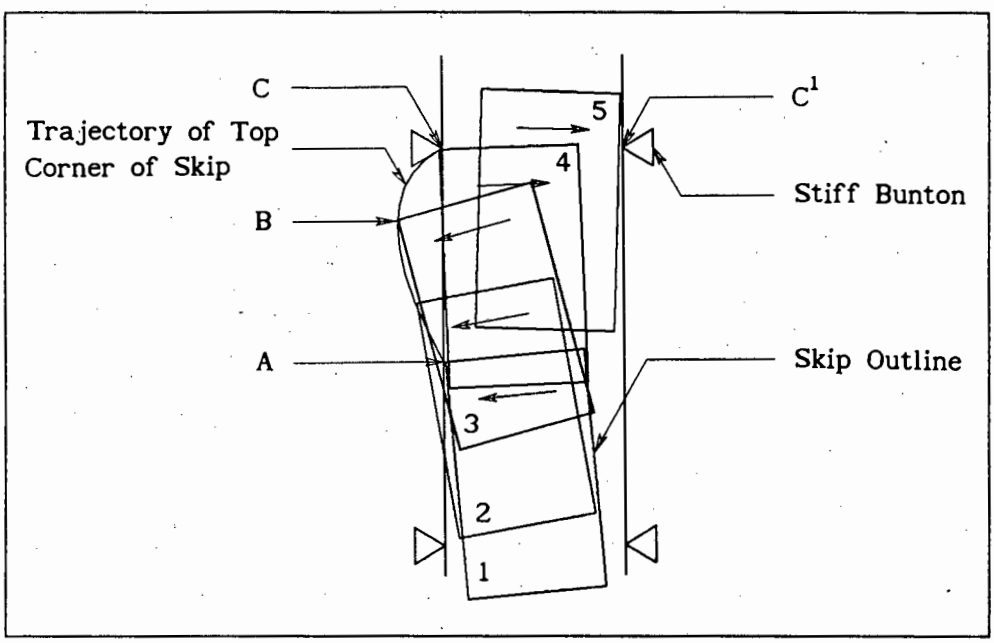

Figure 1.1: Sequence of Skip Positions During a Slamming Event

The event described above does not end when the slipper plate leaves the guide. As a result of the high lateral velocity imparted to the skip, an impact will take place on the opposite guide a fraction of a second later. The sequence of events after this impact is difficult to predict because of the sensitivity of the system to random effects such as guide misalignment, guide gauge variation and other geometric effects.

During the analysis phase [24] an analytical model was developed to model a single slamming event. The SDRC model included the following elements:

- Skip modelled as a lumped mass representing the effective mass of the skip at the contact point;
- Guide a prismatic beam of negligible mass. The beam is assumed to be simply supported at the bunton supports. The centre span stiffness was selected to model the steelwork stiffness at the guide midspan;
- Bunton represented as a spring resisting lateral motion.

The model proved to be a useful tool in modelling a single slamming event and was used for a series of parameter studies. These revealed the following trends:

1. Increasing *skip mass* causes an increase in bunton force and rebound velocity ratio;
2. Increasing *skip velocity* causes an increase in bunton force and rebound velocity ratio;
3. Increasing *bunton spacing* causes an increase in bunton force and rebound velocity ratio;
4. Increasing *guide stiffness* causes a decrease in bunton force and rebound velocity ratio;
5. Increasing *bunton stiffness* causes an increase in bunton force and rebound velocity ratio.

Greenway [6] extended the SDRC [24] analytical phase by nondimensionalising the single slamming event and produced contour plots to simplify the solution. The contour plots were enhanced [7] by including shaded areas representing actual mine shafts. Experimental data [8] was reported for several shafts. Greenway [9] further summarized previous research work and outlined future trends in shaft steel work design. These trends include the use of stiffer guides, more flexible buntons and increased

bunton spacing. He added that owing to the increased understanding of dynamic effects, skip speeds in the region of 20 m/s are within reach.

The SDRC presented the results of a preliminary design guideline phase [27] to establish a design procedure for future designs taking into account dynamic effects. The design guidelines were calibrated [26] with respect to data gathered from a further two mine shafts. The effect of skip flexibility [25] on the analysis was also investigated. The final revision of the SDRC design guidelines [28] represented the culmination of the research programme and contributes greatly to the design of shaft steelwork in South Africa.

Greenway [9] illustrated the advantage to be gained in applying the SDRC design guidelines [27] for the design of the shaft steelwork for Freddies #1 Shaft. The initial shaft steelwork design was reassessed, fully applying the SDRC design guidelines. The bunton spacing was increased from 4.5m to 6.0m and more flexible buntons and stiffer guides were used. A comparison of the two designs indicated that the slamming loads were reduced and a saving of about R2 million in steelwork supply cost was realized. Further savings due to reduced maintenance are also possible.

1.3.2 REVIEW OF WORK BY PRETORIUS [18,19,20,21]

Pretorius [18,19,20,21] extended the analytical work of the SDRC [24] by including the effect of axial compressive forces in the guides. The details of his model are the same as those of the SDRC model described above, except that now the guides are subject to a constant axial compressive force.

The results for the maximum forces, bending moments, displacements and velocities indicated that the slamming event is aggravated when the axial compressive force is present. A simplified analysis based on the assumption that the guide midspan stiffness and the bunton stiffness are

important, while the stiffness distributions between the guide midspan and bunton are not, was also developed. The results of the simplified analysis exhibit errors of up to 20% relative to the previous case. The advantage of the simplified analysis is that it enabled contour plots, giving maximum bunton forces and impact energy magnification, to be generated.

One of the primary assumptions in Pretorius' [18,19,21] analysis was that the guide undergoes only small displacements. As a result, the guide exhibits no secondary stiffening as a result of axial elongation. Pretorius showed, for a specific case, that these stiffening effects could reduce the overall forces in the system. Therefore the severity of the slamming that the skip experiences could be reduced. It was recommended that further work be conducted in this area.

A mathematical model was also developed by Pretorius [18,20] to describe the dynamic behaviour of the skip when the skip rollers are active, i.e. in contact with the guide. The model included the effects of axial compressive forces acting on the guides. Results presented using misalignment data from an actual mine shaft, indicated that axial compressive loads did not significantly influence the response of the skip when the rollers were active.

2 ANALYTICAL MODEL FOR THE SLAMMING ANALYSIS

2.1 INTRODUCTION

In the analytical model for the slamming analysis the skip is modelled as a rigid body with mass, m and a mass moment of inertia, I_G. The centre of gravity is located a distance l_1 below the top of the skip. The skip moves vertically in the shaft at a constant hoisting velocity v_s. The motion of the skip can be described by two degrees of freedom; the translation and rotation of the centre of gravity of the skip. In this analysis only one slamming event is considered and thus the system can be reduced to only one degree of freedom. The top left corner of the skip is assumed to be the point of impact and the motion of this corner is described in terms of a translational degree of freedom y.

The guide is modelled as a massless, prismatic beam which is pinned, on rollers, at the buntons. A bunton set at a specific level of the shaft is modelled as a translational spring, resisting lateral motion. The above description summarises the elements of the SDRC [24] model. The constant axial compressive force investigated by Pretorius [18,19,21] was also assumed to be acting in the guides. So far the model described does not take into account any possible tensile effects due to the axial extension of the guides as they deform, restrained as they are, by the continuous nature of the guide system. In order to model this effect, axial springs are assumed to act on the ends of the guide. The elements of the model are illustrated in Figure 2.1.

It is the inclusion of the axial tension effects (i.e. elongation of the neutral axis) in the model, as bending deformation occurs, that is hereinafter referred to as secondary stiffening.

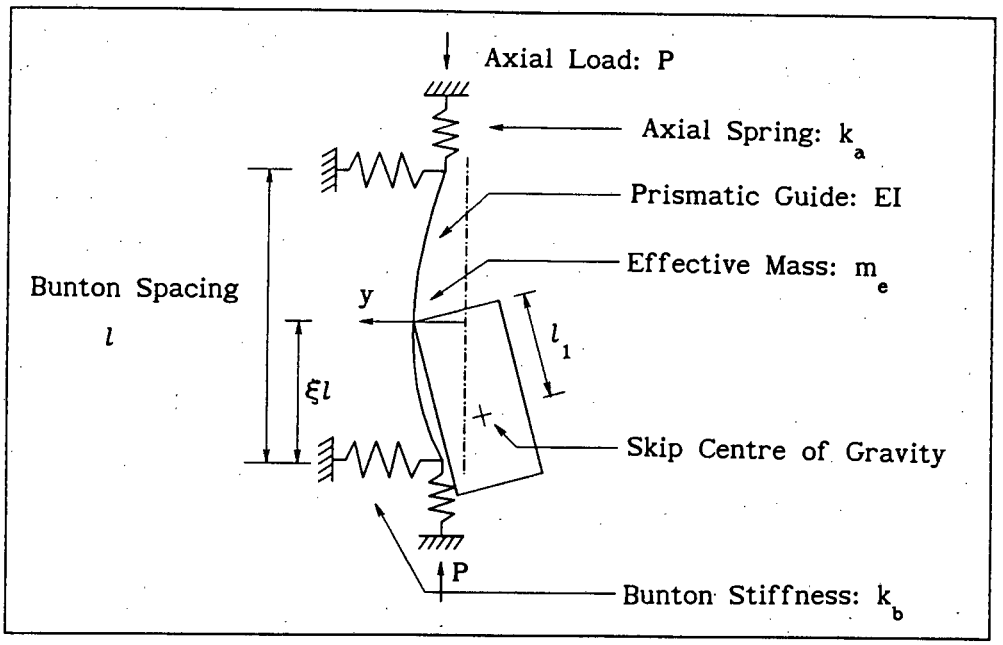

Figure 2.1: Slamming Model Including Axial Compressive Loads and Axial Springs

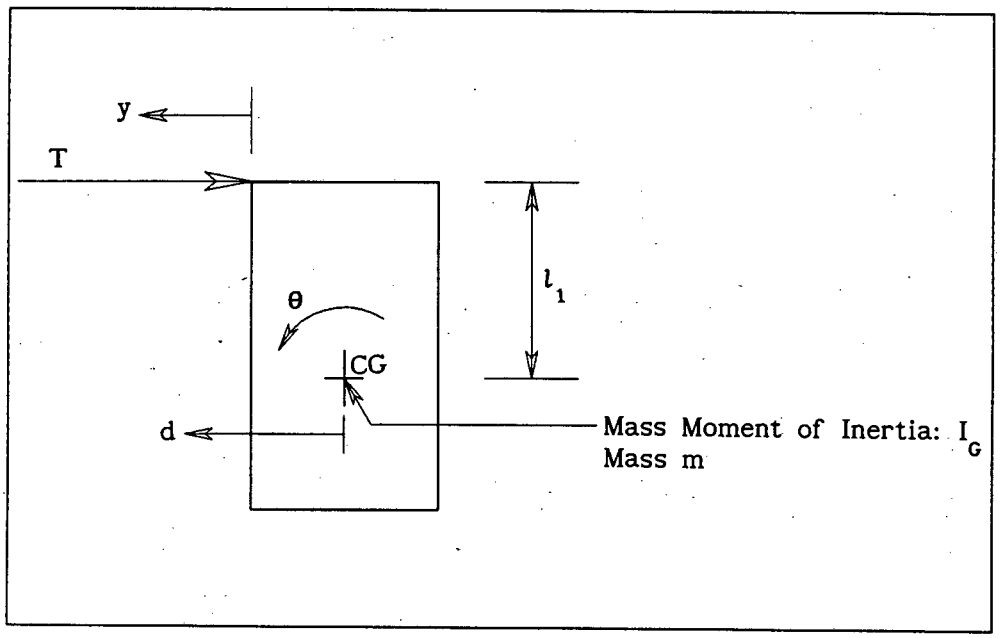

Figure 2.2: Model Showing Notation

2.2 Determination Of The Governing Equations

The derivation of the equations of motion is now discussed using the notation defined in Figure 2.2.

The two equations of motion in terms of the translation, d and rotation, θ are:

$$m\ddot{d} + T = 0 \tag{2.1}$$

and

$$I_G\ddot{\theta} + Tl_1 = 0 \tag{2.2}$$

where T is the skip force, i.e. the force that the guide exerts on the skip. The dots above the variables indicate differentiation with respect to time, i.e. $\ddot{\theta} = \frac{d^2\theta}{dt^2}$. The skip force T is a *nonlinear* function of the beam deflection y, evaluated at a position ξl along the guide ($0 \leq \xi \geq 1$). Thus:

$$T = T(y(\xi)) \tag{2.3}$$

From the geometry of the system and assuming that θ is small, the following relationships between y, d and θ can be obtained:

$$y = d + \theta l_1 \tag{2.4}$$

and,

$$\ddot{y} = \ddot{d} + \ddot{\theta} l_1 \tag{2.5}$$

Substituting equations (2.1), (2.2) and (2.3) into equation (2.5), gives

the following equation describing the motion of the skip:

$$\left[\frac{mI_G}{I_G + ml_1^2}\right] \ddot{y} + T(y(\xi)) = 0 \tag{2.6}$$

A term called the effective mass, m_e, is defined:

$$m_e = \frac{mI_G}{I_G + ml_1^2} \tag{2.7}$$

The equation of motion can be written in terms of the displacement of the corner of the skip $y(\xi)$ (i.e. the beam deflection) as:

$$m_e \ddot{y}(\xi) + T(y(\xi)) = 0 \tag{2.8}$$

and since the skip is hoisted at a constant velocity:

$$\xi = \xi(t) \tag{2.9}$$

2.2.1 CALCULATION OF GUIDE DEFLECTION

The procedure to obtain the relationship between the skip force T and the guide deflection y is now discussed. Firstly, consider an isolated, prismatic beam, pinned at both ends and on rollers. The beam has cross sectional properties EI, length l, an axial compressive force P, and a transverse force T (the force that the skip exerts on the guide), applied at a distance ξl along the beam. The ends of the beam are connected to axial springs, k_a, which restrain the axial translation of the rollers. The displacement under the loads is $y(\xi l)$. The system is illustrated in Figure 2.3.

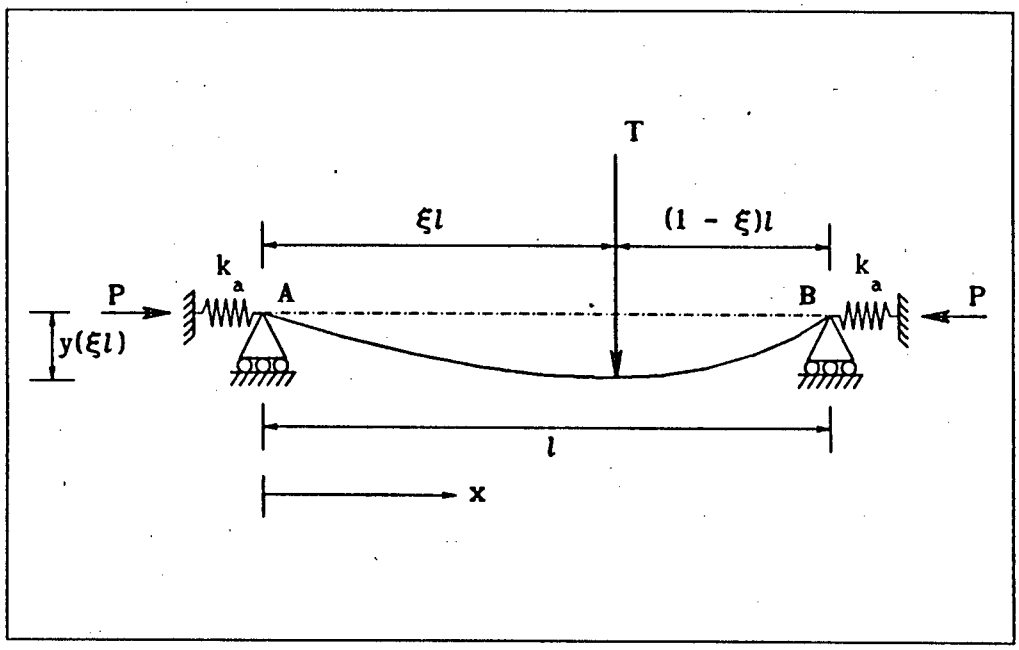

Figure 2.3: An Isolated, Simply-Supported Beam with Axial Load P and Axial Springs k_a

The equations are derived using the *principle of virtual work*. This principle may be expressed as follows:

> *A deformable solid body is in equilibrium if and only if the total virtual work is zero for every kinematically admissible virtual displacement* [4].

Thus the statement of virtual work may be written:

$$\delta W = \delta W_E + \delta W_I = 0 \qquad (2.10)$$

where δW_E is the external virtual work and δW_I is the internal virtual work.

The internal virtual work is given by the negative of the first variation

of the *strain energy*, U, i.e.:

$$\delta W_I = - \delta U \tag{2.11}$$

Substituting equation (2.11) into equation (2.10):

$$\delta W_E - \delta U = 0 \tag{2.12}$$

Writing equation (2.12) in a different way:

$$\delta U - \delta W_E = 0 \tag{2.13}$$

Equation (2.13) can be written as:

$$\delta(U - W_E) = 0 \tag{2.14}$$

where - W_E is the potential of the external forces.

The term in parentheses in equation (2.14) is the *total potential energy*, Π, of the body and thus:

$$\delta\Pi = 0 \tag{2.15}$$

Equation (2.15) is equivalent to the following statement:

> *Of all possible kinematically admissible deflections, those that satisfy equilibrium make the potential energy a minimum* [4].

This is called the *principle of minimum potential energy.*

In order to derive the virtual work expression for the system illustrated in Figure 2.3, first consider half the beam, without the P force acting.

The displacement at **B**, δ_B, due to the induced axial load N and the lateral deflection y in the beam is derived in Appendix A and is:

$$\delta_B = \frac{1}{2}\left(\frac{Nl}{AE} - \frac{1}{2}\int_0^l \left(\frac{dy}{dx}\right)^2 dx\right) \tag{2.16}$$

Also, the displacement at **B** due to the force N in the spring is:

$$\delta_B = -\frac{N}{k_a} \tag{2.17}$$

Equating the displacements and solving for the axial force N:

$$N = \left(\frac{EAk_a}{k_a l + 2EA}\right) \frac{1}{2}\int_0^l \left(\frac{dy}{dx}\right)^2 dx \tag{2.18}$$

which is like an equivalent spring stiffness × the axial displacement.

The virtual work statement for the system illustrated in Figure 2.3 is:

$$\delta W = EI\int_0^l y''\delta y''\ dx + \left(\frac{EAk_a}{k_a l + 2EA}\right)\left(\frac{1}{2}\int_0^l \left(\frac{dy}{dx}\right)^2 dx\right)\left(\int_0^l y'\,\delta y'\ dx\right)$$

$$- P\int_0^l y'\,\delta y'\ dx - T\delta y(\xi l) = 0 \tag{2.19}$$

where:

$EI\int_0^l y''\delta y''\ dx$ represents the virtual work of a beam in bending,

$-P\int_0^l y'\delta y'\,dx$ represents the virtual work due to the beam stretching.

Both of the above expressions are derived in Appendix A.

Writing equation (2.19) as $\delta(U - W_E)$ or $\delta\Pi$ where Π represents the total potential energy of the system:

$$\delta\Pi = \delta\left[\frac{EI}{2}\int_0^l\left(\frac{d^2y}{dx^2}\right)^2 dx + \frac{EAk_a}{2(k_a l+2EA)}\left\{\frac{1}{2}\int_0^l\left(\frac{dy}{dx}\right)^2 dx\right\}^2 - \frac{P}{2}\int_0^l\left(\frac{dy}{dx}\right)^2 dx - Ty(\xi l)\right] \tag{2.20}$$

or, the total potential energy is:

$$\Pi = \frac{EI}{2}\int_0^l\left(\frac{d^2y}{dx^2}\right)^2 dx + \frac{EAk_a}{2(k_a l+2EA)}\left\{\frac{1}{2}\int_0^l\left(\frac{dy}{dx}\right)^2 dx\right\}^2 - \frac{P}{2}\int_0^l\left(\frac{dy}{dx}\right)^2 dx - Ty(\xi l) \tag{2.21}$$

The deflection is assumed to be in the form of a sine series:

$$y(x) = \sum_{n=1}^{\infty} a_n \sin\frac{n\pi x}{l} \tag{2.22}$$

This series automatically satisfies the end conditions $y = y'' = 0$ i.e. the deflections and bending moments at the ends of the beam are zero.

The conditions for termwise differentiation are satisfied [16] and therefore:

$$\frac{dy}{dx} = \frac{\pi}{l}\sum_{n=1}^{\infty} n a_n \cos\frac{n\pi x}{l} \tag{2.23}$$

$$\frac{d^2y}{dx^2} = -\frac{\pi^2}{l^2}\sum_{n=1}^{\infty} n^2 a_n \sin\frac{n\pi x}{l} \tag{2.24}$$

Squaring the series for y′ and y″ we obtain the double series:

$$\left(\frac{dy}{dx}\right)^2 = \frac{\pi^2}{l^2}\sum_{m=1}^{\infty}\sum_{n=1}^{\infty} m a_m \cos\frac{m\pi x}{l}\, n a_n \cos\frac{n\pi x}{l} \tag{2.25}$$

$$\left(\frac{d^2y}{dx^2}\right)^2 = \frac{\pi^4}{l^4}\sum_{m=1}^{\infty}\sum_{n=1}^{\infty} m^2 a_m \sin\frac{m\pi x}{l}\, n^2 a_n \sin\frac{n\pi x}{l} \tag{2.26}$$

The integrals of the cross products cancel because of the relations:

$$\int_0^l \sin\frac{m\pi x}{l}\sin\frac{n\pi x}{l}\,dx = \int_0^l \cos\frac{m\pi x}{l}\cos\frac{n\pi x}{l}\,dx = \begin{cases} 0 & \text{if } m \neq n \\ \frac{l}{2} & \text{if } m = n \end{cases}$$

Thus the following expressions are obtained:

$$\int_0^l \left(\frac{d^2y}{dx^2}\right)^2 dx = \frac{\pi^4}{2l^3}\sum_{n=1}^{\infty} n^4 a_n^2 \tag{2.27}$$

$$\int_0^l \left(\frac{dy}{dx}\right)^2 dx = \frac{\pi^2}{2l}\sum_{n=1}^{\infty} n^2 a_n^2 \tag{2.28}$$

Substituting equations (2.27) and (2.28) into (2.21) we obtain:

$$\Pi = \frac{EI\pi^4}{4l^3}\sum_{n=1}^{\infty} n^4 a_n^2 - \frac{P\pi^2}{4l}\sum_{n=1}^{\infty} n^2 a_n^2$$

$$+ \frac{EAk_a\pi^4}{32l^2(k_a l+2AE)}\left\{\sum_{n=1}^{\infty} n^2 a_n^2\right\}^2 - T\sum_{n=1}^{\infty} a_n \sin n\pi\xi \qquad (2.29)$$

Minimising the total potential energy with respect to the generalized coordinates a_n:

$$\frac{\partial\Pi}{\partial a_n} = \frac{EI\pi^4}{2l^3} n^4 a_n - \frac{P\pi^2}{2l} n^2 a_n$$

$$+ \frac{EAk_a\pi^4}{8l^2(k_a l + 2AE)}\left\{\sum_{r=1}^{\infty} r^2 a_r^2\right\} n^2 a_n - T \sin n\pi\xi = 0 \qquad (2.30)$$

By defining:

$$k_g = \frac{48EI}{l^3} \qquad (2.31)$$

and the dimensionless parameters:

$$p = \frac{P}{\frac{\pi^2 EI}{l^2}} \qquad (2.32)$$

$$\bar{k} = \frac{EA}{l k_a} \qquad (2.33)$$

$$\bar{T} = \frac{T}{k_g}\sqrt{\frac{A}{I}} \qquad (2.34)$$

$$\bar{a}_n = a_n\sqrt{\frac{A}{I}} \qquad (2.35)$$

and multiplying through by $\frac{1}{\bar{k}_g}\sqrt{\frac{\bar{A}}{\bar{I}}}$ equation (2.30) can be written as:

$$\frac{\pi^4 n^2}{96}\left(n^2 - p\right)\bar{a}_n + \frac{\pi^4}{384(1 + 2\bar{k})}\left\{\sum_{r=1}^{\infty} r^2\bar{a}_r^2\right\} n^2\bar{a}_n = \bar{T}\sin n\pi\xi \qquad (2.36)$$

Writing out equation (2.36) for one, two and three Fourier terms we obtain;

for *one* term:

$$\frac{\pi^4}{96}\left[(1 - p)\bar{a}_1 + \frac{1}{4}\left(\frac{1}{1 + 2\bar{k}}\right)\bar{a}_1^3\right] = \bar{T}\sin\pi\xi \qquad (2.37)$$

for *two* terms:

$$\begin{aligned}\frac{\pi^4}{96}\left[(1 - p)\bar{a}_1 + \frac{1}{4}\left(\frac{1}{1 + 2\bar{k}}\right)\left(\bar{a}_1^2 + 4\bar{a}_2^2\right)\bar{a}_1\right] &= \bar{T}\sin\pi\xi \\ \frac{\pi^4}{24}\left[(4 - p)\bar{a}_2 + \frac{1}{4}\left(\frac{1}{1 + 2\bar{k}}\right)\left(\bar{a}_1^2 + 4\bar{a}_2^2\right)a_2\right] &= \bar{T}\sin 2\pi\xi\end{aligned} \qquad (2.38)$$

for *three* terms:

$$\begin{aligned}\frac{\pi^4}{96}\left[(1 - p)\bar{a}_1 + \frac{1}{4}\left(\frac{1}{1 + 2\bar{k}}\right)\left(\bar{a}_1^2 + 4\bar{a}_2^2 + 9\bar{a}_3^2\right)\bar{a}_1\right] &= \bar{T}\sin\pi\xi \\ \frac{\pi^4}{24}\left[(4 - p)\bar{a}_2 + \frac{1}{4}\left(\frac{1}{1 + 2\bar{k}}\right)\left(\bar{a}_1^2 + 4\bar{a}_2^2 + 9\bar{a}_3^2\right)\bar{a}_2\right] &= \bar{T}\sin 2\pi\xi \\ \frac{9\pi^4}{96}\left[(9 - p)\bar{a}_3 + \frac{1}{4}\left(\frac{1}{1 + 2\bar{k}}\right)\left(\bar{a}_1^2 + 4\bar{a}_2^2 + 9\bar{a}_3^2\right)\bar{a}_3\right] &= \bar{T}\sin 3\pi\xi\end{aligned} \qquad (2.39)$$

Equations (2.37), (2.38) and (2.39) thus represent a series of coupled nonlinear equations in $\bar{a}_n$. In order to obtain the guide displacement, and depending on the number of Fourier terms required for the approximation, equation (2.37), (2.38) or (2.39) need to be solved for the $\bar{a}_n$. The corresponding dimensionless guide displacement is then found from:

$$\bar{y}_g = \sum_{n=1} \bar{a}_n \sin n\pi\xi \tag{2.40}$$

The above analysis assumes that bunton supports do not displace. In order to include this displacement, the displacement for a rigid beam acted on by the skip force T is superimposed on the guide displacement calculated from equation (2.40).

Consider a rigid beam (as illustrated in Figure 2.4) supported at its ends by linear springs k_b and acted upon by a lateral force T at $x = \xi l$. The deflection y_b at $x = \xi l$ is:

$$y_b(\xi) = \frac{T}{k_b}\left[\xi^2 + (1 - \xi)^2\right] \tag{2.41}$$

Equation (2.41) can be non-dimensionalised by multiplying through by $\frac{1}{k_g}\sqrt{\frac{A}{I}}$ thus we obtain:

$$\bar{y}_b(\xi) = \frac{1}{r}\left[\xi^2 + (1 - \xi)^2\right] \tag{2.42}$$

where:

$$r = \frac{k_b}{k_g} \tag{2.43}$$

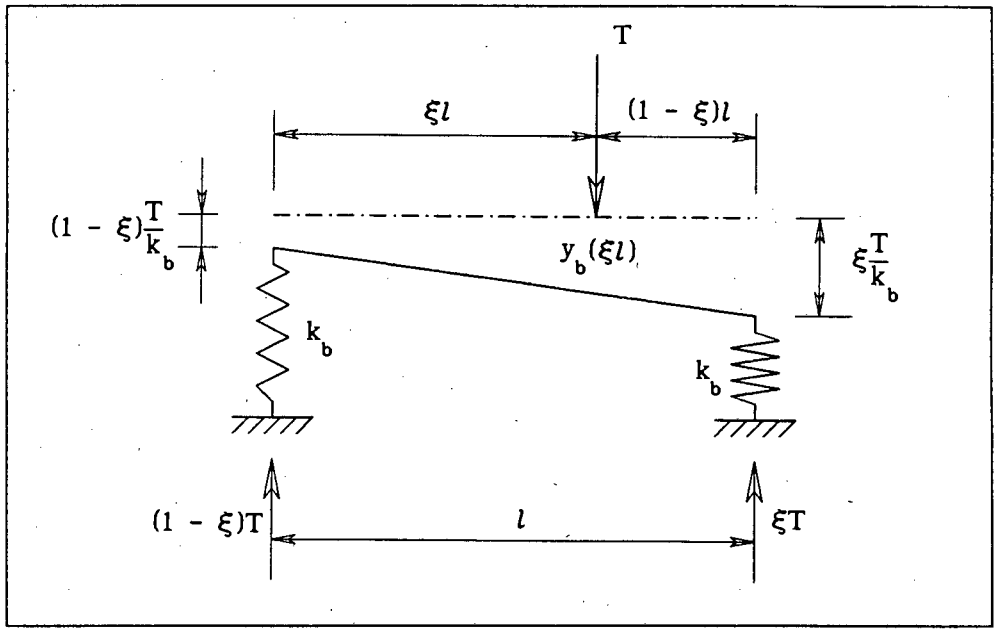

Figure 2.4: Displacements of the Buntons

2.2.2 DIMENSIONLESS FORMULATION OF THE EQUATION OF MOTION

It is desirable to write the equation of motion in a dimensionless form so that parametric studies can be performed for a general class of problems rather than for specific cases.

The equation of motion, equation (2.8), is rewritten:

$$m_e \ddot{y}(\xi) + T(y(\xi)) = 0 \ , \quad \xi = \xi(t) \tag{2.44}$$

with the initial conditions: $y(\xi(0)) = 0$ and $\dot{y}(\xi(0)) = \dot{u}_0$.

Multiplying through by $\frac{1}{k_g}\sqrt{\frac{A}{I}}$, equation (2.44) can be expressed as:

$$\frac{1}{\omega^2}\frac{d^2Y}{dt^2} + \bar{T}(Y) = 0 \tag{2.45}$$

where Y is the total dimensionless displacement, i.e.:

$$Y = y\sqrt{\frac{A}{I}}\ ,\ y = y_g + y_b \text{ and where } \omega = \sqrt{\frac{k_g}{m_e}}$$

By defining $\tau = \omega t$ equation (2.45) can be written as:

$$\frac{d^2Y}{d\tau^2} + \bar{T}(Y) = 0 \tag{2.46}$$

The initial conditions in the dimensionless equations are obtained as follows:

$$\frac{dy(\xi(0))}{dt} = \dot{u}_0 \tag{2.47}$$

where $\dot{u}_0$ is the initial translational velocity of the skip.

Making use of the dimensionless form of the displacement we obtain:

$$\frac{d}{dt}\left(\frac{Y}{\sqrt{\frac{A}{I}}}\right) = \frac{\omega}{\sqrt{\frac{A}{I}}}\frac{dY}{d\tau} = \dot{u}_0$$

which gives the dimensionless initial velocity as:

$$\frac{dY(\xi(0))}{d\tau} = \frac{\dot{u}_0}{\omega}\sqrt{\frac{A}{I}} \tag{2.48}$$

The parameter ξ is a function of time, defined by the relationship:

$$\xi(t) = \xi_0 + \frac{v_s}{l}t \tag{2.49}$$

where v_s is the constant vertical velocity of the skip and ξ_0 is the initial point of impact of the corner of the skip. The following

dimensionless parameter for the skip velocity is introduced:

$$\bar{V}_s = \frac{v_s}{l}\sqrt{\frac{m_e}{k_g}} = \frac{v_s}{\omega l} \tag{2.50}$$

The dimensionless relationship between ξ and τ is therefore:

$$\xi(\tau) = \xi_0 + \bar{V}_s\tau \tag{2.51}$$

2.2.3 SYSTEM PARAMETERS

The solution of the equation of motion, equation (2.46) depends on the following six dimensionless parameters:

$r = \frac{k_b}{k_g}$ the ratio of the bunton stiffness to the guide stiffness,

$\bar{k} = \frac{AE}{k_a l}$ the ratio of the axial stiffness of the guide to the stiffness of the end springs,

$p = \frac{P}{P_{cr}}$ the ratio of the applied axial compressive load to the critical buckling load of the guide,

$\bar{V}_s = \frac{v_s}{\omega l}$ the dimensionless form of the vertical velocity of the skip,

$\xi_0 = \frac{x_0}{l}$ the initial position of impact between the skip and the guide,

$\frac{dY}{d\tau} = \frac{\dot{u}_0}{\omega}\sqrt{\frac{A}{I}}$ the initial translational impact velocity of the skip.

2.2.4 CALCULATION OF THE FORCES IN THE SYSTEM

The forces in the buntons as defined in Figure 2.4, are:

$$B_1(\xi) = (1 - \xi)T(\xi) \quad \text{and}$$

$$B_2(\xi) = \xi T(\xi)$$

The bunton forces can be written in dimentionless form as:

$$\bar{B}_1(\xi) = (1 - \xi)\bar{T}(\xi) \tag{2.52}$$

$$\bar{B}_2(\xi) = \xi\bar{T}(\xi) \tag{2.53}$$

where: $\bar{B}(\xi) = \dfrac{B(\xi)}{k_g}\sqrt{\dfrac{A}{I}}$

The maximum bunton force at any instant is the maximum of $\bar{B}_1(\xi)$ and $\bar{B}_2(\xi)$.

The maximum bending moment due to the transverse load T will occur at the position of the load, while the maximum bending moment due to the resultant axial load will occur at the position of maximum beam deflection. The positions of these two maxima will not always occur at the same place. Since the beam deflection is only known at the position of maximum load it is assumed that the maximum bending moment occurs at the position of the transverse load T, i.e. at position ξl.

The bending moment due to the skip force $T(\xi)$ is:

$$M_s(\xi) = \xi(1 - \xi)lT(\xi)$$

and the bending moment due to the resultant axial forces is:

$$M_a(\xi) = (P - N)y(\xi)$$

The total bending moment at position ξl is therefore:

$$M(\xi) = \xi(1 - \xi)lT(\xi) + (P - N)y(\xi)$$

Substituting equation (2.18) for the axial tension N we obtain:

$$\bar{M}(\xi) = \xi(1 - \xi)l\bar{T}(\xi) + \frac{\pi^2}{48}\left\{p - \frac{1}{4(1 + 2\bar{k})}\sum_{n=1}^{\infty} n^{2-2}a_n\right\} Y(\xi) \qquad (2.54)$$

where:

$$\bar{M}(\xi) = \frac{1}{lk_g}\sqrt{\frac{A}{I}}\, M(\xi) \qquad (2.55)$$

3 NUMERICAL IMPLEMENTATION OF THE MODEL

3.1 INTRODUCTION

In this chapter the numerical implementation of the model is described. An integration algorithm is used for the time-stepping and the solution procedure is discussed, along with a scheme to terminate the solution. Finally, the model is verified by comparing results to those obtained by a previous model.

The numerical integration of the equation of motion, equation (2.46), is based on two ideas. The first is that equilibrium of the equation of motion will only be sought at discrete time intervals Δt apart. The second is that a variation of displacements, velocities and accelerations within each time interval Δt is assumed. The form of the assumption on the variation of displacements, velocities and accelerations determines the accuracy, stability and cost of the solution procedure.

3.2 THE NEWMARK METHOD

The Newmark integration scheme [1,17] uses the following assumptions:

$$\dot{Y}_{\tau+\Delta\tau} = \dot{Y}_{\tau} + \left[(1 - \delta)\ddot{Y}_{\tau} + \delta\ddot{Y}_{\tau+\Delta\tau}\right]\Delta\tau \tag{3.1}$$

$$Y_{\tau+\Delta\tau} = Y_{\tau} + \dot{Y}_{\tau}\Delta\tau + \left[\left(\frac{1}{2} - \alpha\right)\ddot{Y}_{\tau} + \alpha\ddot{Y}_{\tau+\Delta\tau}\right]\Delta\tau^2 \tag{3.2}$$

where α and δ are parameters that are chosen to determine the integration accuracy and stability. When $\delta = \frac{1}{2}$ and $\alpha = \frac{1}{4}$ the scheme is unconditionally stable and assumes that the acceleration over a specific time interval is constant.

The acceleration at any arbitrary time $\tilde{\tau}$ ($\tau \leq \tilde{\tau} \geq (\tau + \Delta\tau)$) is taken as the average of the accelerations at the preceding and the following time steps (see Figure 3.1) i.e.:

$$\ddot{Y}(\tilde{\tau}) \approx \frac{1}{2}\left(\ddot{Y}_{\tau} + \ddot{Y}_{\tau+\Delta\tau}\right) \tag{3.3}$$

Expressing the differential equation describing the motion of the system, equation (2.46), at time $\tau + \Delta\tau$, we obtain the following equation:

$$\ddot{Y}_{\tau+\Delta\tau} + \bar{T}\left(Y_{\tau+\Delta\tau}\right) = 0 \tag{3.4}$$

Solving equation (3.2) for $\ddot{Y}_{\tau+\Delta\tau}$ in terms of $Y_{\tau+\Delta\tau}$ and then substituting for $\ddot{Y}_{\tau+\Delta\tau}$ into equation (3.1) we obtain the following equations for $\ddot{Y}_{\tau+\Delta\tau}$ and $\dot{Y}_{\tau+\Delta\tau}$, each in terms of unknown displacements $Y_{\tau+\Delta\tau}$:

$$\dot{Y}_{\tau+\Delta\tau} = \frac{2}{\Delta\tau}\left(Y_{\tau+\Delta\tau} - Y_{\tau}\right) - \dot{Y}_{\tau} \tag{3.5}$$

$$\ddot{Y}_{\tau+\Delta\tau} = \frac{4}{\Delta\tau^2}\left(Y_{\tau+\Delta\tau} - Y_{\tau} - \dot{Y}_{\tau}\Delta\tau - \frac{\Delta\tau^2}{4}\ddot{Y}_{\tau}\right) \tag{3.6}$$

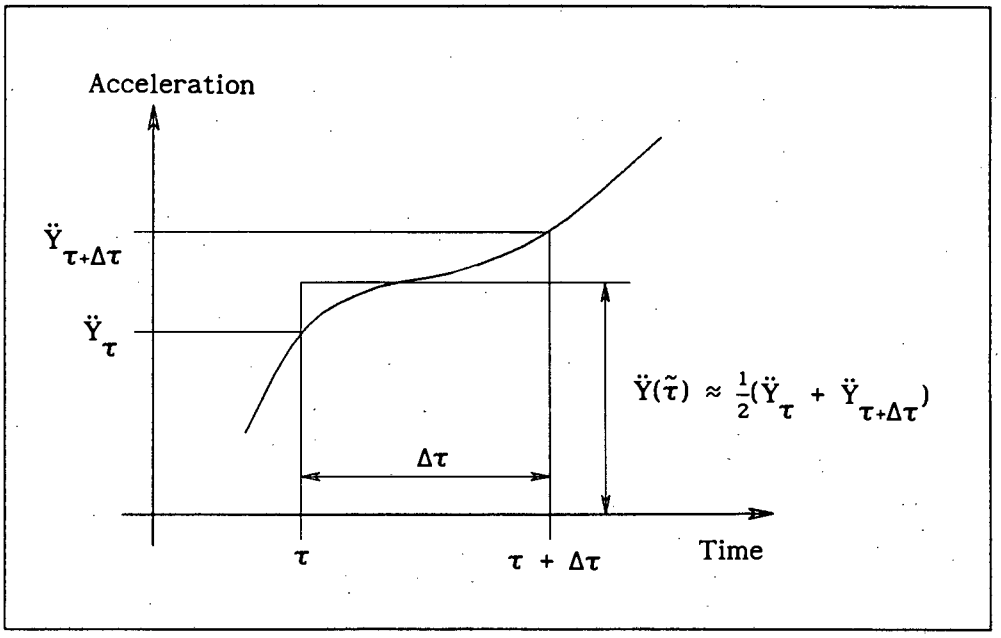

Figure 3.1: Plot of Acceleration versus Time Showing Acceleration Approximation

Substituting equation (3.6) into the equation of motion, equation (3.4), we obtain:

$$Y^{i+1}_{\tau+\Delta\tau} = Y_{\tau} + \Delta\tau\ \dot{Y}_{\tau} + \frac{\Delta\tau^2}{4}\ \ddot{Y}_{\tau} - \frac{\Delta\tau^2}{4}\ \bar{T}\left(Y^{i}_{\tau+\Delta\tau}\right) \tag{3.7}$$

where the i superscript represents an iteration to ensure equilibrium between the displacement and the force. In order to start the iteration, the following starting value for the displacement is assumed:

$$Y^{0}_{\tau+\Delta\tau} = \Delta\tau\ \dot{Y}_{\tau}$$

The iteration is continued until the difference between two successive displacements is less than a chosen tolerance, i.e.:

$$\left(Y^{i+1}_{\tau+\Delta\tau} - Y^{i}_{\tau+\Delta\tau}\right) / Y^{i}_{\tau+\Delta\tau} \leq \varepsilon_1$$

3.2.1 CALCULATION OF THE SKIP FORCE

In order to solve equation (3.7) a method for determining the force $\bar{T}\left(Y^1_{\tau+\Delta\tau}\right)$ corresponding to the displacement $Y^1_{\tau+\Delta\tau}$ is required. It must be remembered that Y is the total displacement (guide + bunton). Because the force-displacement relation for the guide is nonlinear an iterative procedure is required to obtain $\bar{T}$. A predictor-corrector type of solution strategy is employed whereby a prediction of the skip force is made using a linear stiffness. The deflection of the skip due to the linear predicted force is then calculated as the corrector phase. The two values of displacement are then compared and if the difference is not less than a specified tolerance, a new force is calculated, and so on, until convergence is achieved. The procedure is detailed below and illustrated in Figure 3.2.

The linear stiffness, derived in Appendix B, is:

$$K^L = \left\{\frac{96\sin^2\pi\xi}{\pi^4(1-p)} + \frac{1}{r}\left[\xi^2 + (1-\xi)^2\right]\right\}^{-1} \tag{3.8}$$

using the linear stiffness, the force corresponding to the displacement $Y^1_{\tau+\Delta\tau}$ is calculated as:

$${}^j\bar{T}^1_{\tau+\Delta\tau} = Y^1_{\tau+\Delta\tau}\left\{\frac{96\sin^2\pi\xi}{\pi^4(1-p)} + \frac{1}{r}\left[\xi^2 + (1-\xi)^2\right]\right\}^{-1} \tag{3.9}$$

where the j superscript is the iteration counter.

The bunton deflection corresponding to the force ${}^j\bar{T}^1_{\tau+\Delta\tau}$ is calculated using:

$${}^j\bar{y}^1_{b_{\tau+\Delta\tau}} = \frac{1}{r}\left[\xi^2 + (1-\xi)^2\right]{}^j\bar{T}^1_{\tau+\Delta\tau} \tag{3.10}$$

while the guide displacement, ${}^{J}\bar{y}^{1}_{g_{\tau+\Delta\tau}}$, is calculated using the non-linear guide equations, equation (2.40). Details of the solution procedure may be found in Appendix C.

The bunton and guide deflections are added to obtain the total deflection:

$$ {}^{J}Y^{1}_{\tau+\Delta\tau} = {}^{J}\bar{y}^{1}_{b_{\tau+\Delta\tau}} + {}^{J}\bar{y}^{1}_{g_{\tau+\Delta\tau}} \tag{3.11} $$

As a convergence check, ${}^{J}Y^{1}_{\tau+\Delta\tau}$ is compared to the target displacement, $Y^{1}_{\tau+\Delta\tau}$, i.e.:

$$ \left(Y^{1}_{\tau+\Delta\tau} - {}^{J}Y^{1}_{\tau+\Delta\tau} \right) / {}^{J}Y^{1}_{\tau+\Delta\tau} \leq \varepsilon_2 $$

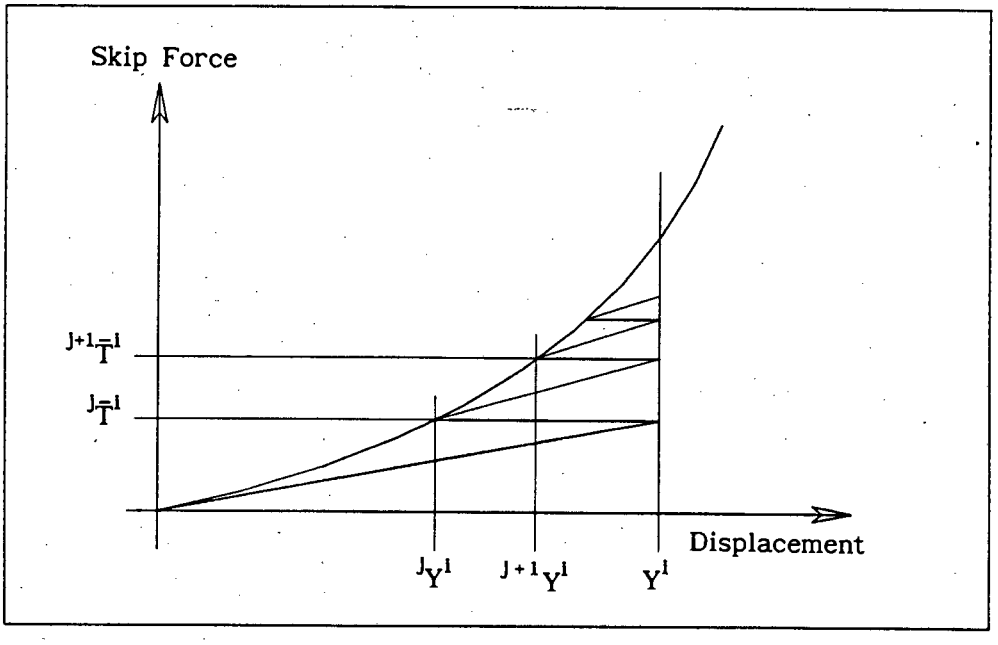

Figure 3.2: Solution Algorithm for Skip Force $\bar{T}$

Should convergence not be achieved, a further approximation to the force is calculated:

$$^{j+1}\bar{T}^{i}_{\tau+\Delta\tau} = \left(Y^{i}_{\tau+\Delta\tau} - {}^{j}Y^{i}_{\tau+\Delta\tau}\right)\left\{\frac{96\sin^2\pi\xi}{\pi^4(1-p)} + \frac{1}{r}\left[\xi^2 + (1-\xi)^2\right]\right\}^{-1} + {}^{j}\bar{T}^{i}_{\tau+\Delta\tau} \qquad (3.12)$$

and so on, until the force corresponding to the equilibrium displacement, $Y^{i}_{\tau+\Delta\tau}$, is attained within the desired degree of accuracy.

3.3 COMPUTER PROGRAM UCTSTIFF

A computer program called **UCTSTIFF** was developed in order to perform the slamming analysis described in section 3.1. The program was written in FORTRAN 77 and implemented on a DEC VAX 6000-330. The relevant code can be found in Appendix D.

3.3.1 TERMINATION OF THE SOLUTION

The solution of the equation of motion (3.4) is terminated when the skip leaves the guide, i.e. when $Y_{\tau>0} = 0$. The time at which the skip leaves the guide will not necessarily fall precisely at the end of a time-step. A linear interpolation is performed to obtain a better approximation of the time when the skip leaves the guide. This new time increment is used to calculate the values of the velocity and acceleration when the skip leaves the guide, as well as the position at which the skip left the guide.

3.3.2 VERIFICATION OF THE MODEL

In order to verify the model, the program **UCTSTIFF** was run using the following data. This choice allows a direct comparison to be made with the results obtained by Pretorius [18,19,21]. Two cases of the axial compressive force ratio, p, and the initial impact position, ξ_0, were used for the comparison.

$r = \frac{k_b}{k_g}$ was kept constant at a value of $r = \frac{26330}{810} = 32.506$

$\bar{k} = \frac{AE}{k_a l}$ was set to 1000 in order to negate, for comparison purposes, the effect of the axial end springs, k_a.

$p = \frac{P}{P_{cr}}$ was set to p = 0.0 for the first case and to p = 0.5 for the second.

$V_s = \frac{v_s}{\omega l}$ was kept constant at a value of $V_s = \frac{15.24}{\sqrt{\frac{810}{6.95}} \times 6.1} = 0.2314$

$\xi_0 = \frac{x_0}{l}$ was set to $\xi_0 = 0.1$ for the first case and to $\xi_0 = 0.25$ for the second.

The initial translation velocity, $\dot{u}_0$, was set at 1 m/s for all examples in this thesis and is the same value used by the SDRC [24]. Three Fourier terms were used to approximate the guide displacement.

The results that were obtained are tabulated in Tables 3.1 and 3.2 below. Plots of the displacement of the skip and the force exerted by the corner of the skip are presented graphically in Figures 3.3 to 3.6. The values of the variables have been converted to dimensional numbers as Pretorius [18,19,21] used dimensionless numbers different from those used in this work.

	UCTSTIFF	Pretorius
Skip Left Guide (x/l)	0.7484	0.7571
Rebound Velocity [m/s]	0.7002	0.7155
Max. Skip Force [kN]	69.00	67.77
Max. Bunton Force [kN]	55.31	53.70
Max. Bending Moment [kNm]	81.41	82.08
Max. Displacement [m]	0.062	0.063

Table 3.1: Comparison between Pretorius' Results and **UCTSTIFF** (p = 0.0, $\xi_0 = 0.1$)

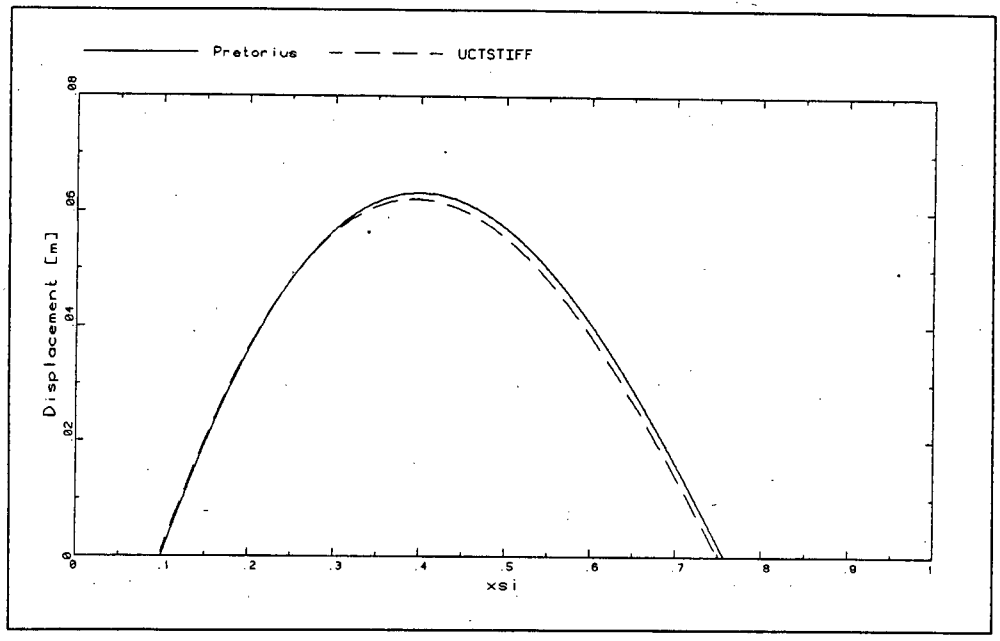

Figure 3.3: Displacement Comparison Between Pretorius' Results and **UCTSTIFF** ($p = 0.0$, $\xi_0 = 0.1$)

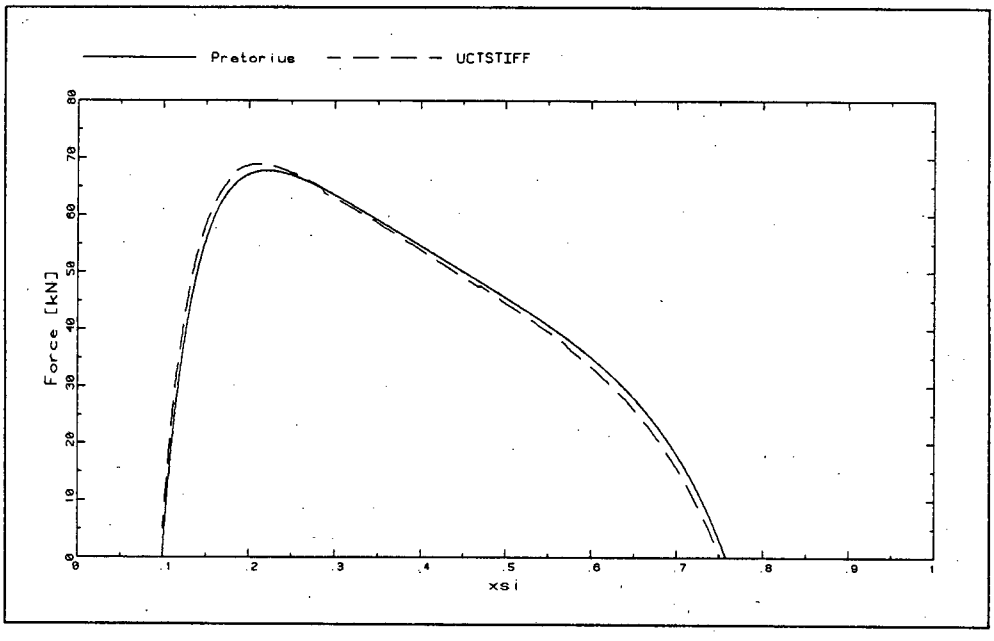

Figure 3.4: Force Comparison Between Pretorius' Results and **UCTSTIFF** ($p = 0.0$, $\xi_0 = 0.1$)

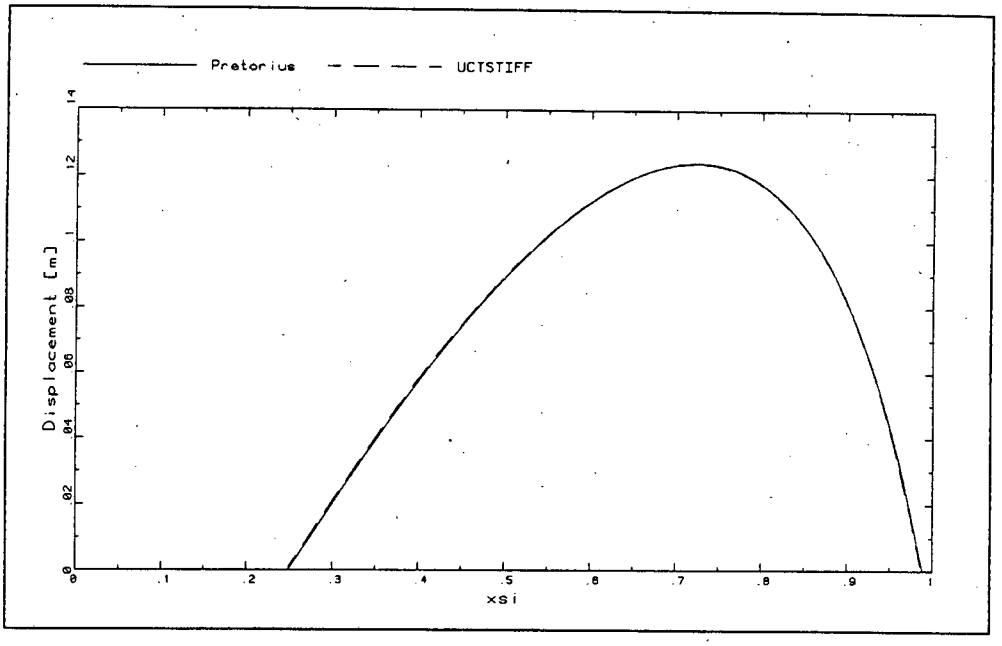

Figure 3.5: Displacement Comparison Between Pretorius' Results and **UCTSTIFF** (p = 0.5, ξ_0 = 0.25)

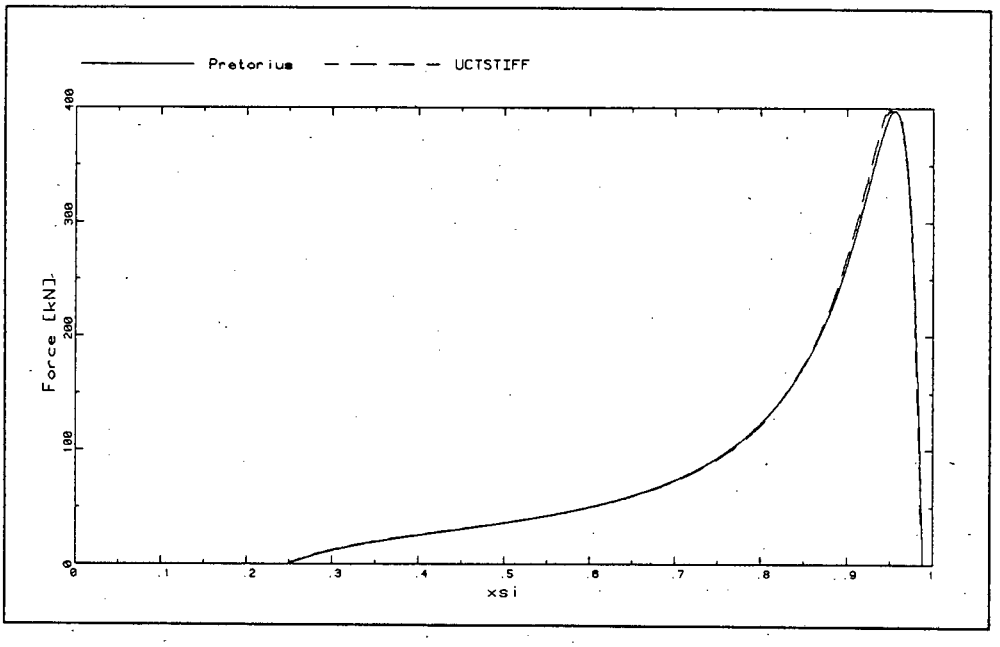

Figure 3.6: Force Comparison Between Pretorius' Results and **UCTSTIFF** (p = 0.5, ξ_0 = 0.25)

3.3.3 CALCULATION OF GUIDE STIFFNESS

As discussed in Chapter 1, previous work by SDRC [24] and Pretorius [18,19,21] did not model the continuous nature of the guide string and thereby the axial stiffening effects. However, in order to include these effects, the midspan stiffness of the simply supported beam was multiplied by a factor and this increased stiffness value was used in the computations. The SDRC [24] reported that a multispan continuous beam is 1.90 times as stiff as a simply supported beam of the same size and length.

The model developed in this thesis models the continuous nature of the guide string by means of axial springs. The stiffness of the springs used to simulate the continuous structure was obtained from a frame analysis [12] involving several layers of the shaft steelwork which are linked together by the guides. A spring stiffness of k_a = 49145 kN/m was used.

Figures 3.7 and 3.8 illustrate the force deflection curves at the *midpoint* of a guide for the following three cases:

- **A** Simply-supported, on rollers,
- **B** Simply-supported, on rollers, with constant factor to simulate the axial effects of the rest of the structure,
- **C** Simply-supported, on rollers, with end springs to simulate the axial effects of the rest of the structure.

The guide in Figure 3.7 has no axial compressive force acting while in Figure 3.8 an axial compressive load of p = 0.9 is present.

In both Figures 3.7 and 3.8, the secondary stiffening effect is clearly evident in curve **C** with the nonlinear effect being greater for large deflections. Curve **C** is initially asymptotic to the linear curve, **A**. This is to be expected as the secondary stiffening effects only influence the

response of the structure for large deflections. Curve **B**, the linear curve used by the SDRC [24] to include the axial effects, attempts to approximate a nonlinear curve with a linear curve. The ineffectiveness of the approximation is particularly evident in Figure 3.8 where an axial compressive load of $p = 0.9$ is present. Curves for p ratios between $p = 0.0$ and $p = 0.9$ lie between those illustrated in Figures 3.7 and 3.8. In general it can be said that the approximation over-estimates the stiffness for small displacements while under-estimating the stiffness for larger displacements.

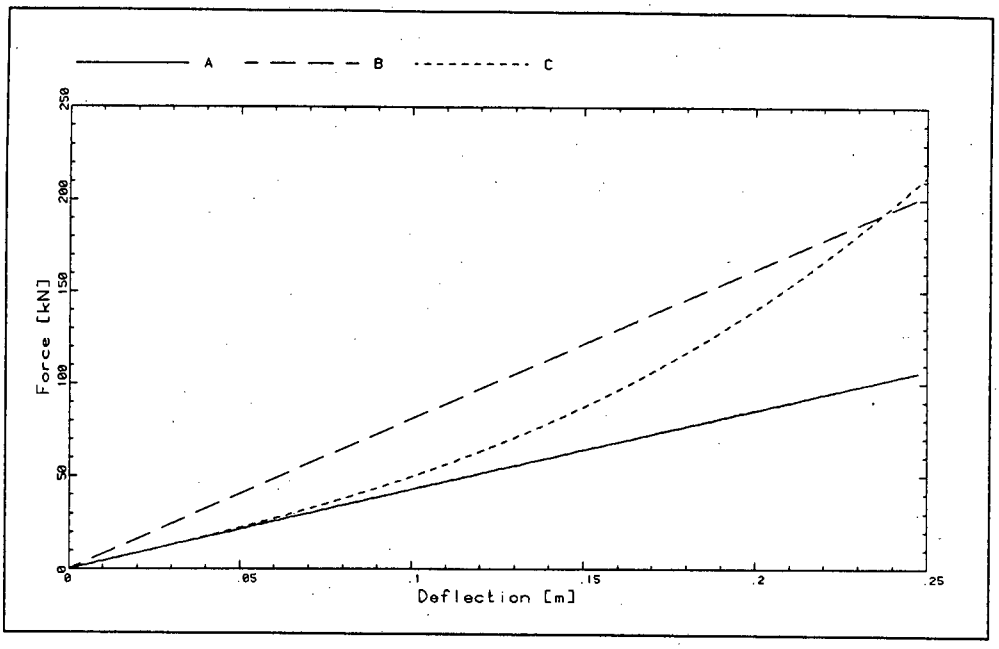

Figure 3.7: Comparison of Force-Displacement Curves (p = 0 0)

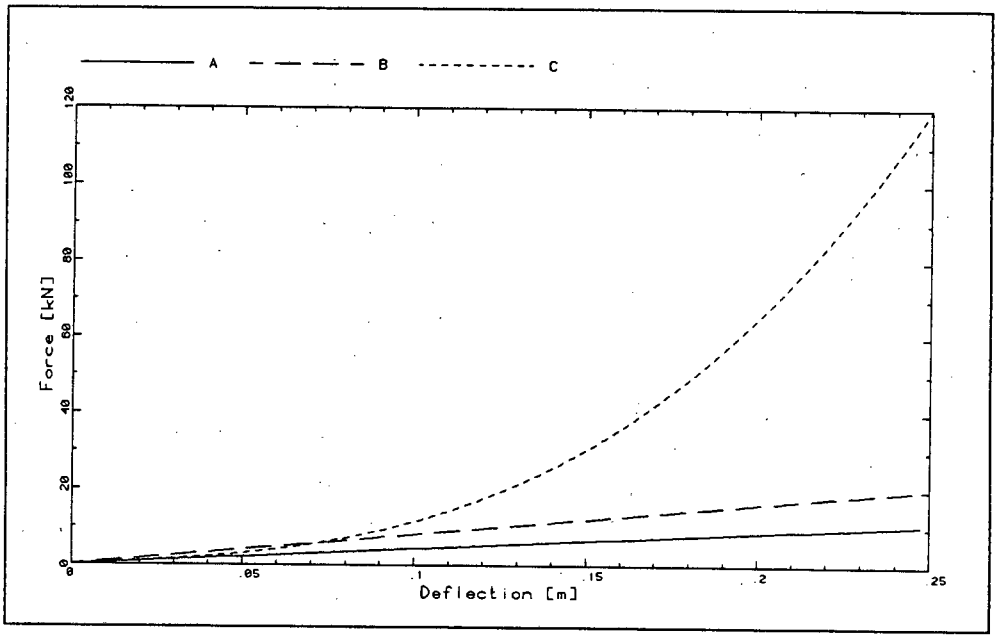

Figure 3.8: Comparison of Force-Deflection Curves (p = 0.9)

Figures 3.9 and 3.10 illustrate the response to a slamming event using the linear and nonlinear curves, discussed above. The skip force and displacement are plotted against the position of the skip on the guide. The input data for each case was the same, except for the method of including the end effects. For the nonlinear case the midpoint stiffness for the simply supported guide was calculated using:

$$k_g = \frac{48EI}{l^3}$$

while the end effects are modelled using the axial springs.

For the linear case the end effects are approximated using a factor, thus:

$$k_g = 1.9 \times \frac{48EI}{l^3}$$

Curve **B** in Figure 3.9 and 3.10 is the response of the skip during a slamming event using the factor to approximate the end effects of the guide. Curve **C** is the response of the skip using the nonlinear force deflection relationship, i.e. axial springs are included to model the end effects. Figure 3.9 shows that the skip or guide deflects less and leaves the guide earlier when the linear guide stiffness is used. Figure 3.10 illustrates that although the maximum force is of comparable magnitude, the maximum force occurs at different positions along the guide. This behaviour is a result of the fact that the linear guide stiffness used in the determination of curve **B** is higher, for the relatively low deflections in this example, than the nonlinear guide stiffness used for the determination of curve **C**. This is a consequence of trying to approximate a nonlinear curve with a linear one.

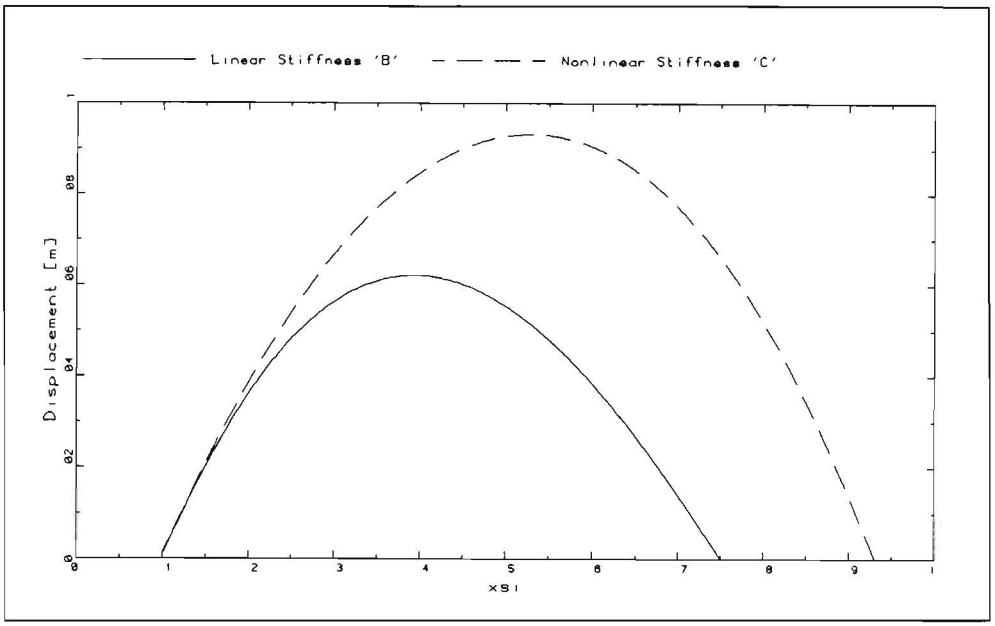

Figure 3.9: Comparison of Slamming Displacement for Linear and Nonlinear Guide Stiffness

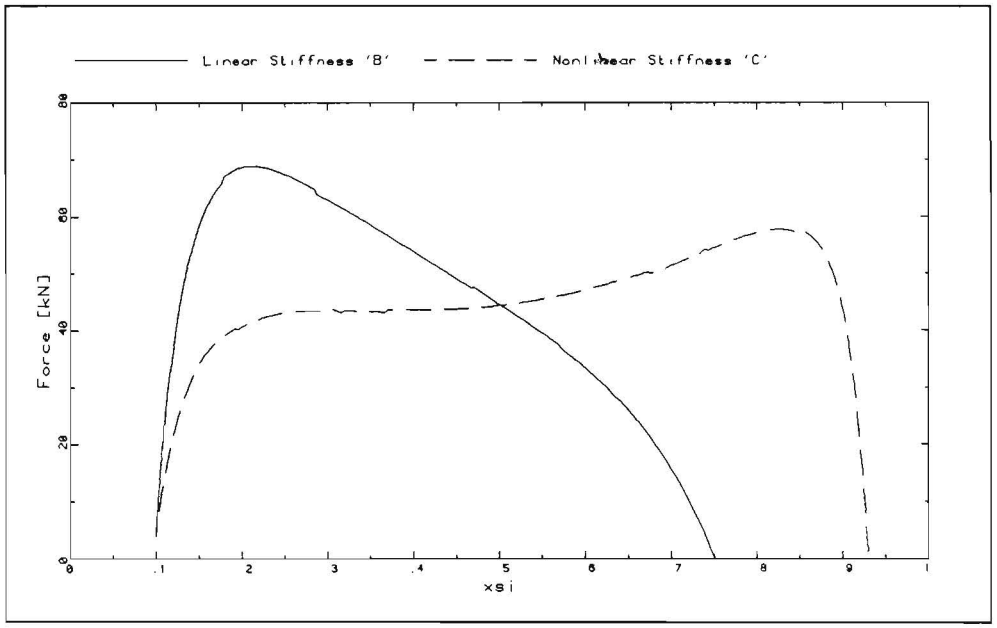

Figure 3.10: Comparison of Slammming Force for Linear and Nonlinear Guide Stiffness

3.3.4 EFFECT OF SECONDARY STIFFENING

The effect of the axial springs, k_a, on the system is now discussed. Two slamming events are considered. The first, illustrated in Figure 3.11 and 3.12 has no axial force in the guides while the second (Figure 3.13 and 3.14) has an axial load of half the critical force acting in the guides. The guide midspan stiffness was calculated using $k_g = \frac{48EI}{l^3}$ for *both* cases. (i.e. the 1.9 factor is *not* included)

Figures 3.11 to 3.14 illustrate that the inclusion of secondary stiffening has the effect of reducing the displacements and forces experienced by the skip. The skip also leaves the guide earlier when secondary stiffening is present. The slamming event is thus less severe when secondary stiffening is present. This is particularly true when there are compressive forces acting on the guides. Figure 3.14 illustrates the skip force during a slamming event when there is a compressive force of half the critical force acting in the guide. The skip force is increased by about 220 % when secondary stiffening is not present.

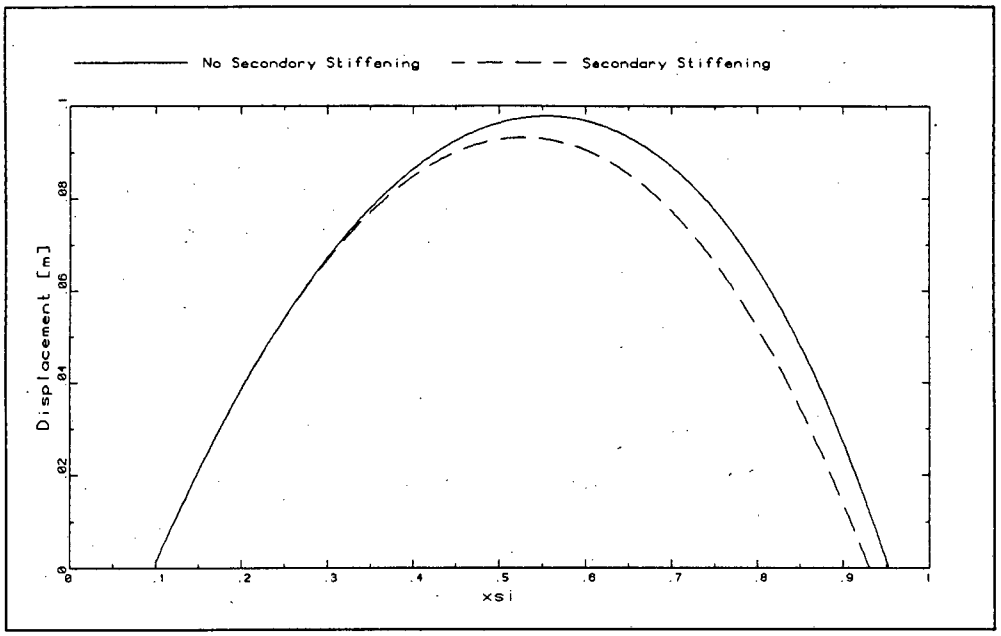

Figure 3.11: Effect of Secondary Stiffening on Skip Displacement (p = 0.0)

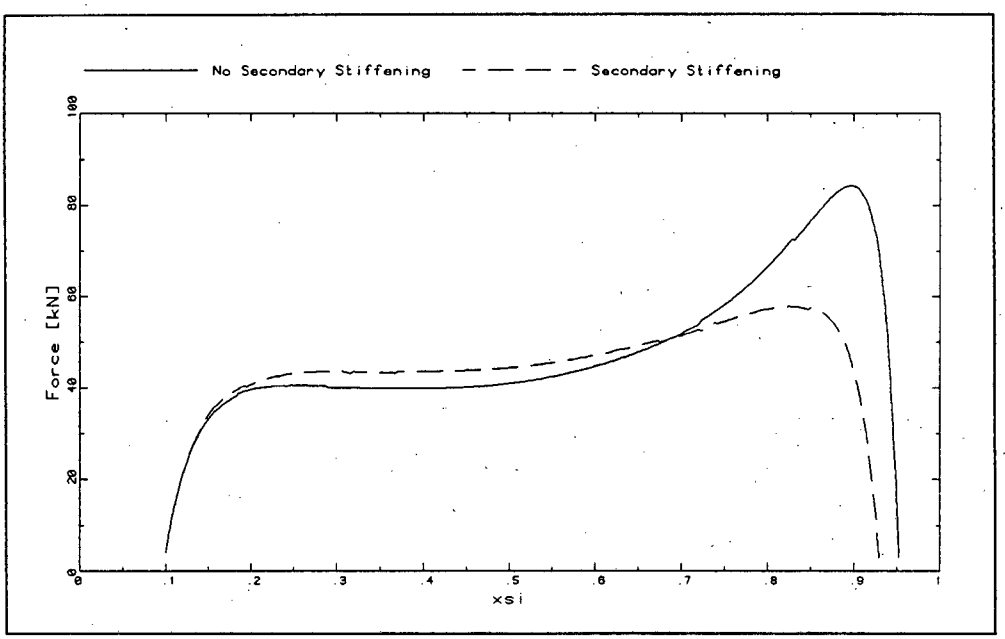

Figure 3.12: Effect of Secondary Stiffening on Skip Force (p = 0.0)

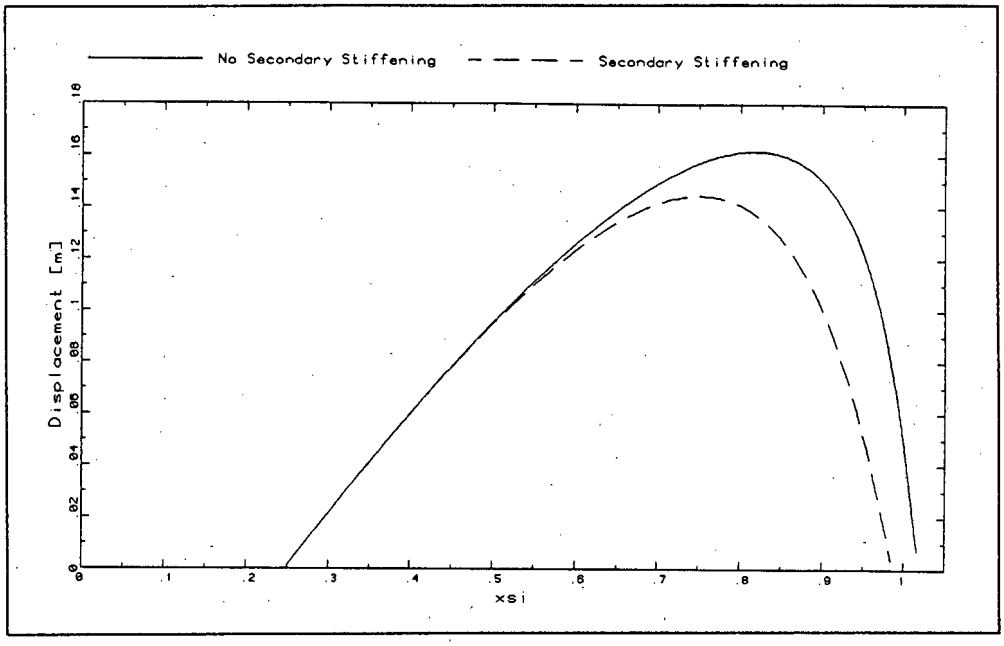

Figure 3.13: Effect of Secondary Stiffening on Skip Displacement (p = 0.5)

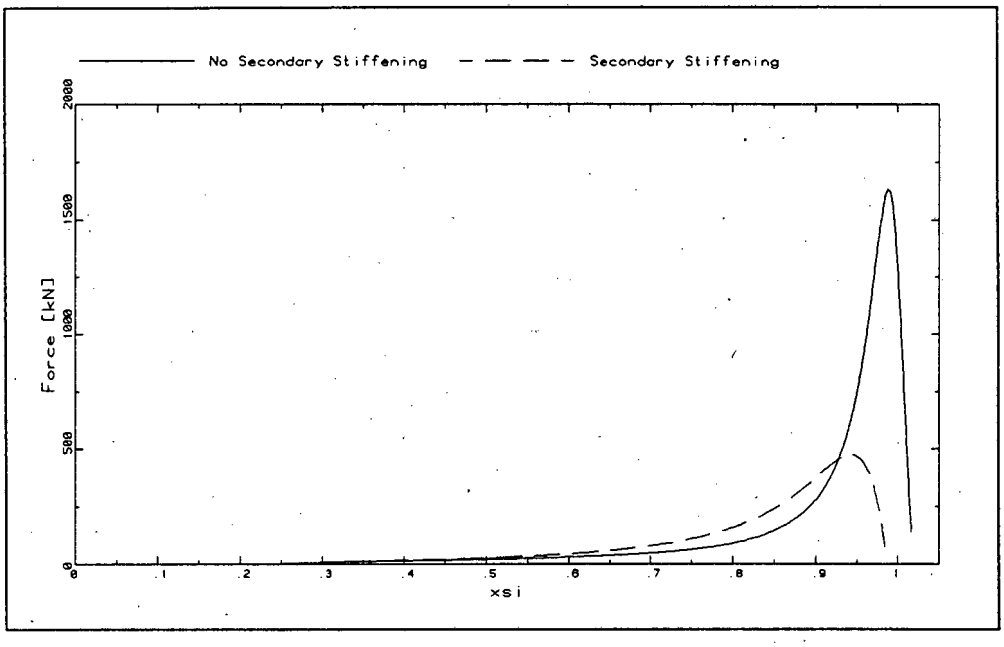

Figure 3.14: Effect of Secondary Stiffening on Skip Force (p = 0.5)

4 RESULTS OF NUMERICAL MODELLING

4.1 INTRODUCTION

In this section the detailed response of one particular system is reviewed so that a better understanding of the slamming phenomenon is obtained. The influence of the axial load P on the system with secondary stiffening is then presented. Finally the results of a parametric study of the major variables are presented and discussed. In order to make comparisons with the results obtained by Pretorius [18,19,21], a set of datum results was required. The configuration selected corresponds to the President Steyn Gold Mine #4 shaft and is detailed as follows:

$r = \frac{k_b}{k_g}$ was kept constant at a value of $r = \frac{26330}{427} = 61.663$

$\bar{k} = \frac{AE}{k_a l}$ was kept constant at $\bar{k} = \frac{7.213\times10^{-3}\times200\times10^{9}}{49145\times10^{3}\times6.1} = 4.812$

$p = \frac{P}{P_{cr}}$ was varied from p = 0.0 to p = 0.9

$V_s = \frac{v_s}{\omega l}$ was kept constant at a value of $V_s = \frac{15.24}{\sqrt{\frac{427}{6.95}} \times 6.1} = 0.3179$

$\xi_0 = \frac{x_0}{l}$ was varied from $\xi_0 = 0.0$ to $\xi_0 = 0.9$

4.2 System Behaviour with Secondary Stiffening - Example

Figures 4.1 to 4.4 show the skip displacement and skip force during a slamming event. In Figures 4.1 and 4.2 the system has no axial compressive force in the guides while in Figures 4.3 and 4.4 an axial force of 0.9 times the critical load is acting on the guides. There are five lines on each plot corresponding to five different impact locations. In each case a lateral impact velocity of 1 m/s is used.

When the skip impacts the guide anywhere other than at the bunton ($\xi_0 = 0.0$), the skip leaves the guide at a point close to the bunton. As the skip is hoisted at a constant velocity, the position of the skip along the guide, ξ, is equivalent to a time variable. Thus the slopes of the displacement curves represent the velocity of the skip. The rebound velocity of the skip can be seen to be higher than the velocity at impact. This is particularly evident when an axial compressive force acts in the guides (Figure 4.3). The skip forces during the slamming event are illustrated in Figures 4.2 and 4.4.

The increase in lateral velocity after impact distinguishes the slamming phenomenon from other impacts the skip may experience. Greenway [9] discusses the source of the lateral velocity gained as a result of the impact. A small component of the reaction between the skip and the guide acts in the direction of the vertical motion of the skip - due to the shape adopted by the guide during impact. When the work done against this force is computed, it is found that it equals the gain in lateral kinetic energy. Thus the winder does work in order to keep the skip moving at constant speed. Slamming thus provides a mechanism whereby energy can be transferred from the winder to the lateral motion of the skip. The larger the guide deflection the more work done by the winder and the larger the rebound velocity.

When the skip impacts at a bunton (ξ_0 = 0.0) the behaviour differs from the previous cases. When there is no axial compressive force in the guide (Figure 4.1) the stiff bunton initially limits the lateral motion of the skip. As the skip moves along the guide it is subjected to the reduced displacement with the result that the associated forces are much lower. The maximum force occurs near the point of impact and slamming does not occur.

For the case where an axial force acts in the guides (Figure 4.3 and 4.4) the lateral stiffness of the guide is reduced, so that a combination of events occurs when the skip impacts at a bunton (ξ_0= 0.0). Initially the stiff bunton limits the lateral motion of the skip but when the skip moves onto the guide, the reduced stiffness allows large guide deflections to result and slamming occurs. The force shows a peak near the point of impact and then rises sharply as the skip is 'catapulted' off the guide near the following bunton.

In this thesis the lateral impact velocity, $\dot{u}_0$, of the skip was kept constant at a value of 1 m/s for all cases. Results (not shown here) for higher lateral impact velocities indicated an increase in the response of the skip. The increase is not a linear one, due to the nonlinear nature of the problem. A value of 1 m/s was also used by the SDRC [24] and is considered realistic.

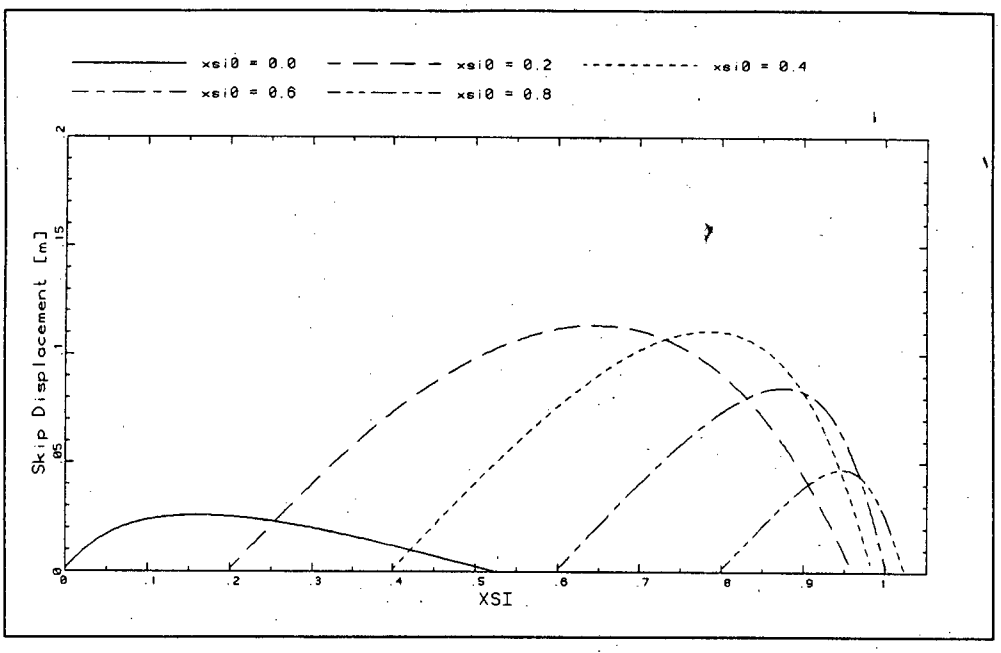

Figure 4.1: Skip Displacement During Slamming for Various Impact Positions (p = 0.0)

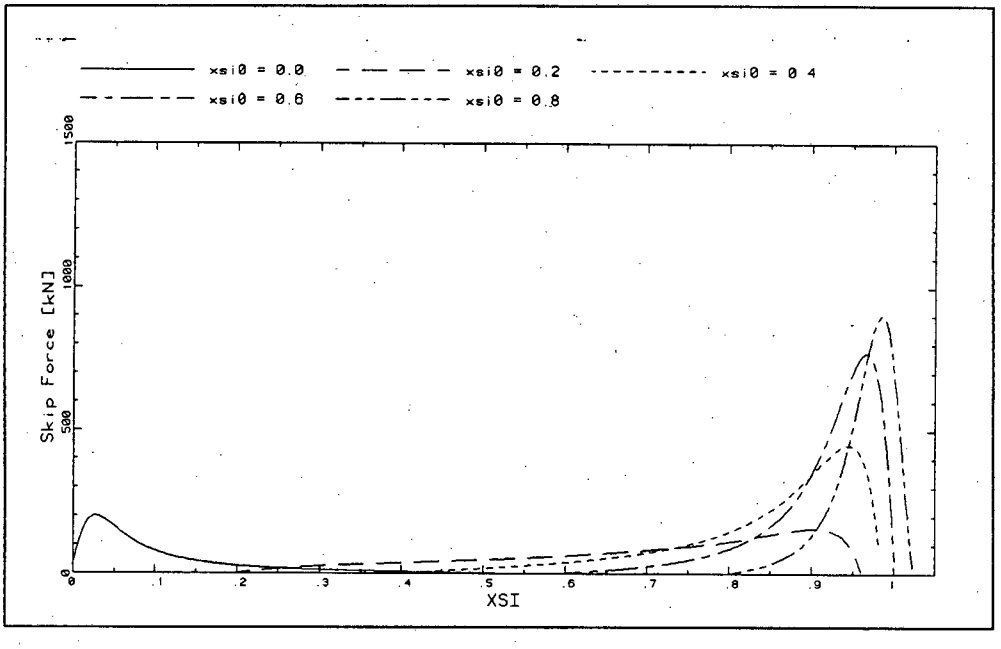

Figure 4.2: Skip Force During Slamming for Various Impact Positions (p = 0.0)

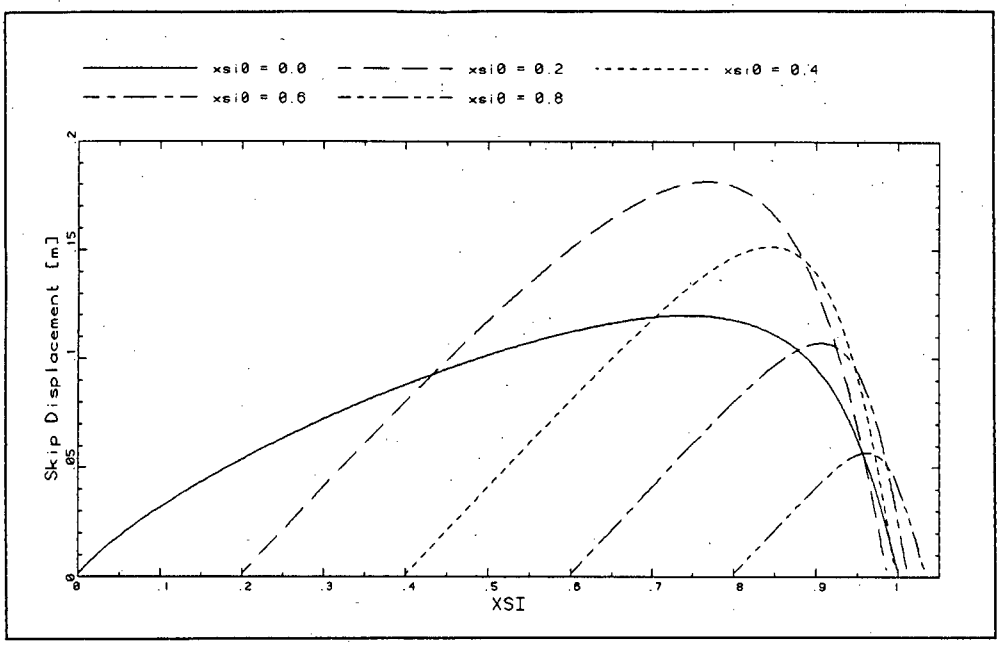

Figure 4.3: Skip Displacement During Slamming for Various Impact Positions (p = 0.9)

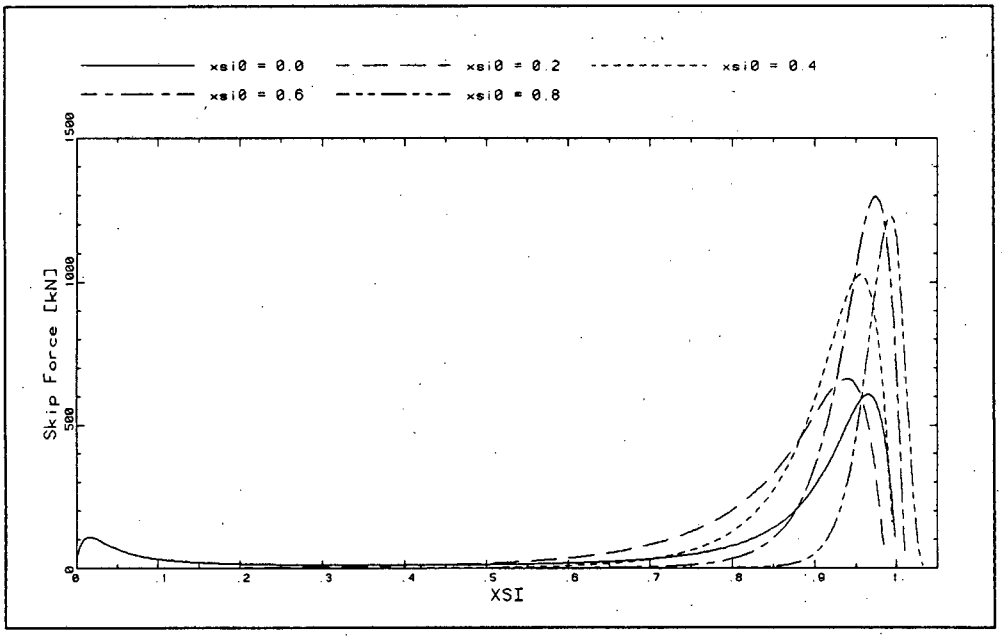

Figure 4.4: Skip Force During Slamming for Various Impact Positions (p = 0.9)

4.3 Influence Of The Axial Compressive Load

The influence of the axial load P on the system is now shown. The data listed in section 4.1 is used as the input to program **UCTSTIFF**. The results are presented graphically, showing the relevant component versus the initial impact position between the skip and the guide. The results show the locus of the maxima for the whole time that the skip was in contact with the guide for a specific impact position. The plots are presented for various values of $p = P/P_{cr}$, the ratio of the axial load to the critical load of the guide. These plots are the same as those presented by Pretorius [18,19,21], except that now the nonlinear effect of secondary stiffening is included, instead of the multiplying factor used by Pretorius [18,19,21].

The general trends of the results are discussed and amplification factors are given to show the effect of the axial compressive load P. The amplification factors are relative to the values for p = 0.0. The amplification factors obtained by Pretorius [18,19,21] are also presented for comparison purposes. Because Pretorius' amplification factors are also relative to his values for p = 0.0, the amplification factors cannot be compared directly. Care should be taken in interpreting these comparisons but the results are included to show *relative* reductions. Further plots allowing direct comparison, for the skip force and rebound velocity for various p ratios, are presented in order to make specific conclusions regarding the effects of secondary stiffening.

The following results were calculated by the program **UCTSTIFF**:

(a) The *maximum displacement* of the skip corner,
(b) the position where the skip leaves the guide, called the *rebound position*,
(c) the time when the skip leaves the guide called the *contact time*,

(d) the maximum velocity at which the skip leaves the guide, called the *rebound velocity*,

(e) the maximum force at the corner of the skip, called the *skip force*,

(f) the maximum force that the buntons experience due to the impact of the skip with the guide, called the *bunton force*.

(g) the *maximum bending moment* that the guide experiences due to the impact of the skip with the guide.

4.3.1 PRESENTATION AND DISCUSSION OF RESULTS

Maximum Deflection of the Guide

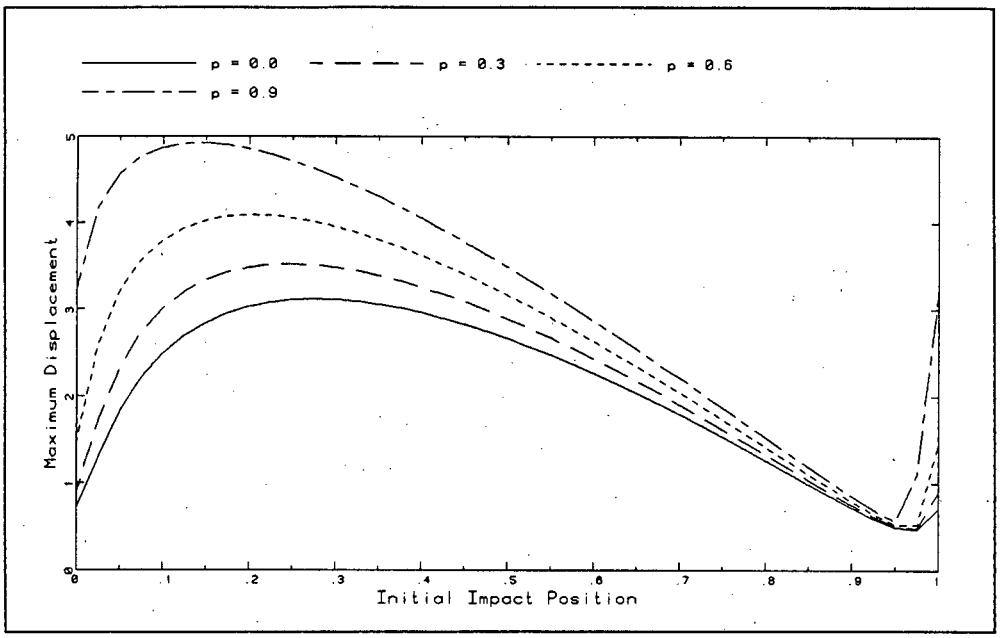

Figure 4.5: Maximum Deflection of the Guide

When the skip impacts the guide near the first bunton (i.e. when $0.1 < \xi_0 > 0.4$), large displacements of the skip corner result, as illustrated in Figure 4.5. As the skip impact position nears the bunton so the maximum displacement decreases until near $\xi_0 = 0.95$ a minimum is reached. For values of ξ_0 between 0.95 and 1.0 the displacements increase dramatically. This occurs because the skip does not rebound at the bunton and is pulled through to the more flexible region of the following guide span. The effects of the axial loads are illustrated by means of amplification factors relative to the results for p = 0.0. These factors are presented in Table 4.1. Table 4.1 also includes the amplification factors presented by Pretorius [18,19,21]. A comparison of the factors shows the relative decrease in response due to the effect of the secondary stiffening in the guides.

p	Amplification Factor	
	UCTSTIFF	Pretorius
0.3	1.1	1.2
0.6	1.3	1.5
0.9	1.6	2.5

Table 4.1: Amplification Factors for Guide Deflection

Rebound Position

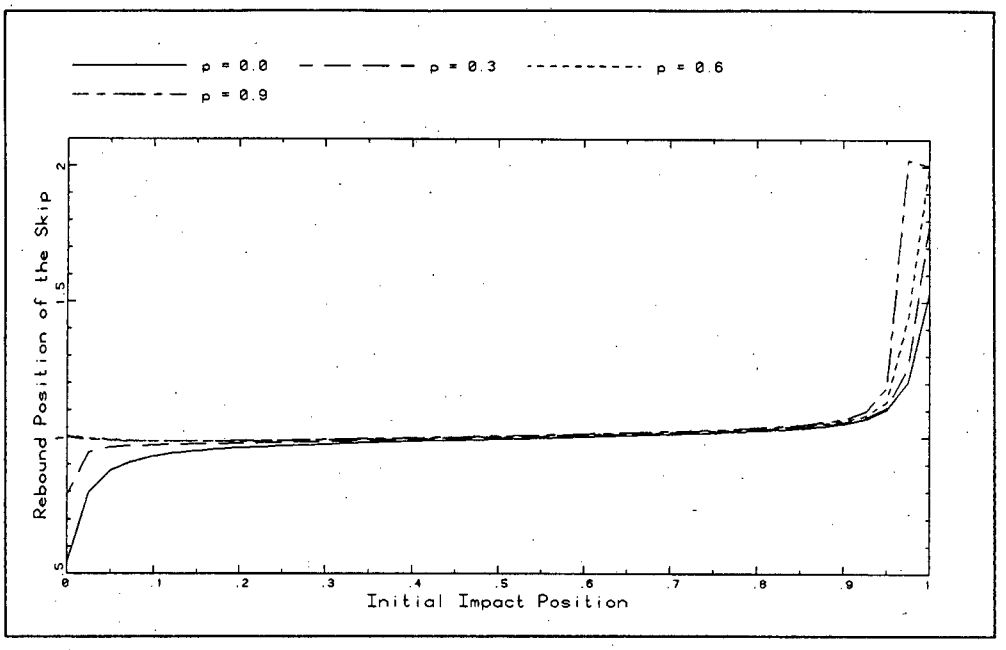

Figure 4.6: Position at which the Skip leaves the Guide

Figure 4.6 illustrates the position at which the skip rebounds from the guide. A rebound position of 1.0 thus indicates that the skip rebounded from the guide at the first bunton the skip reached after impact. Figure 4.6 shows that, in general, the skip rebounds from the guide at the first bunton it reaches after impact. An exception occurs when the skip initially impacts the guide between $\xi_0 = 0.0$ and $\xi_0 = 0.15$. Here the skip rebounds before the bunton is reached. Also, a trend towards a rebound position at the first bunton is evident as p increases. When the skip initially impacts at the end of the guide i.e. $\xi_0 \approx 0.95$, the rebound position tends to occur near the following bunton, i.e. when the rebound position approaches a value of two.

Contact Time

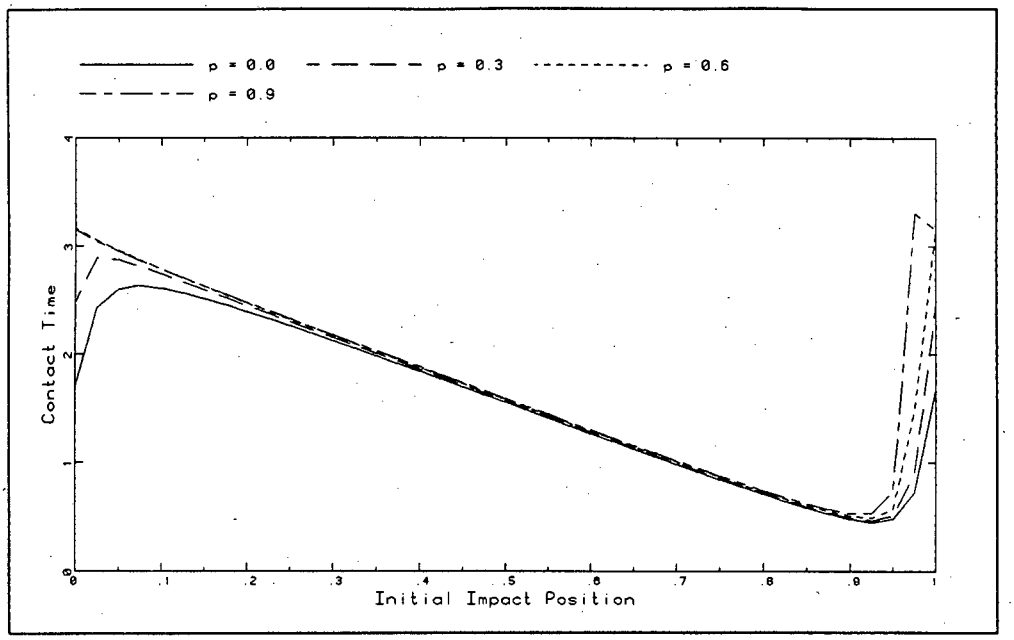

Figure 4.7: Time of Contact between the Skip and the Guide

Figure 4.7 is a plot of the dimensionless contact time, τ, versus the initial impact position ξ_0. Figure 4.7 illustrates that the contact time decreases almost linearly from $\tau \approx 3.2$ at $\xi_0 = 0.0$ to $\tau \approx 0.5$ at $\xi_0 = 0.9$. For impact positions between $\xi_0 = 0.0$ and $\xi_0 = 0.2$ and low p values the relationship is not linear, but as the p ratio increases so the trend becomes more linear. The contact time is directy related to the contact length through the hoisting speed and therefore to the rebound position of the skip, discussed above.

Rebound Velocity

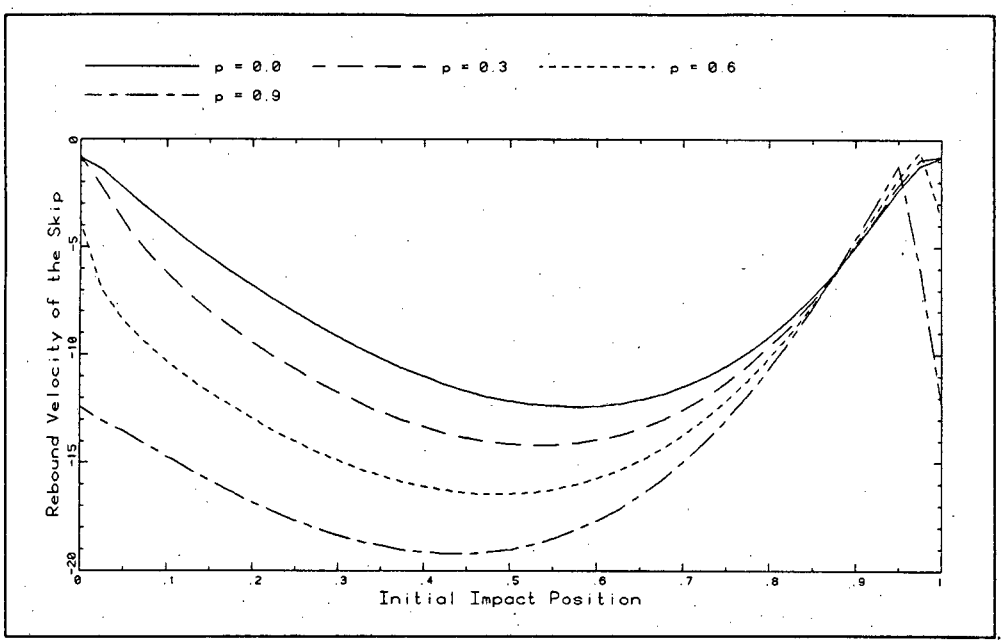

Figure 4.8: Velocity at which the Skip leaves the Guide

Figure 4.8 is a plot of the dimensionless rebound velocity of the skip versus the initial impact position ξ_0. The velocity varies from about 1.0 for impacts at the guides to about 12.5 for impacts near midspan for p = 0.0. The increase in the rebound velocity due to the axial force p is clearly evident and amplification factors, based on the results for p = 0.0 are presented in Table 4.2. The amplification factors calculated by Pretorius [18,19,21] are also presented for comparison purposes. The inclusion of secondary stiffening reduces the effect of increasing the p ratio as Table 4.2 indicates. Pretorius [18,19,21] reported an amplification factor of 3.8 for a p ratio of 0.9 while when secondary stiffening effects are included the amplification factor drops to 1.6.

p	Amplification Factor	
	UCTSTIFF	Pretorius
0.3	1.1	1.2
0.6	1.3	1.8
0.9	1.6	3.8

Table 4.2: Amplification Factors for Rebound Velocities

Maximum Skip Force

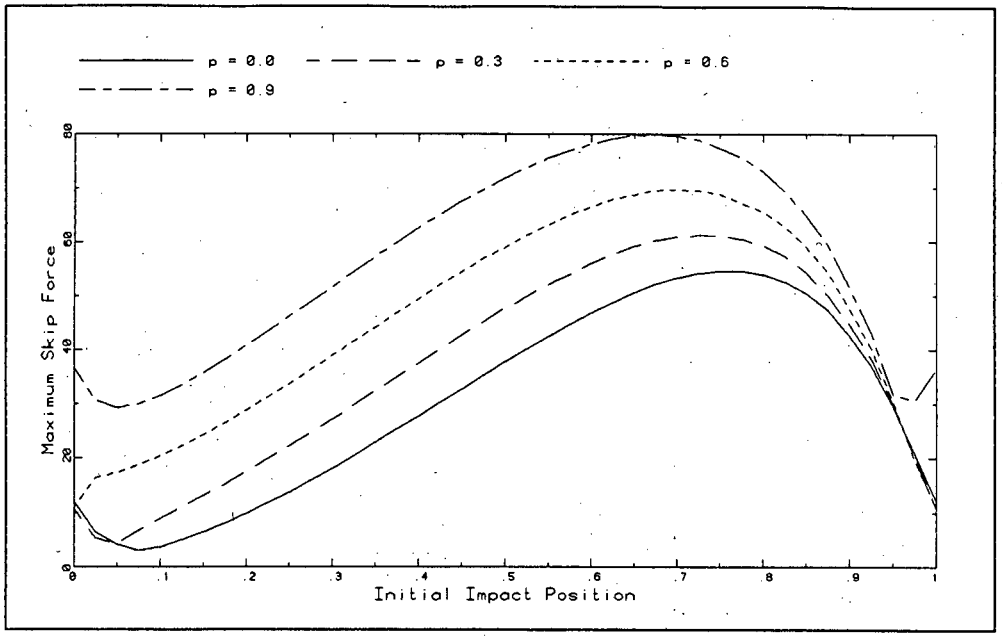

Figure 4.9: Maximum Force acting on the Skip

Figure 4.9 is a plot of the maximum dimensionless skip force versus the initial impact position ξ_0. Impact positions around ξ_0= 0.75 result in the highest skip forces for all p ratios. The increase in skip force for increasing p ratios is evident and amplification ratios are listed in Table 4.3. The decrease in response due to the inclusion of secondary stiffening is illustrated when comparing the amplification factors reported by Pretorius [18,19,21] to these results. The drop in amplification factors is particularly significant for the high p ratios.

p	Amplification Factor	
	UCTSTIFF	Pretorius
0.3	1.1	1.1
0.6	1.3	1.7
0.9	1.5	6.5

Table 4.3: Amplification Factors for Maximum Skip Forces

Maximum Bunton Force

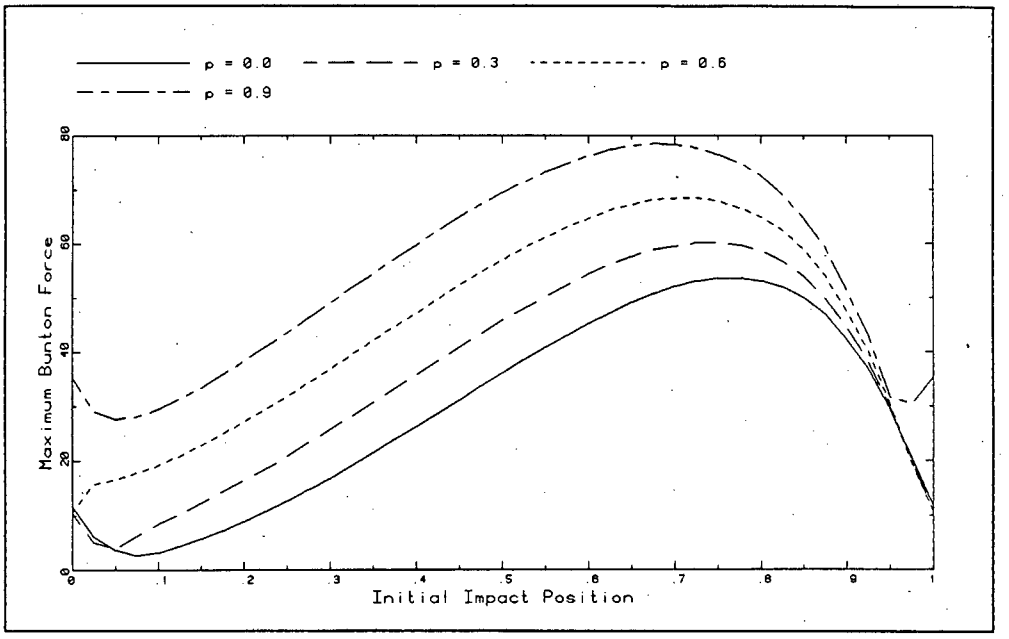

Figure 4.10: Maximum Force in the Buntons

Figure 4.10 illustrates the maximum dimensionless force in the buntons. The forces are similar to those of the maximum skip force, illustrated in Figure 4.9. This is to be expected because the bunton force depends on the skip force and the location of the skip. Since the maximum skip force generally occurs near a bunton, the results are similar. Amplification factors are presented in Table 4.4. The effect of secondary stiffening is again evident when comparing the results to Pretorius [18,19,21].

p	Amplification Factor	
	UCTSTIFF	Pretorius
0.3	1.1	1.1
0.6	1.3	1.7
0.9	1.5	6.5

Table 4.4: Amplification Factors for Maximum Bunton Forces

Maximum Guide Bending Moment

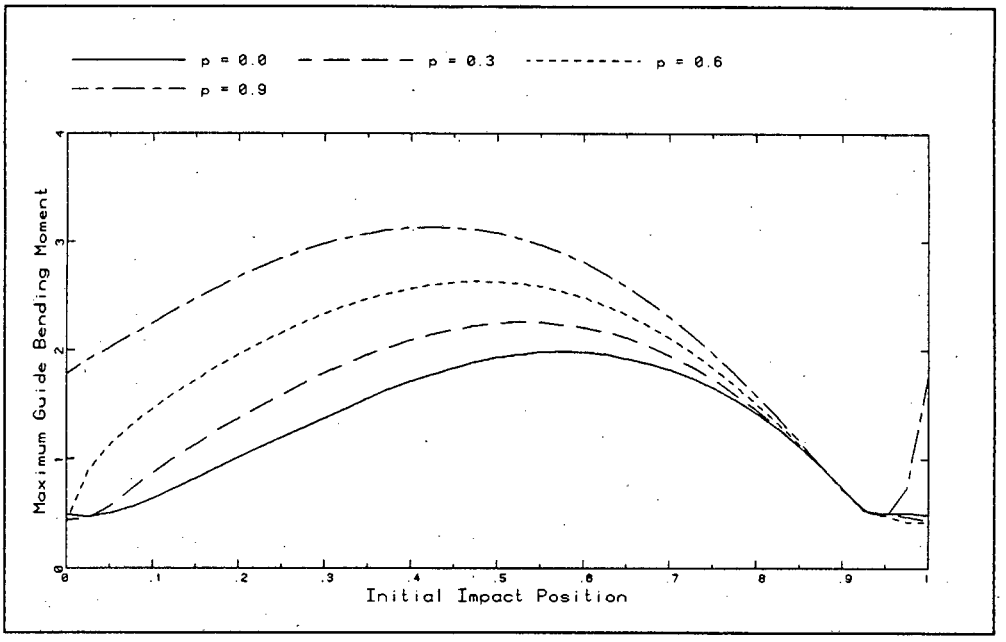

Figure 4.11: Maximum Bending Moment in the Guide

Figure 4.11 is a plot of the maximum dimensionless bending moment in the guide versus the initial impact position ξ_0. Impact positions around midspan result in the highest bending moments. Increasing the axial compressive force P in the guides causes an increase in the bending moment in the guide. Amplification factors of the bending moments are presented in Table 4.5. The inclusion of secondary stiffening results in a relative decrease in the maximum bending moment but to a lesser extent than for the skip force.

p	Amplification Factor	
	UCTSTIFF	Pretorius
0.3	1.2	1.1
0.6	1.4	1.4
0.9	1.7	2.5

Table 4.5: Amplification Factors for Maximum Guide Bending Moments

4.3.2 COMPARISON BETWEEN RESULTS PRESENTED BY PRETORIUS [18, 19,21] AND UCTSTIFF

This section presents direct comparisons between the results presented by Pretorius [18,19,21] and those generated by **UCTSTIFF**. The results are presented in the same manner as those of the previous section, i.e. the results show the maximum for the whole time the skip was in contact with the guide, for various impact positions. Plots of maximum skip force and rebound velocity are presented. Because Pretorius [18,19,21] used dimensionless numbers different to those used in this this study, the force and velocity are converted to dimensional numbers to allow comparison.

Figures 4.12 to 4.15 compare the *forces* predicted by Pretorius [18,19,21] to those predicted by **UCTSTIFF** for various p ratios. When p = 0.0 and 0.3, Figures 4.12 and 4.13 indicate that **UCTSTIFF** predicts a higher maximum skip force than Pretorius [18,19,21]. When p = 0.6, Figure 4.14, the maxima are of similar magnitudes (1150 kN). When p = 0.9 the results differ markedly, with **UCTSTIFF** predicting much lower maximum values than Pretorius [18,19,21]. Similar trends are evident in Figures 4.16 to 4.19 where the results for the *rebound velocity* of the skip are illustrated. For the low p ratios, Figures 4.16 and 4.17, **UCTSTIFF** predicts higher rebound velocities than Pretorius [18,19,21]. For p = 0.6, Figure 4.18, the results are of similar magnitudes while for p = 0.9, Figure 4.19, **UCTSTIFF** predicts much lower maximum rebound velocity (5.5 m/s as against 10.5 m/s) than Pretorius [18,19,21].

Section 3.3.3 showed that for *low* p ratios the linear curve predicted a 'stiffer' response than the nonlinear one. When the p ratio was *high* the nonlinear curve was 'stiffer' than the linear approximation. The results in this section can be explained in this context. For cases of low p ratio **UCTSTIFF** predicts a greater skip response than that of Pretorius [18,19,21] as the lower guide stiffness allows larger deflections to

result, with correspondingly higher slamming forces and rebound velocities. When the axial compressive force in the guide is high (p = 0.9), the nonlinear curve used by **UCTSTIFF** is significantly stiffer than the linear approximation used by Pretorius [18,19,21]. The lower deflections that result lead to lower slamming forces and rebound velocities. The case of p = 0.6, Figures 4.14 and 4.18, represents the case when the linear approximation provides a relatively good average approximation to the nonlinear guide stiffness.

The fact that the linear approximation curve used by Pretorius [18,19,21] is too stiff for p = 0.0 and not stiff enough for p = 0.9 explains in part the high amplification factors for the high p ratios reported by Pretorius [18,19,21].

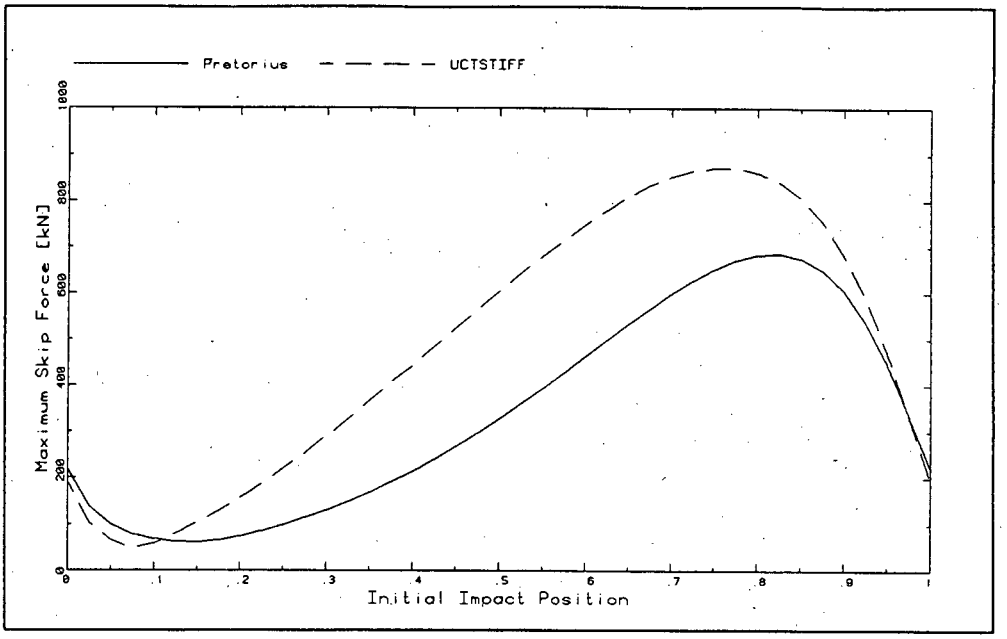

Figure 4.12: Comparison of Maximum Skip Force (p = 0.0)

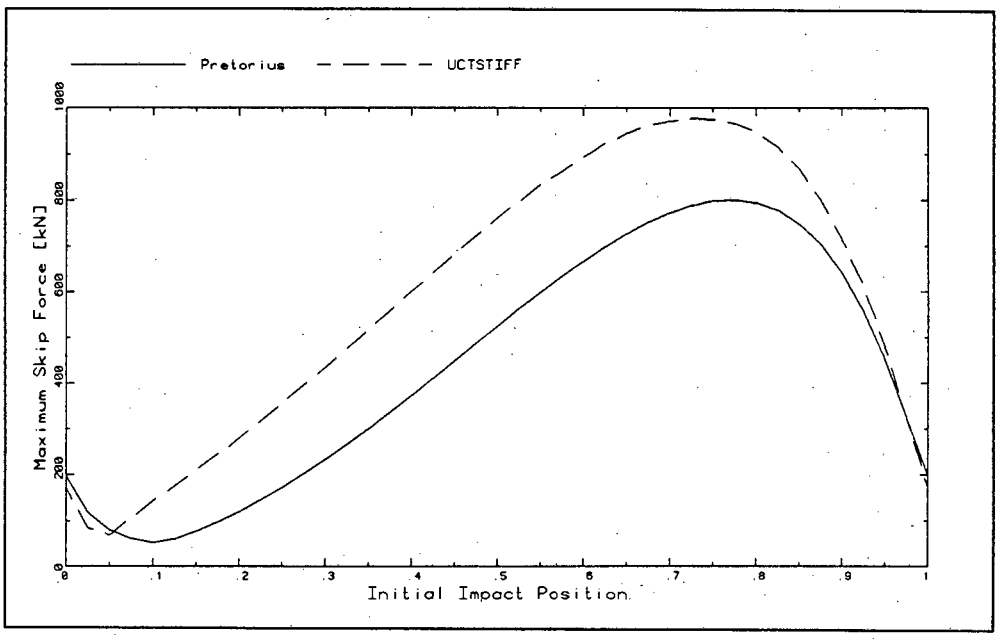

Figure 4.13: Comparison of Maximum Skip Force (p = 0.3)

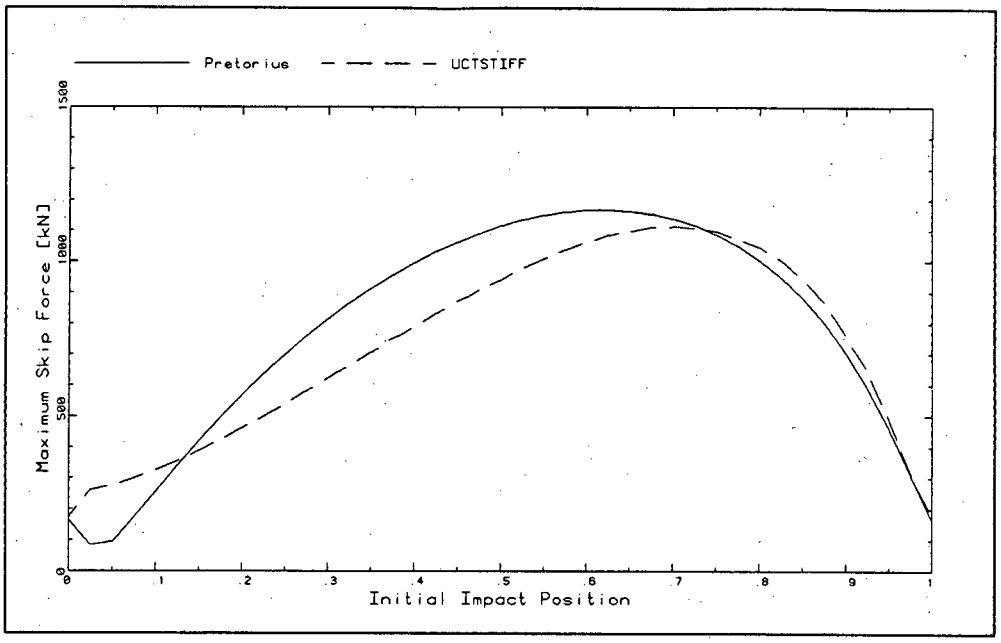

Figure 4.14: Comparison of Maximum Skip Force (p = 0.6)

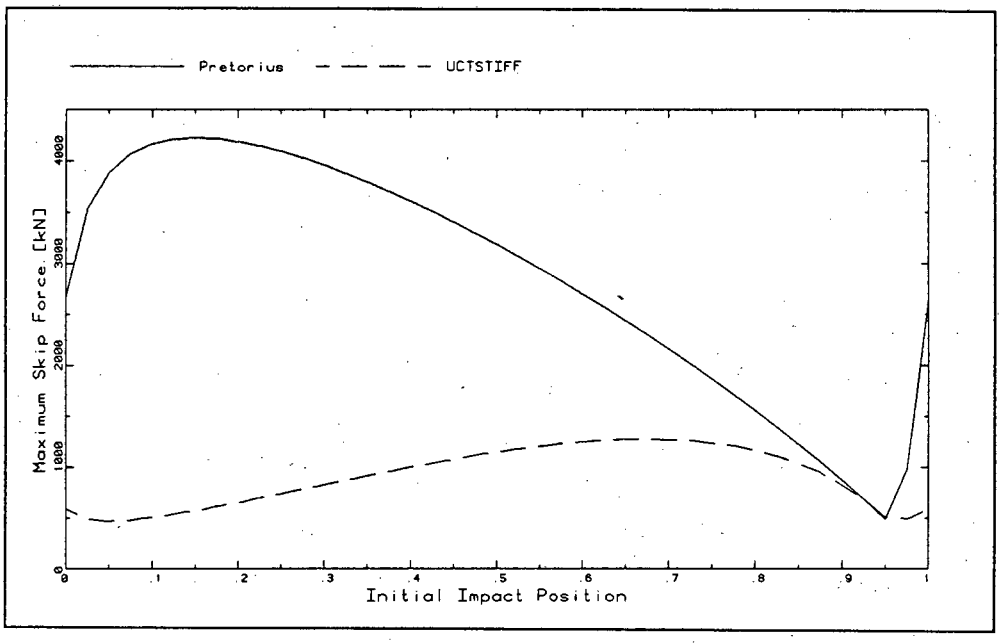

Figure 4.15 Comparison of Maximum Skip Force (p = 0.9)

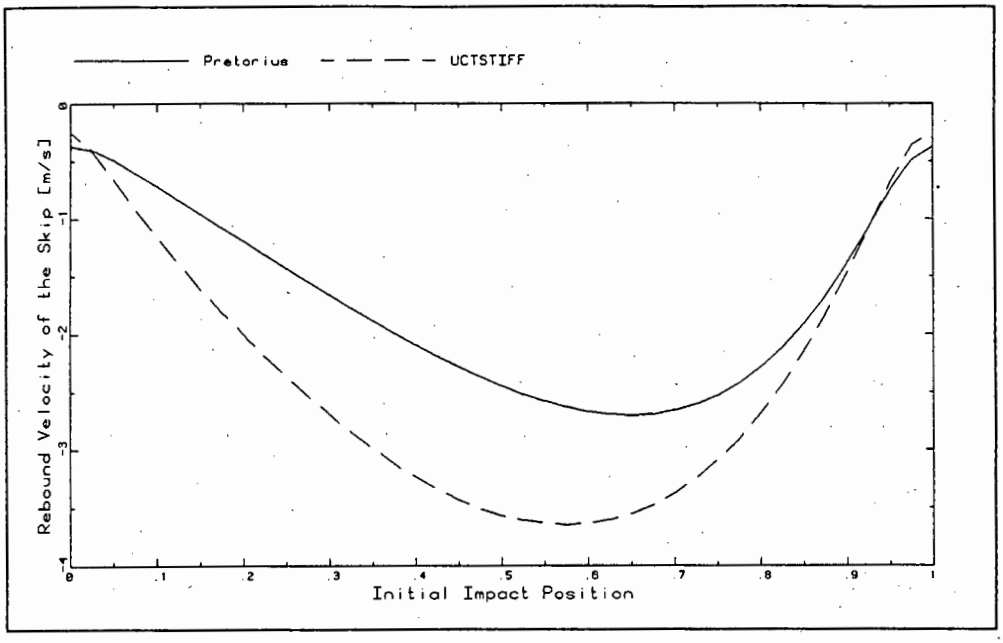

Figure 4.16: Comparison of Rebound Velocity (p = 0.0)

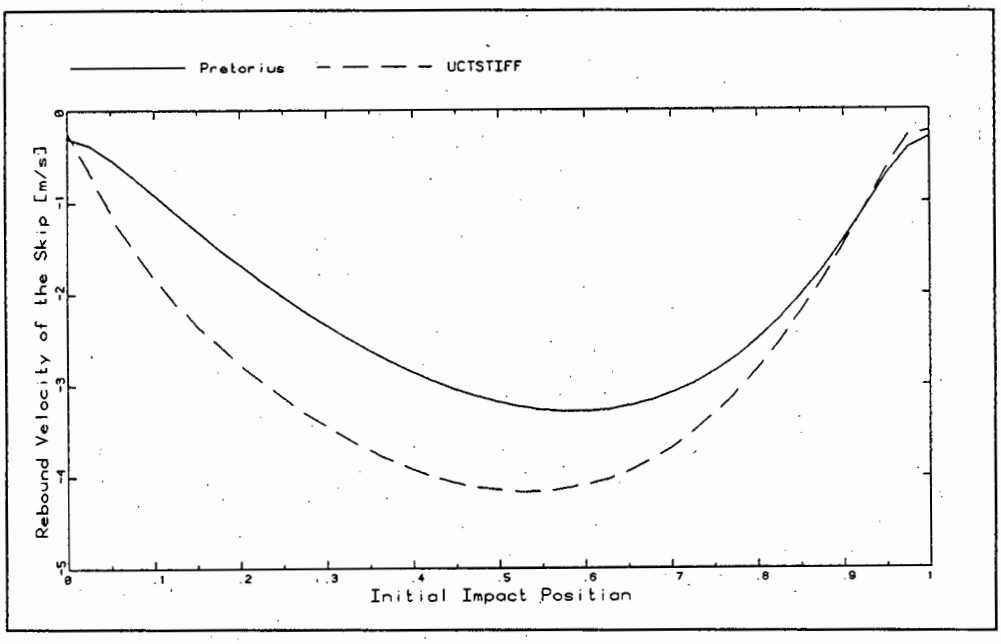

Figure 4.17: Comparison of Rebound Velocity (p = 0.3)

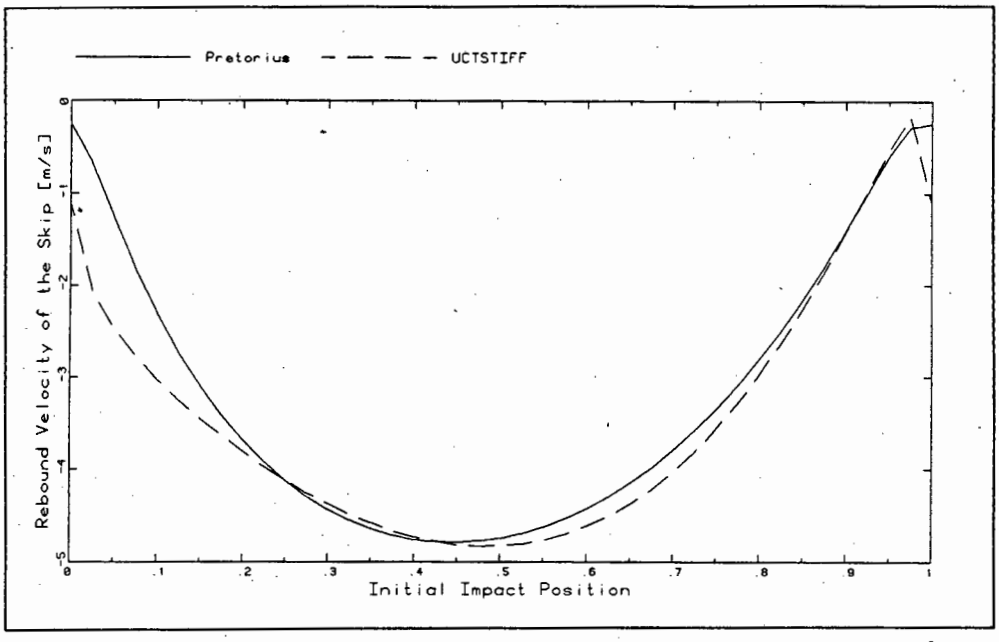

Figure 4.18: Comparison of Rebound Velocity (p = 0.6)

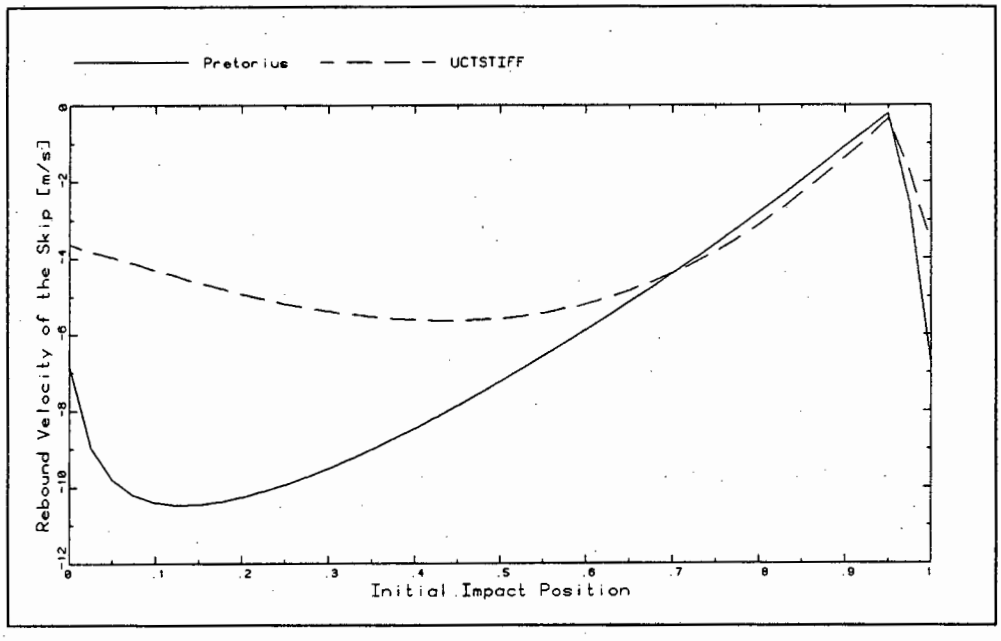

Figure 4.19: Comparison of Rebound Velocity (p = 0.9)

4.4 PARAMETRIC STUDY

In this section the effects of varying the input parameters on the response of the system are investigated. In each case only one parameter is varied with all the other values held constant. The base data used is that for the President Steyn Gold Mine and is listed below. In order to show the influence of the axial compressive force, the p ratio for each case, was varied from p = 0.0 to p = 0.9. The translational impact velocity of the skip was taken to be 1 m/s for all cases. As has been illustrated in section 4.3, the initial point of impact of the skip, ξ_0, has a large influence on the resultant behaviour of the skip. For this reason a search was conducted for each set of variables to find the worst impact location and then the corresponding results presented.

The base data for the President Steyn Gold Mine is:

$$r = \frac{k_b}{k_g} = \frac{26330}{427} = 61.663$$

$$\bar{k} = \frac{AE}{k_a l} = \frac{7.213\times10^{-3}\times200\times10^{9}}{49145\times10^{3}\times6.1} = 4.812$$

$$\bar{V}_s = \frac{v_s}{\omega l} = \frac{15.24}{\sqrt{\frac{427}{6.95}}\times 6.1} = 0.3179$$

The results are presented graphically showing the maximum bunton force and maximum rebound velocity versus the varying parameter. Each graph consists of four curves, corresponding to the various axial compressive ratios, p.

The following six parameters were varied in the study:

- Skip Mass
- Guide Stiffness
- Bunton Stiffness
- Bunton Spacing
- Skip Speed
- Axial Spring Stiffness

The general trends of the results are discussed and presented in Figures 4.20 to 4.31 below.

4.4.1 PRESENTATION AND DISCUSSION OF RESULTS

Skip Mass

Figures 4.20 and 4.21 illustrate the effect of varying the skip mass on the maximum rebound velocity and maximum bunton force respectively. The skip mass is varied from 10 to 60 tons.

The rebound velocity increases from a value of 2.4 m/s for a skip mass of 10 tons to 4.6 m/s for a skip mass of 60 tons for p = 0.0. For a p ratio of 0.9 the rebound velocity varies from 4.2 m/s for a 10 ton skip to 6.4 m/s for a 60 ton skip. These results are expected because of the decreasing effectiveness of the guide to retard the transverse motion of the skip. The axial compressive load P has the effect of reducing the transverse stiffness of the guide, thus resulting in higher rebound velocities. As the skip mass is increased so the buntons become relatively less stiff and are 'pushed' out of the way by the passing skip, thus reducing the slamming effect. This effect is visible for the higher skip masses where the rate of increase in rebound velocity is decreasing.

The maximum bunton force illustrated in Figure 4.21 increases linearly over the range of skip masses and p ratios. Again this trend is expected for the same reasons outlined above.

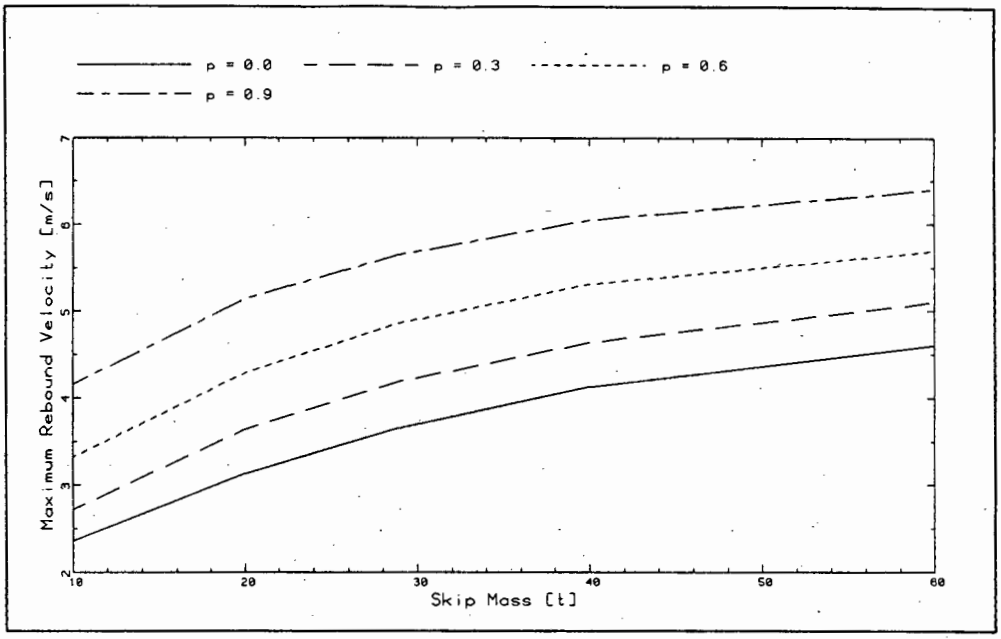

Figure 4.20: Maximum Rebound Velocity as a Function of Skip Mass

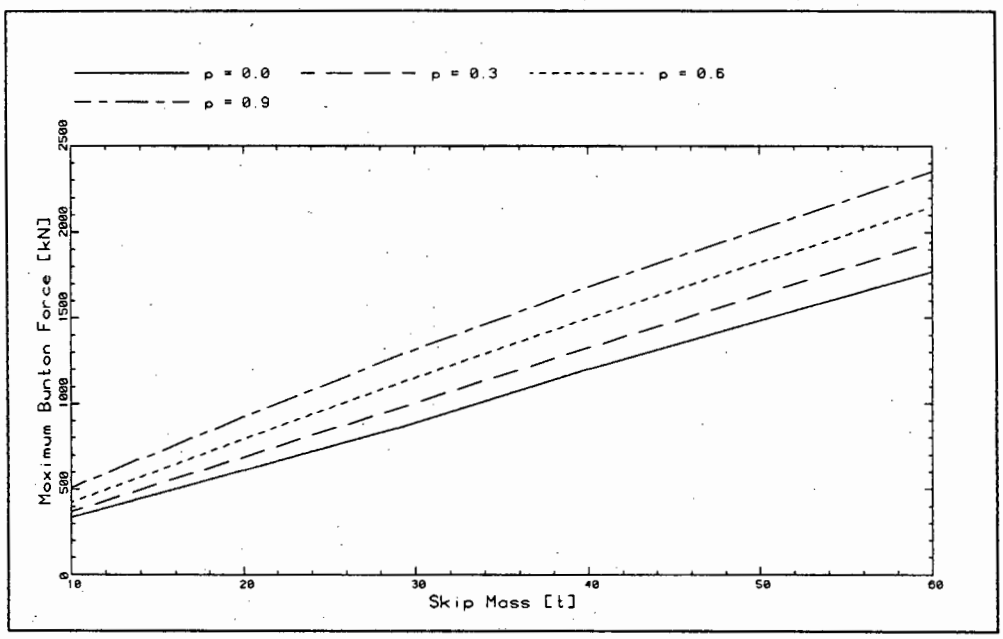

Figure 4.21: Maximum Bunton Force as a Function of Skip Mass

Guide Stiffness

Figures 4.22 and 4.23 illustrate the effect of varying the guide stiffness on the rebound velocity and bunton force respectively. Both the maximum rebound velocity and the maximum bunton force show decreasing trends for increasing guide stiffness. As the guide stiffness is increased so the lateral skip deflection that the skip experiences decreases. The reduced deflection, in turn, results in a lower acceleration of the skip and thus the rebound velocity and bunton force are reduced.

When axial compressive forces are present in the guides, the maximum rebound velocity and bunton force increase. This is because the lateral stiffness of the guide is reduced, with a corresponding increase in guide deflection, acceleration, force and the severity of slamming.

Figures 4.22 and 4.23 also indicate that as the guide stiffness increases so the difference between the curves for p = 0.0 and p = 0.9, for example, increases. This effect can be linked to the inclusion of secondary stiffening. For the very low guide stiffnesses and high p ratios the guide deflection will be larger than for a high guide stiffness and p ratio. The secondary stiffening effect is greater for large deflections and thus the increased stiffness reduces the response.

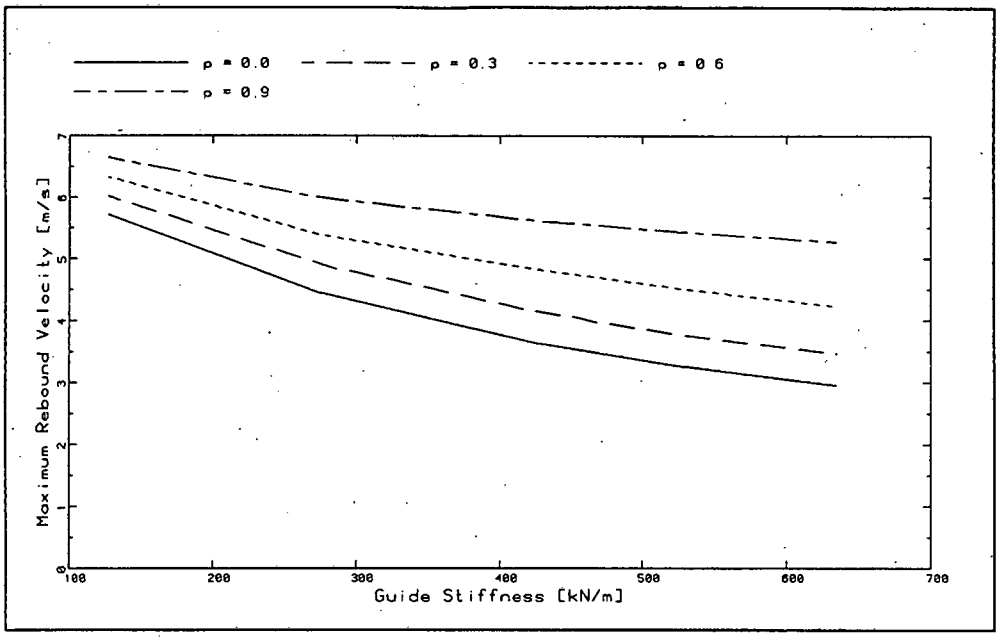

Figure 4.22: Maximum Rebound Velocity as a Function of Guide Stiffness

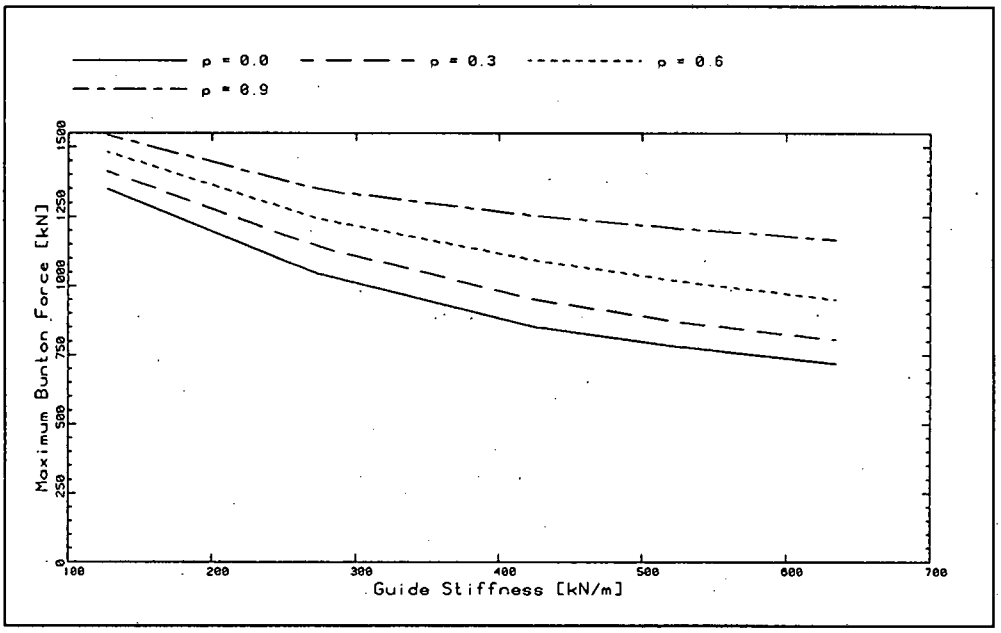

Figure 4.23: Maximum Bunton Force as a Function of Guide Stiffness

Bunton Stiffness

Figure 4.24 and 4.25 illustrate the effect of varying the bunton stiffness on the maximum rebound velocity and bunton force respectively. Both the maximum rebound velocity and maximum bunton force show increasing trends for increasing bunton stiffness. When the buntons are relatively flexible they are able to be pushed aside by the passing skip. The slamming effect, where the guide stiffness suddenly increases (due to the presence of the stiff bunton), is thus avoided. The reduction in the slamming effect accounts for the reduction in bunton forces and the rebound velocity for low bunton stiffnesses.

The presence of the axial compressive forces in the guide leads to increased rebound velocities and bunton forces. This is because the guide lateral stiffness is reduced when axial forces are present. This results in larger guide deflections which aggravate the slamming effect.

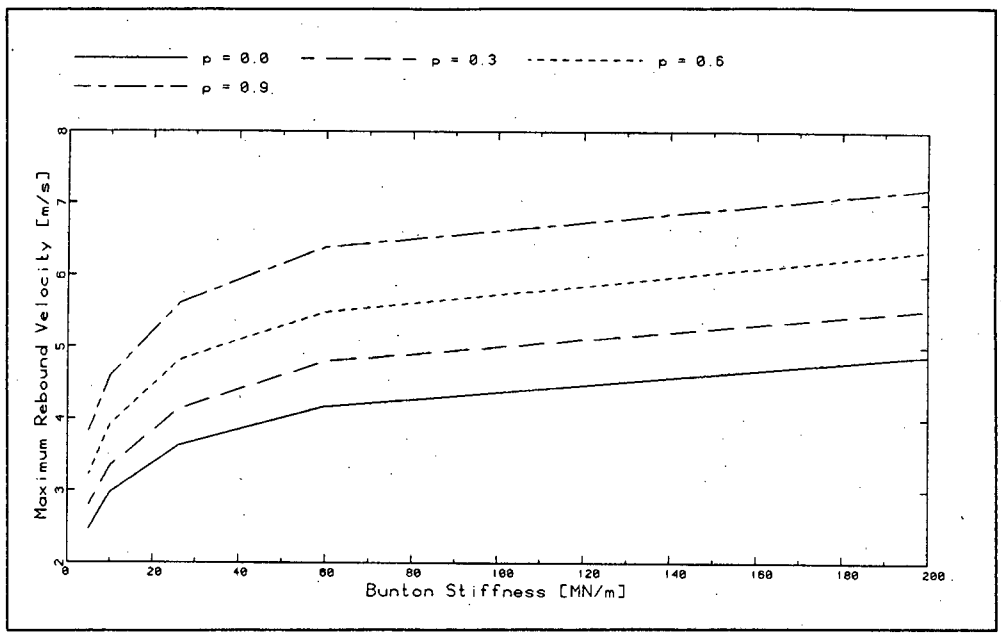

Figure 4.24: Maximum Rebound Velocity as a Function of Bunton Stiffness

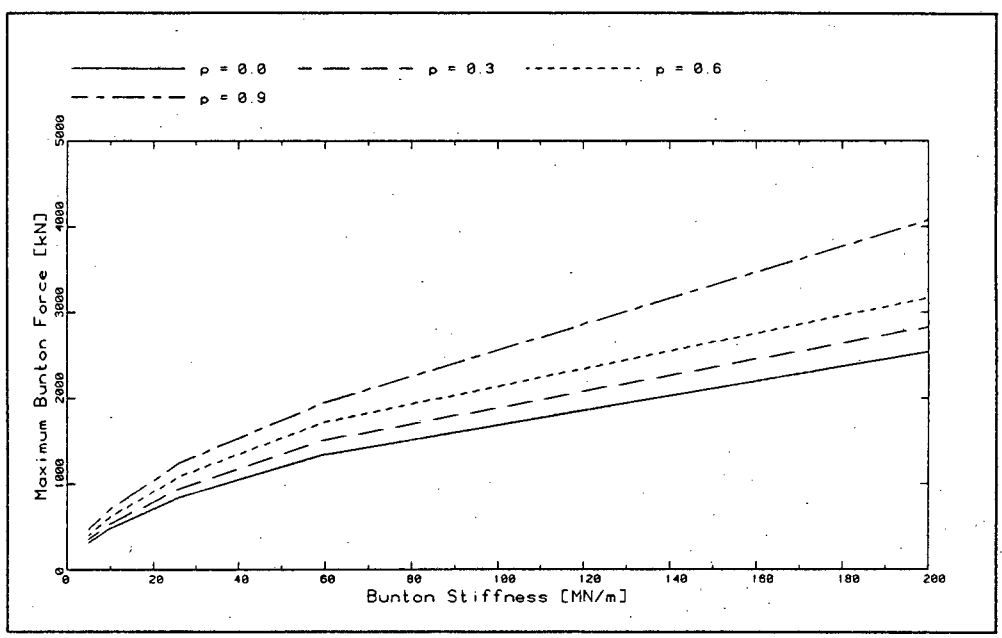

Figure 4.25: Maximum Bunton Force as a Function of Bunton Stiffness

Bunton Spacing

Figure 4.26 and 4.27 illustrate the effect of increasing the bunton spacing on the maximum rebound velocity and maximum bunton force respectively. Both the rebound velocity and bunton force increase for increasing bunton spacing. This trend is due to the fact that as the bunton spacing is increased so the guide stiffness decreases. The results accord with those obtained earlier for a change in guide stiffness. As the guide stiffness decreases so the guide deflections increase. This aggravates the slamming effect and leads to higher rebound velocities and bunton forces.

The presence of compressive forces in the guides also leads to a reduction in the lateral stiffness of the guide. This also aggravates the slamming effect for the same reasons described above.

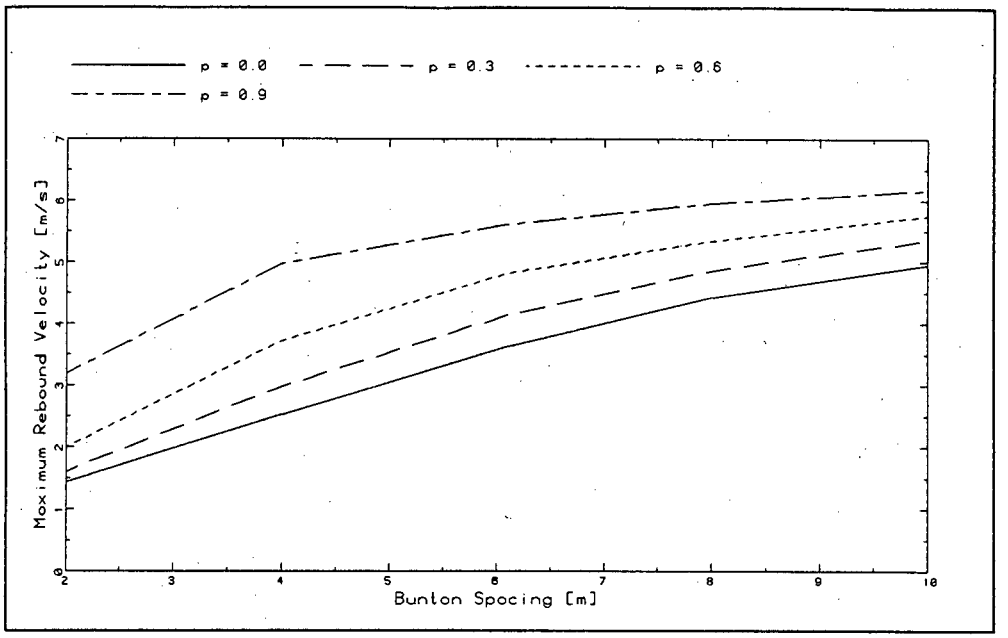

Figure 4.26: Maximum Rebound Velocity as a Function of Bunton Spacing

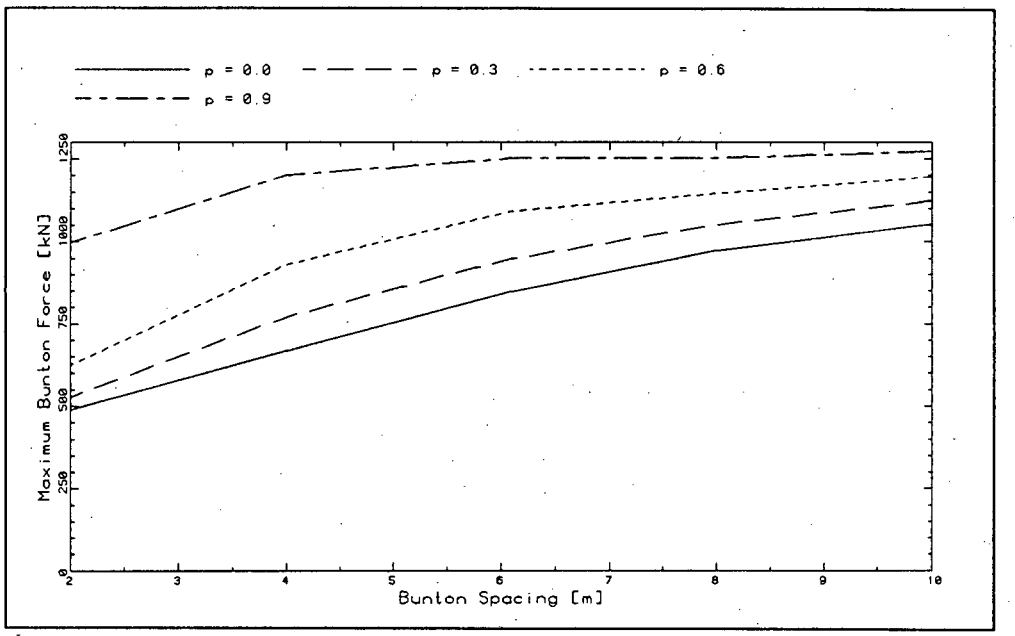

Figure 4.27: Maximum Bunton Force as a Function of Bunton Stiffness

Skip Speed

Figure 4.28 and 4.29 illustrate the effect of the skip speed on the rebound velocity and bunton force respectively. Both the rebound velocity and the bunton force show increasing trends as the skip speed is increased. The rebound velocity curves exhibit a leveling off and reduction at skip speeds greater than about 25 m/s. This is a result of the skip starting to push the buntons aside at the high speeds. At present such skip speeds are not practically feasible, but the fact that the rebound velocity has a limiting value might be important in future studies into sustained slamming.

The effect of axial compressive forces in the guides is also illustrated in Figures 4.28 and 4.29. As in previous cases the compressive forces cause a decrease in the guide stiffness which aggravate the slamming phenomenon.

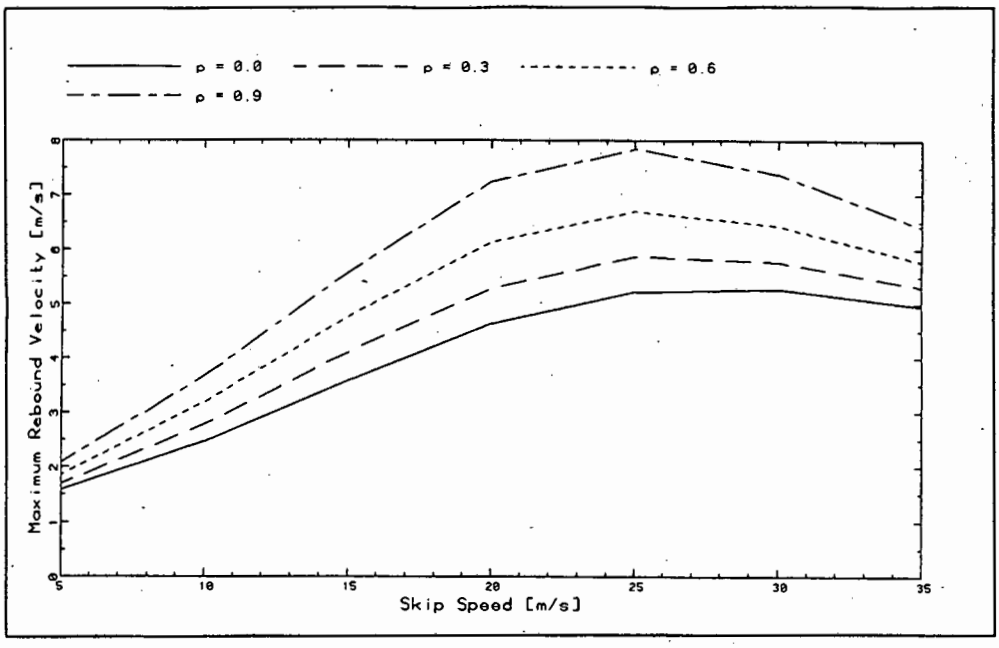

Figure 4.28: Maximum Rebound Velocity as a Function of Skip Speed

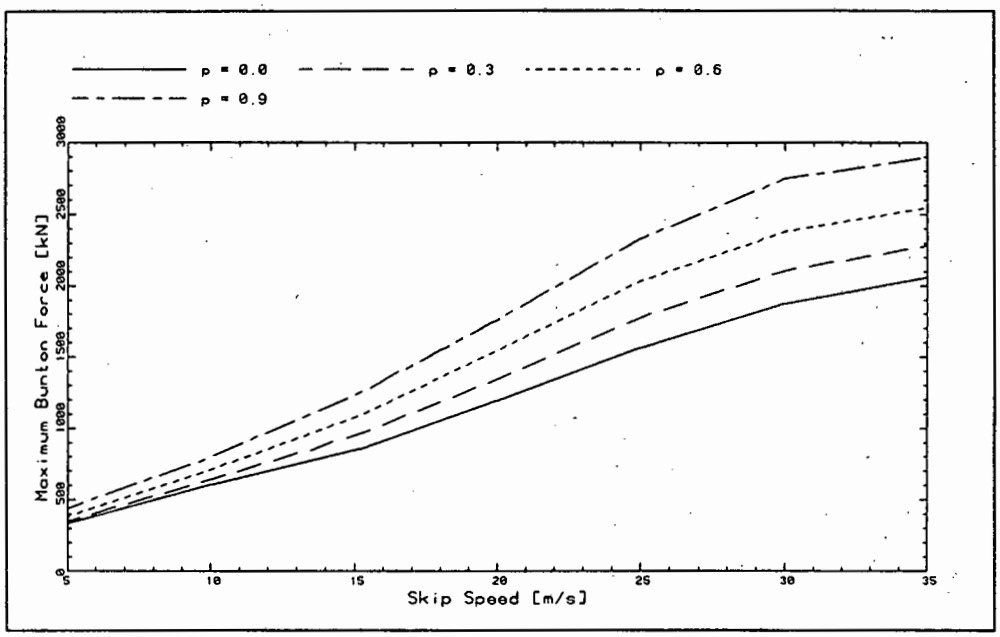

Figure 4.29: Maximum Bunton Force as a Function of Skip Speed

Axial Spring Stiffness

Figures 4.30 and 4.31 illustrate the effect of the axial spring stiffness on the rebound velocity and the bunton force respectively. The case of no axial spring stiffness corresponds to a simply supported guide, while the higher stiffnesses approximate the guide on supports that allow no axial movement.

For *low* p ratios the graphs show a gradual decrease in response as the axial spring stiffness is increased. The influence of secondary stiffening is particularly significant when high axial compressive forces are present in the guides. When there is no secondary stiffening present ($k_a = 0$) the amplification ratio of p = 0.9 relative to p = 0.0 is 4.9. When $k_a = 50000$ kN/m the amplification ratio drops to 1.5. Similar trends occur for the rebound velocity. Thus secondary stiffening has a dramatic effect on the slamming phenomenon when high axial compressive forces are present in the guides.

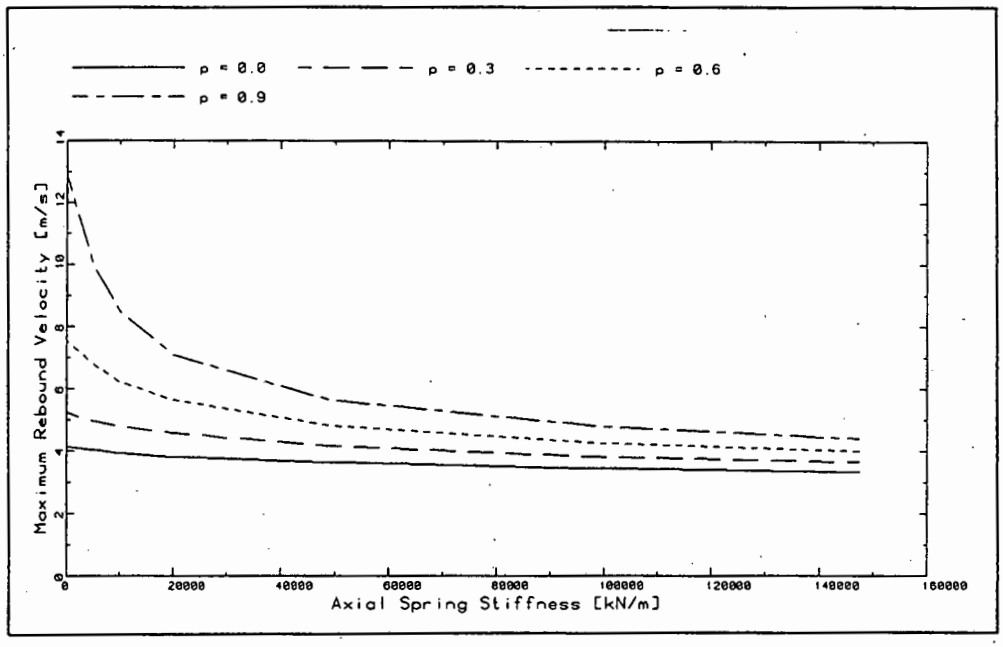

Figure 4.30: Maximum Rebound Velocity as a Function of Axial Spring Stiffness

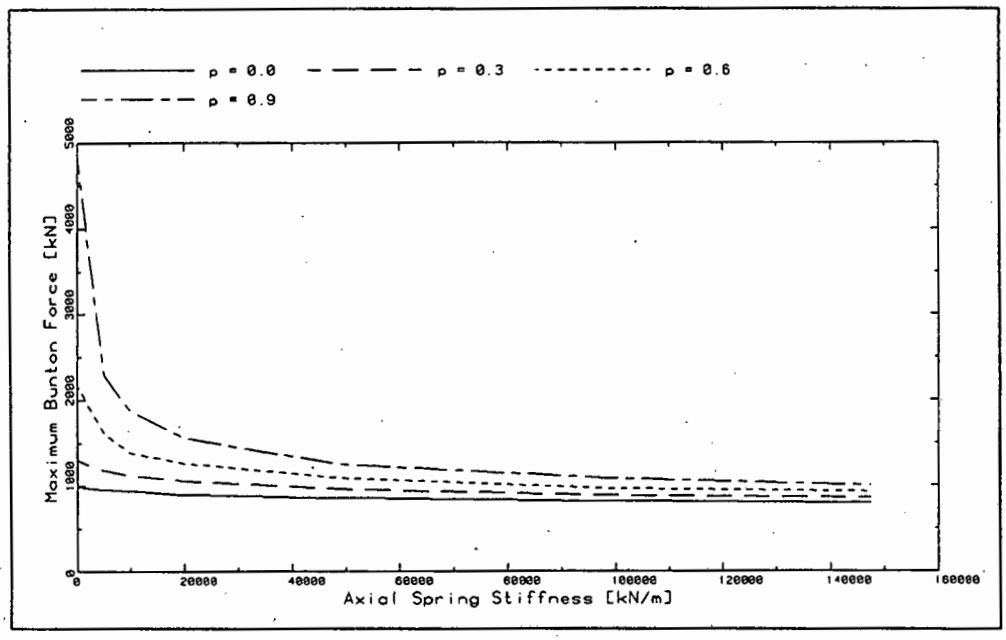

Figure 4.31: Maximum Bunton Force as a Function of Axial Spring Stiffness

5 SUMMARY

5.1 INTRODUCTION

A model has been presented in this thesis to include the effects of secondary stiffening, that result from axial tension effects, for a single slamming event. Results have been presented showing the system response for various axial compressive forces in the guides. A parameter study was performed to show the effects of changes in the various parameters. This section summarizes the results and draws conclusions. Finally, possible future research areas for further study are suggested, which include sustained slamming.

5.2 CONCLUSIONS

The inclusion of secondary stiffening, due to axial tension effects, results in a nonlinear force-displacement curve for the guide. Previous researchers accounted for the axial restraint of the guide by multiplying the simply-supported guide stiffness by a constant factor. Thus the force-deflection curve remained linear but of steeper slope. This thesis showed that for *low* p ratios (the ratio of the axial load to the critical load for the guide) the linear approximation resulted in a stiffer guide than the nonlinear curve. The more flexible guide leads to larger deflections resulting in higher forces and rebound velocities during a slamming event than a stiffer guide. When the p ratio is *greater* than about p = 0.6 the nonlinear guide stiffness is *stiffer* than the linear approximation and the reduced guide deflections result in a reduced slamming response. To summarize, the new model, with the effect of secondary stiffening included, predicts an *increased* skip response, relative to previous models, for a slamming event when the p ratio is *less* than about 0.6. When the p ratio *exceeds* about 0.6 the slamming response is *reduced* relative to previous reported results.

Amplification factors, relative to the response for no compressive load, showed the increased response when axial loads are present. The axial compressive forces, induced by shaft wall strains, reduce the lateral stiffness of the guide. The resulting increased displacements lead to increased forces and rebound velocities. The inclusion of secondary stiffening results in a considerable reduction of amplification factors. For example, the maximum bunton force with no secondary stiffening for p = 0.9 is 6.5 times the value for p = 0.0. When secondary stiffening effects are present the amplification factor drops to 1.5.

A parametric study was carried out in order to show the effects of varying the input parameters, for various p ratios, on the response of the system. A brief summary of the results is presented below:

- Skip mass: Increasing skip mass results in an increased response of the system for all p ratios.
- Guide Stiffness: Increasing guide stiffness reduces the response of the system for all p ratios.
- Bunton Stiffness: Increasing bunton stiffness increases the system response for all p ratios.
- Bunton Spacing: Increasing the bunton spacing increases the system response for all p ratios.
- Skip Speed: Increasing the skip speed increases the system response for all p ratios.
- Axial Spring Stiffness: Increasing the axial spring stiffness reduces the system response. This trend is particularly significant for high p ratios.

Since slamming is a severe event and in respect of shaft steelwork design is responsible for the maximum loads experienced by the shaft system, the effects of axial compressive loads in the steelwork are important. The inclusion of secondary stiffening, due to axial tension effects, represents a significant refinement of the slamming model.

5.3 Scope For Future Work

Owing to the fact that slamming is such a severe event it is desirable that a complete understanding of the phenomenon be acquired. The scope of this thesis was to include the effects of secondary stiffening in the formulation of the model for a single slamming event. A result of a single slamming event is that the skip rebounds with an increased velocity. A consequence of this is that a further slamming event is usually initiated. The resulting behaviour is called sustained slamming. What is significant about the resulting observed behaviour is that the oscillations do not increase infinitely but are limited in amplitude. An extension of the work presented in this thesis should investigate sustained slamming and the parameters that limit its behaviour.

REFERENCES

[1] BATHE, K-J. and WILSON, E.L., **NUMERICAL METHODS IN FINITE ELEMENT ANALYSIS**, Prentice-Hall Inc., Englewood Cliffs, New Jersey, U.S.A., pp 322-324, (1976).

[2] BENTLY, D.M., *"The Equipment of Vertical Shafts - Present South African Mining Practice and Development Trends"*, Paper presented to the Seventh Commonwealth Mining and Metallurgical Congress.

[3] BUDYNAS, R.G., **ADVANCED STRENGTH AND APPLIED STRESS ANALYSIS**, McGraw-Hill Book Company, New York, U.S.A., pp 240-244, (1977).

[4] EISLEY, J.G., **MECHANICS OF ELASTIC STRUCTURES: CLASSICAL AND FINITE ELEMENT METHODS**, Prentice-Hall Inc., Englewood Cliffs, New Jersey, U.S.A., pp 124-127, (1989).

[5] GALLOWAY, L.G. and TILEY, P.M., *"The Performance of Fixed Guidance Systems in Mine Shafts"*, CIM Bulletin, pp 45-60, November 1982.

[6] GREENWAY, M.E., *"Analysis of Skip Slamming"*, Mechanical Engineering Department, Anglo American Corporation of South Africa, Johannesburg, 8 August 1985.

[7] GREENWAY, M.E., Communication with SDRC on COM Steelwork Programme, Mechanical Engineering Department, Anglo American Corporation of South Africa, Johannesburg.

[8] GREENWAY, M.E., *"Further Test Data on Skip and Shaft Steelwork Dynamic Behaviour - Free State Geduld No. 5 Shaft"*, Mechanical Engineering Department, Anglo American Corporation of South Africa, Johannesburg, Submitted to the Chamber of Mines, February 1986.

[9] GREENWAY, M.E., *"Future Trends in the Design of Shaft Steelwork and Conveyances"*, Anglo American Corporation of South Africa Group Engineering Symposium, pp 301-313.

[10] HOISCHEN, I.A., *"Schachteinbauten für Hauptschächte"*, Glückauf, No 14, July 1970.

[11] HUTTON, F.C.L., JAMES, C.L. and SCHWARTZ, C.R., *"Design of Shaft Systems at Depth"*, Rock Mechanics, South Div., Western Deep Levels, LTD, Anglo American Corporation of South Africa, Johannesburg.

[12] JOYCE, P. and HALBAUER, S., Private Communication with T.S. Pretorius on Shaft Steelwork Analyses, Mechanical Engineering Department, Anglo American Corporation of South Africa, Johannesburg, 20 September 1988.

[13] KRIGE, G.J., *"The Behaviour and Design of Mineshaft Steelwork and Conveyances"*, PhD thesis, University of the Witswatersrand, 1983.

[14] KRIGE, G.J., *"Some Initial Findings on the Behaviour and Design of Mine Shaft Steelwork and Conveyances"*, Journal of the South African Institute of Mining and Metallurgy, v 86 n 6 June 1986, pp 205-215.

[15] KRIGE, G.J. and KEMP, A.R., *"Behaviour and Design of Mineshaft Steelwork and Conveyances: A Summary of a Current Research Programme"*, South African Mechanical Engineer, v 32 n 7 July 1982, pp 163-169.

[16] LANGHAAR, H.L., **ENERGY METHODS IN APPLIED MECHANICS**, John Wiley and Sons, Inc., New York, pp 44-46, (1962).

[17] NEWMARK, N.M., *"A Method of Computation for Structural Dynamics"*, J. Eng.Mech. ASCE, pp 67-94, (1959).

[18] PRETORIUS, T.S., *"Vibration Problems of Skips in Mine Shafts: The Effect of Compressive Forces in the Guides"*, MSc dissertation, University of Cape Town 1989.

[19] PRETORIUS, T.S., MERCER, C.D. and MARTIN, J.B., *"Slamming Analysis of Mine Skips: The Effect of Compressive Forces in the Guides"*, University of Cape Town CERECAM Report No. 123, Revised December 1989.

[20] PRETORIUS, T.S., MERCER, C.D. and MARTIN, J.B., *"The Response of Mine Skips with Rollers: The Effect of Compressive Forces in the Guides"*, University of Cape Town CERECAM Report No. 139, December 1989.

[21] PRETORIUS, T.S., MERCER, C.D. and MARTIN, J.B., *"Slamming Analysis of Skips in Mine Shafts"*, University of Cape Town CERECAM Report No. 143, January 1990.

[22] REDPATH, J.S. and SHAVER, W.M., *"Towards a Better Understanding of Mine Shaft Guides"*, CIM Bulletin, pp 90-100, September 1977.

[23] STRUCTURAL DYNAMICS RESEARCH CORPORATION, *"An Investigation into Shaft Steelwork and Skip Dynamics, Phase I - Experimental Programme"*, SDRC Project No. 11251, Milford Ohio, June 1983.

[24] STRUCTURAL DYNAMICS RESEARCH CORPORATION, *"An Investigation into Shaft Steelwork and Skip Dynamics, Phase II - Analytical Programme"*, SDRC Project No. 11801, Milford Ohio, February 1984.

[25] STRUCTURAL DYNAMICS RESEARCH CORPORATION, *"An Investigation into the Slamming Behaviour of Flexible Skips"*, SDRC Project No. 12207, Milford Ohio, May 1985.

[26] STRUCTURAL DYNAMICS RESEARCH CORPORATION, *"An Investigation into Shaft Steelwork and Skip Dynamics, Phase IV - Calibration"*, SDRC Project No. 11964, Milford Ohio, February 1987.

[27] STRUCTURAL DYNAMICS RESEARCH CORPORATION, *"An Investigation into Shaft Steelwork and Skip Dynamics, Phase III - Design Guidelines"*, SDRC Project No. 11964, Milford Ohio, August 1987.

[28] STRUCTURAL DYNAMICS RESEARCH CORPORATION, *"Design Guidelines for the Dynamic Performance of Shaft Steelwork and Conveyances"*, SDRC Project No. 11964, Milford Ohio, September 1990.

[29] YAKOWITZ, S. and SZIDAROVSZKY, F., **AN INTRODUCTION TO NUMERICAL COMPUTATIONS**, Macmillan Publishing Company, New York, U.S.A., pp 283-285, (1989).

APPENDIX A: DERIVATION OF VIRTUAL WORK TERMS

The derivation of the virtual work terms used in section 2.2.1. for the determination of the guide displacement, is presented below.

A.1 DISPLACEMENT AT POINT B

Referring to Figure A.1, and considering first only the extension of the beam (i.e. no bending) the displacement, δ_{B1}, due to the axial tension N, is:

$$\delta_{B1} = \frac{Nl}{AE} \tag{A.3}$$

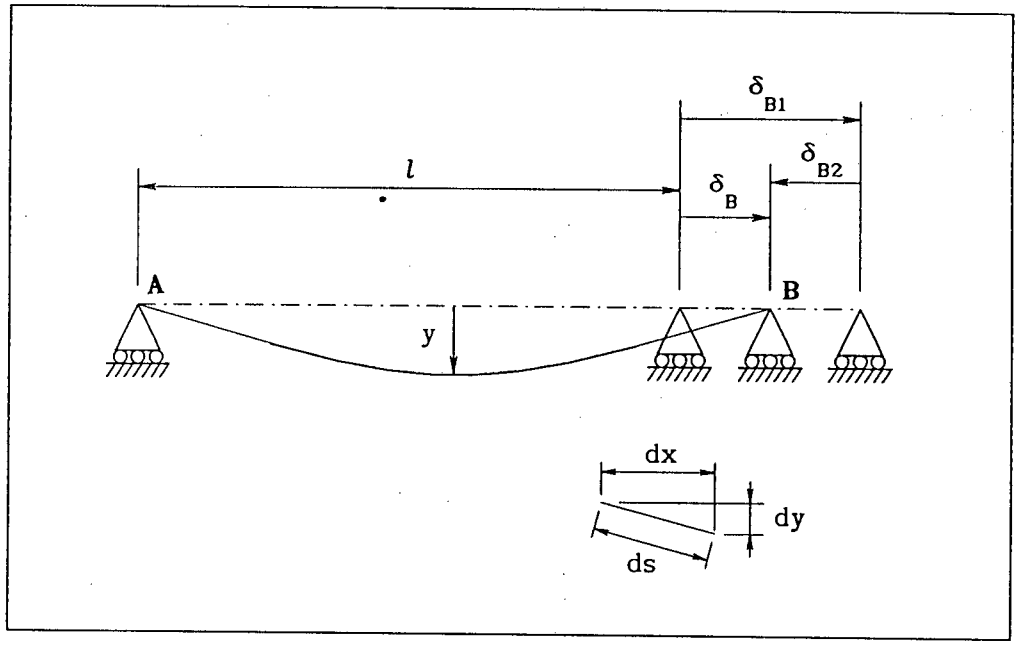

Figure A.1: Deflection of end of beam due to bending and extension

Consider now the application of a transverse load. The displacement, δ_{B2}, due to the bending deflection y, is derived as follows [3].

Assuming that bending does not cause any axial stress along the centroidal axis of the beam, the deflection δ_{B2} is the difference between the straight line **AB** and the arc **AB**.

Using the curvilinear variable s, one can view a segment of the beam centroid where:

$$ds^2 = dx^2 + dy^2$$

$$ds = dx \left[1 + \left(\frac{dy}{dx}\right)^2\right]^{1/2} \tag{A.1}$$

For small slopes, $\frac{dy}{dx} \ll 1$ and the term in the brackets can be expanded using the binomial expansion theorem. When terms $(dy/dx)^4$ and higher are neglected equation (A.1) is approximated by:

$$ds \approx dx \left[1 + \frac{1}{2}\left(\frac{dy}{dx}\right)^2\right]$$

Integration yields:

$$\int_0^l ds \approx \int_0^l dx + \frac{1}{2}\int_0^l \left(\frac{dy}{dx}\right)^2 dx$$

Since: $$\int_0^l ds = \text{arc } \mathbf{AB} \text{ and } \int_0^l dx = \mathbf{AB}$$

we have:

$$\delta_{B2} = \text{arc } \mathbf{AB} - \mathbf{AB} = \int_0^l ds - \int_0^l dx \approx \frac{1}{2}\int_0^l \left(\frac{dy}{dx}\right)^2 dx \tag{A.2}$$

The resultant deflection of point **B**, δ_B, (due to both the bending and extension) is given by:

$$\delta_B = \frac{Nl}{AE} - \frac{1}{2}\int_0^l \left(\frac{dy}{dx}\right)^2 dx \qquad (A.4)$$

Thus for the case when only half the beam is considered, as in section 2.21, the deflection at point **B** is:

$$\delta_B = \frac{1}{2}\left(\frac{Nl}{AE} - \frac{1}{2}\int_0^l \left(\frac{dy}{dx}\right)^2 dx\right) \qquad (A.5)$$

A.2 BEAM IN BENDING

The internal virtual work δU represents the work done by the actual stresses during the virtual distortion and is written:

$$\delta U = \iiint \underset{\sim}{\sigma}\ \delta\underset{\sim}{\varepsilon}\ dxdydz \tag{A.6}$$

Since the beam is in pure bending and we assume that plane sections remain plane subsequent to bending:

$$\varepsilon = \frac{du}{dx} = \frac{d}{dx}\left(-z\,\frac{dw}{dx}\right) = -z\,\frac{d^2w}{dx^2} = -zw''$$

$$\Rightarrow \delta\varepsilon = -z\ \delta w'' \tag{A.7}$$

Also:

$$\sigma = E\varepsilon = -zEw'' \tag{A.8}$$

Substituting equations (A.7) and (A.8) into equation (A.6) we obtain:

$$\delta U_{EI} = E \iiint z^2 w''\delta w''\ dxdydz$$

$$= EI \int_0^l w''\delta w''\ dx \tag{A.9}$$

A.3 BEAM STRETCHING

Figure A.2 illustrates the neutral axis of the beam having under gone a virtual displacement δw. From Figure A.2:

$$dx^2 + (w' + \delta w')^2 dx^2 = ds^2 \tag{A.10}$$

$$\Rightarrow ds - dx = dx \left\{ \left[1 + (w' + \delta w')^2 \right]^{1/2} - 1 \right\} \tag{A.11}$$

Using the binomial expansion theorem to expand the term in square brackets equation (A.11) is approximated by:

$$ds - dx = dx \left\{ 1 + \frac{1}{2}(w' + \delta w')^2 + \ldots - 1 \right\}$$

$$\Rightarrow ds - dx = \left\{ \frac{1}{2} w'^2 + w' \delta w' + \frac{1}{2} \delta w'^2 \right\} dx$$

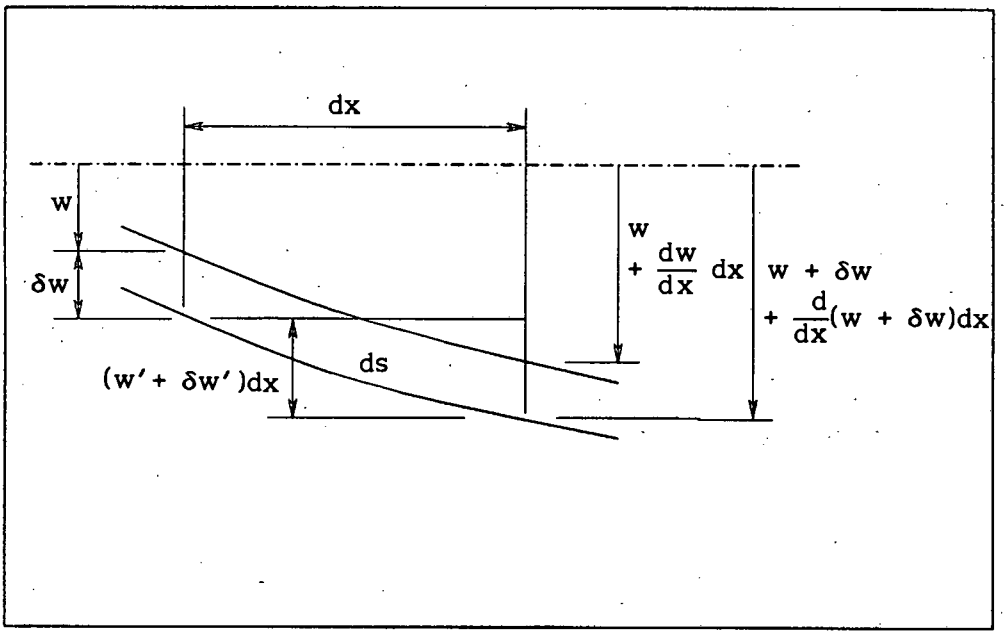

Figure A.2: Deformed Beam subject to a Virtual Displacement

Dropping the term of order $\delta w'^2$ we have for the axial elongation with virtual displacement δw:

$$ds - dx = \left\{\frac{1}{2}w'^2 + w'\delta w'\right\} dx$$

The $\frac{1}{2}w'^2$ term arises from the *actual* elongation due to a displacement w. Therefore the resulting virtual elongation is given by:

$$\delta u = w'\delta w' \; dx \qquad \text{(A.12)}$$

APPENDIX B: DERIVATION OF LINEAR PREDICTOR

The derivation of the linear predictor used in section (3.2.1) to determine the skip force is presented below.

The guide deflection equation (equation 2.40) for one Fourier term is:

$$\bar{y}_g = \bar{a}_1 \sin \pi\xi \tag{B.1}$$

where the $\bar{a}_1$ is solved from:

$$\frac{\pi^4}{96}\left[(1 - p)\bar{a}_1 + \frac{1}{4}\left(\frac{1}{1 + 2\bar{k}}\right)\bar{a}_1^3\right] = \bar{T} \sin \pi\xi \tag{B.2}$$

Linearising equation (B.2) by truncating after the first term we obtain:

$$\frac{\pi^4}{96}\left[(1 - p)\bar{a}_1\right] = \bar{T} \sin \pi\xi \tag{B.3}$$

Substituting for $\bar{a}_1$ from equation (B.1) into (B.3) we obtain:

$$\bar{y}_g = \left[\frac{96 \sin^2\pi\xi}{\pi^4(1 - p)}\right] \bar{T} \tag{B.4}$$

The bunton deflection was derived as:

$$\bar{y}_b = \frac{1}{r}\left[\xi^2 + (1 - \xi)^2\right] \bar{T} \tag{B.5}$$

The total *linear* displacement is the sum of the bunton and guide displacements:

$$Y^L = \left\{\frac{96 \sin^2\pi\xi}{\pi^4(1 - p)} + \frac{1}{r}\left[\xi^2 + (1 - \xi)^2\right]\right\} \bar{T} \tag{B.6}$$

thus the *linear* stiffness is:

$$K^L = \left\{ \frac{96 \sin^2 \pi\xi}{\pi^4 (1 - p)} + \frac{1}{r}\left[\xi^2 + (1 - \xi)^2\right] \right\}^{-1} \qquad \text{(B.7)}$$

APPENDIX C: SOLVING THE EQUATIONS FOR THE GUIDE DISPLACEMENT

The equations governing the guide displacement derived in section 2.2.1, are repeated below:

$$\bar{y}_g(x) = \sum_{n=1}^{\infty} \bar{a}_n \sin n\pi\xi \tag{C.1}$$

where the $\bar{a}_n$ are calculated from:

$$\frac{\pi^4 n^2}{96}\left(n^2 - p\right)\bar{a}_n + \frac{\pi^4}{384(1 + 2\bar{k})}\left\{\sum_{r=1}^{\infty} r^2\bar{a}_r^2\right\} n^2\bar{a}_n = \bar{T}\sin n\pi\xi \tag{C.2}$$

The number of simultaneous non-linear equations depends on how many terms are required for the deflection approximation. The solution of systems of non-linear equations is normally achieved by a generalization of the single-variable Newton's method [29]. The solution procedure is sketched below.

The equations can be expressed as:

$$f_i(x_1, \ldots, x_n) = 0 \qquad (i = 1, 2, \ldots, n) \tag{C.3}$$

where the f_i's represent real-valued functions. A *root* is any vector $\tilde{\mathbf{x}} = (\tilde{x}_1, \ldots, \tilde{x}_n)$ of real numbers for which (C.3) is satisfied simultaneously for all i.

Defining the (i, j)th element of the *Jacobian matrix*, $\mathbf{J}(\mathbf{x})$ to be:

$$J_{ij}(\mathbf{x}) = \frac{\partial}{\partial x_j} f_i(x_1, x_2, \ldots, x_n).$$

Define $\mathbf{J}^{(k)} = \mathbf{J}(\mathbf{x}^{(k)})$ to be the Jacobian matrix of $(f_1(\mathbf{x}), \ldots, f_n(\mathbf{x}))$, evaluated at the kth iteration estimate $\mathbf{x}^{(k)}$, and introduce the vector:

$$\mathbf{f}^{(k)} = \begin{bmatrix} f_1(\mathbf{x}^{(k)}) \\ \vdots \\ f_1(\mathbf{x}^{(k)}) \end{bmatrix}$$

The multivariable Newton method is expressible as:

$$\mathbf{x}^{(k+1)} = \mathbf{x}^{(k)} - (\mathbf{J}^{(k)})^{-1}\mathbf{f}^{(k)} \tag{C.3}$$

for computational reasons equation (C.3) is rewritten as:

$$\mathbf{J}^{(k)}(\mathbf{x}^{(k+1)} - \mathbf{x}^{(k)}) = -\mathbf{f}^{(k)} \tag{C.4}$$

and solved by Gauss elimination methods.

APPENDIX D: COMPUTER CODE FOR UCTSTIFF

```
      program STIFF
c=============================================================
c     Program:       STIFF
c     Purpose:       Compute the response to a slamming event, including
c                    the effect of secondary stiffening.
c     Programmer:    A Darcy-Evans, CERECAM, UCT
c     Date:          August 1990
c     Language:      VMS Fortran
c     Revisions:     None
c     Installation:  Vax 6330
c     Add S/Ware:    None
c=============================================================
c
      implicit       none
      integer        inpfil,outfil,datfil,kk,n
      real*8         pi,
     &               rratio,pratio,kratio,vbar,xsi0,tol,
     &               t,dt,
     &               disp0,vel0,accn0,
     &               displ0,displ1,
     &               tmax,bmax,bmmax,dspmax,
     &               xsi,
     &               disp,displ,vel1,accn1,
     &               tbar,btndsp,abar(3),gdedsp,
     &               b,c,d,e,
     &               lstiff,deldsp,cordsp,resid,
     &               dtstar,xleft,delf,dylin,
     &               bf1,bf2,bm,
     &               mass,Kg,A,I,L,
     &               force,def1,
     &               atmax,abmax,abmmax,admax
      parameter      (inpfil=10,outfil=20,datfil=30)
c
      pi = 4.0d0*dATAN(1.0d0)
c
      open (unit=inpfil,status='old',readonly)
      open (unit=outfil,status='new')
      open (unit=datfil,status='new')
c
      read (inpfil,*) rratio, pratio, kratio, vbar, xsi0, vel0
      read (inpfil,*) tol, n, kk
      read (inpfil,*) mass, Kg, A, I, L
c
      write(outfil,1000)
      write(outfil,1001) rratio,pratio,kratio,vbar,
```

```
     &                          xsi0,vel0,mass,Kg,A,I,L,tol,n
c
c---  initialise the global constants
c
      t       = 0.0d0
      dt      = 1.0d-2
c
      disp0   = 0.0d0
c---  non-dimensional initial translational velocity
      vel0    = vel0 * dSQRT(mass*A/Kg/I)
      accn0   = 0.0d0
c
      dspmax = 0.0d0
      tmax    = 0.0d0
      bmax    = 0.0d0
      bmmax = 0.0d0
c
      admax = 0.0d0
      atmax = 0.0d0
      abmmax = 0.0d0
      admax = 0.0d0
      abmmax = 0.0d0
c
      tbar    = 0.0d0
c
10    continue
c
c---  main analysis loop starts here
c---  increment position
      xsi = (xsi0+vbar*t) - DINT(xsi0+vbar*t)
      write(*,*)'xsi = ',xsi
c
      b = (96.0d0*(dsin(pi*xsi))**2)/(pi**4*(1.0d0-pratio))
      e = (1.0d0/rratio)*(xsi**2+(1.0d0-xsi)**2)
      lstiff = 1.0d0/(b+e)
c
      disp10 = dt * vel0
c
20    continue
c
      deldsp = disp10
c
30    continue
c
      delf    = lstiff * deldsp
      tbar    = tbar + delf
c
c--   calculate the bunton displacement using the predicted force
      btndsp = tbar * (xsi**2+(1.0d0-xsi)**2) / rratio
```

```
c
c---  calculate the guide displacement using the non-linear equations
      call NEWTON(kratio,pratio,tbar,xsi,n,abar)
      gdedsp = abar(1)*dSIN(pi*xsi) + abar(2)*dSIN(2.0*pi*xsi) +
     &         abar(3)*dSIN(3.0*pi*xsi)
c
c---  calculate the corrected total displacement
      cordsp = gdedsp + btndsp
c
c---  check for convergence - if not iterate
      resid  = displ0 - cordsp
      if (ABS(resid/displ0) .gt. tol) then
         deldsp = resid
         goto 30
      end if
c
      displ1 = disp0 + dt*vel0 + dt*dt/4.0d0*accn0 - dt*dt/4.0d0*tbar
c
      if (ABS((displ1-displ0)/displ0) .gt. tol) then
         displ0 = displ1
         goto 20
      end if
c
c---  update acceleration, velocity
      displ = displ1
      vel1  = (2.0d0/dt)*(displ-disp0) - vel0
      accn1 = (2.0d0/dt)*(vel1-vel0)   - accn0
c
      force = tbar * Kg * dSQRT(I/A) / 1.0d3
      defl  = displ * dSQRT(I/A)
      write(datfil,2000)xsi,force,defl
c
c---  Check to see if the skip has left the guide, if it has do a
c     linear interpolation to get the approximate position where it
c     left the guide, and the time it left the guide.
c
      if (displ .le. 0.0d0) then
         t      = t - dt
         dtstar = (disp0*dt)/(-displ+disp0)
         t      = t + dtstar
         displ  = 0.0d0
         accn1  = 4.0d0/dtstar**2*(displ - dtstar*vel0 - disp0) - accn0
         vel1   = dtstar/2.0d0*(accn0 + accn1) + vel0
         xleft  = (xsi0+vbar*t)
         xsi    = xleft - DINT(xleft)
      end if
c
c---  Compute the forces and the guide bending moment
      bfl    = (1.0d0-xsi)*tbar
```

```
      bf2    = xsi*tbar
      bm     = xsi*(1.0d0-xsi)*tbar +
     &         (pi*pi/48.0d0)*pratio*displ -
     &         (pi*pi/192.0d0)*1.0d0/(1.0d0+2.0d0*kratio) *
     &         (abar(1) + 4.0d0*abar(2) + 9.0d0*abar(3))*displ
c
c---  if the output parameter is 1, output the results at each time step
      if (kk.eq.1) then
         write (outfil,1002) xsi,t,tbar,bf1,bf2,bm
      end if
c
c---  get the maximum forces, displacement and maximum bending moment
c     also convert to actual values for comparison purposes
      if (tbar  .gt. tmax) then
         tmax   = tbar
         atmax  = tbar * Kg * dSQRT(I/A)
      end if
      if (displ .gt. dspmax) then
         dspmax = displ
         admax  = displ * dSQRT(I/A)
      end if
      if (bf1 .gt. bmax) then
         bmax   = bf1
         abmax  = bf1 * Kg * dSQRT(I/A)
      end if
      if (bf2 .gt. bmax) then
         bmax   = bf2
         abmax  = bf2 * Kg * dSQRT(I/A)
      end if
      if (bm  .gt. bmmax) then
         bmmax  = bm
         abmmax = bm * L * Kg * dSQRT(I/A)
      end if
c
c---  if the skip has left the guide then write the results to file
      if (displ .le. 0.0d0) then
         write(outfil,1003) xleft,t,vel1,tmax,bmax,bmmax,dspmax
         write(outfil,1005) atmax,abmax,abmmax,admax
      end if
c
c---  if the skip has not left the guide then update variables
      if (displ.gt.0.0d0) then
         disp0 = displ
         vel0  = vel1
         accn0 = accn1
         t     = t + dt
         goto 10
      end if
c
```

```
      close (unit=inpfil,status='keep')
      close (unit=outfil,status='keep')
      close (unit=datfil,status='keep')
c
1000  format(/,'*****************************************************',/,
     &         '** SLAMMING ANALYSIS OF A SIMPLY SUPPORTED GUIDE **',/,
     &         '**        INCLUDING SECONDARY STIFFENING           **',/,
     &         '*****************************************************',/)
c
1001  format(/,'   Stiffness Ratio (r)            =',f8.4,/,
     &         '   Axial Force Ratio (p)           =',f8.4,/,
     &         '   Axial Stiffness Ratio (k)       =',f8.4,/,
     &         '   Dimensionless Velocity (vbar) =',f8.4,/,
     &         '   Initial Impact Position (xsi) =',f8.4,/,
     &         '   Translational Impact Velocity =',f8.4,' m/s',/,
     &         '   Skip Effective Mass             =',f8.1,' kg',/,
     &         '   Guide Midspan Stiffness         =',e11.4e1,' N/m',/,
     &         '   Guide Cross-Sectional Area      =',e11.4e1,' m^2',/,
     &         '   Guide Second Moment of Area     =',e11.4e1,' m^4',/,
     &         '   Guide Length                    =',f8.4,' m',/,
     &         '   Tolerance on Displacements      =',f8.4,/,
     &         '   Number of Fourier Terms         =',i3,/)
c
1002  format(/,'          Position (xsi)           =',f8.4,/,
     &         '          Time                      =',f8.4,/,
     &         '          Skip Force                =',f8.4,/,
     &         '          Bunton Force 1            =',f8.4,/,
     &         '          Bunton Force 2            =',f8.4,/,
     &         '          Bending Moment            =',f8.4,/)
c
1003  format(/,'   Skip Left Guide at x/l          =',f8.4,/,
     &         '                     at time        =',f8.4,/,
     &         '   Velocity                        =',f8.4,/,
     &         '   Maximum Skip Force              =',f8.4,/,
     &         '   Maximum Bunton Force            =',f8.4,/,
     &         '   Maximum Bending Moment          =',f8.4,/,
     &         '   Maximum Displacement            =',f12.8,/)
c
1005  format(/,'   Maximum Skip Force              =',e11.4e1,' N ',/,
     &         '   Maximum Bunton Force            =',e11.4e1,' N ',/,
     &         '   Maximum Bending Moment          =',e11.4e1,' Nm',/,
     &         '   Maximum Displacement            =',e11.4e1,' m ',/)
c
2000  format(3d12.4)
2005  format(5d12.4)
      stop '$ Normal Termination of program STIFF!'
      end
```

```
      subroutine   Newton(k,p,force,xsi,n,a)
c=====================================================================
c     Function:    Solve the system of non-linear equations for the Fourier
c                  coefficients using Newtons method for systems.
c     Parameters:
c i      k         Ratio of axial stiffness of guide to axial spring
c i      p         Ratio of axial to Euler critical buckling load
c i      force     Non-dimensional skip force
c i      xsi       Non-dimensional skip position
c i      n         Number of Fourier Terms to be used
c o      a         Fourier Coefficients
c     Programmer: A Darcy-Evans, CERECAM, UCT
c     Date:       September 1990
c     Language:   VMS Fortran
c=====================================================================
c
      implicit    none
      integer     n
      real*8      k,p,force,xsi,
     &            a0(3),a(3),eps
c
      a0(1) = 5.0d0
      a0(2) = 1.0d0
      a0(3) = 1.0d0
      eps   = 0.1d-6
c
      call MVNE(n,a0,a,k,p,force,xsi,eps)
c
      end
c
      double precision function F1(i,a,force,p,xsi,k)
c=====================================================================
      implicit    none
      integer     i
      real*8      fnctn(3),a(3),force,xsi,p,k,
     &            pi,fact1,fact2,fact3
c
      pi    = 4.0d0*dATAN(1.0d0)
c
      fact1 = (2.0d0*p*k) / (1.0d0+2.0d0*k)
      fact2 = 1.0d0 / (1.0d0+2.0d0*k)
      fact3 = 1.0d0 + ( k / (1.0d0+2.0d0*k))

      fnctn(1)  =  pi**4/96.0d0*((1.0d0-p)*a(1) +
     &             0.25d0*fact2*a(1)**3) -
     &             force*dSIN(pi*xsi)
c
      F1 = fnctn(i)
c
```

```
      return
      end
c
      double precision function F2(i,a,force,p,xsi,k)
c=================================================================
      implicit     none
      integer      i
      real*8       fnctn(3),a(3),force,xsi,p,k,
     &             pi,fact1,fact2,fact3
c
      pi      = 4.0d0*dATAN(1.0d0)
c
      fact1  = (2.0d0*p*k) / (1.0d0+2.0d0*k)
      fact2  = 1.0d0 / (1.0d0+2.0d0*k)
      fact3  = 1.0d0 + ( k / (1.0d0+2.0d0*k))

      fnctn(1)  =  pi**4/96.0d0*((1.0d0-p)*a(1) +
     &             0.25d0*fact2*(a(1)**2 + 4.0d0*a(2)**2)*a(1)) -
     &             force*dSIN(pi*xsi)
      fnctn(2)  =  pi**4/24.0d0*((4.0d0-p)*a(2) +
     &             0.25d0*fact2*(a(1)**2 + 4.0d0*a(2)**2)*a(2)) -
     &             force*dSIN(pi*2.0d0*xsi)
c
      F2 = fnctn(i)
c
      return
      end
c
      double precision function F3(i,a,force,p,xsi,k)
c=================================================================
      implicit     none
      integer      i
      real*8       fnctn(3),a(3),force,xsi,p,k,
     &             pi,fact1,fact2,fact3
c
      pi      = 4.0d0*dATAN(1.0d0)
c
      fact1  = (2.0d0*p*k) / (1.0d0+2.0d0*k)
      fact2  = 1.0d0 / (1.0d0+2.0d0*k)
      fact3  = 1.0d0 + ( k / (1.0d0+2.0d0*k))
c
      fnctn(1)  =  pi**4/96.0d0*((1.0d0-p)*a(1) +
     &             0.25d0*fact2*
     &             (a(1)**2 + 4.0d0*a(2)**2 + 9.0d0*a(3)**2)*a(1)) -
     &             force*dSIN(pi*xsi)
      fnctn(2)  =  pi**4/24.0d0*((4.0d0-p)*a(2) +
     &             0.25d0*fact2*
     &             (a(1)**2 + 4.0d0*a(2)**2 + 9.0d0*a(3)**2)*a(2)) -
     &             force*dSIN(pi*2.0d0*xsi)
```

```
      fnctn(3)  =  9.0d0*pi**4/96.0d0*((9.0d0-p)*a(3) +
     &             0.25d0*fact2*
     &             (a(1)**2 + 4.0d0*a(2)**2 + 9.0d0*a(3)**2)*a(3)) -
     &             force*dSIN(pi*3.0d0*xsi)
c
      F3 = fnctn(i)
c
      return
      end
c
      double precision function DF1(i,j,a,p,k)
c=======================================================================
      implicit      none
      integer       i,j
      real*8        jac(3,3),a(3),p,k,
     &              pi,fact1,fact2,fact3
c
      pi     = 4.0d0*dATAN(1.0d0)
c
      fact1  = (2.0d0*p*k) / (1.0d0+2.0d0*k)
      fact2  = 1.0d0 / (1.0d0+2.0d0*k)
      fact3  = 1.0d0 + ( k / (1.0d0+2.0d0*k))

      jac(1,1) =    pi**4/96.0d0*((1.0d0-p) +
     &              3.0d0/4.0d0*fact2*a(1)**2)
c
      DF1 = jac(i,j)
c
      return
      end
c
      double precision function DF2(i,j,a,p,k)
c=======================================================================
      implicit      none
      integer       i,j
      real*8        jac(3,3),a(3),p,k,
     &              pi,fact1,fact2,fact3
c
      pi     = 4.0d0*dATAN(1.0d0)
c
      fact1  = (2.0d0*p*k) / (1.0d0+2.0d0*k)
      fact2  = 1.0d0 / (1.0d0+2.0d0*k)
      fact3  = 1.0d0 + ( k / (1.0d0+2.0d0*k))
c
      jac(1,1) =    pi**4/96.0d0*((1.0d0-p) +
     &              fact2*(3.0d0/4.0d0*a(1)**2 +
     &              a(2)**2))
      jac(1,2) =    pi**4/96.0d0*(2.0d0*fact2*a(1)*a(2))
      jac(2,1) =    pi**4/24.0d0*(0.5d0*fact2*a(1)*a(2))
```

```
      jac(2,2) =   pi**4/24.0d0*((4.0d0-p) +
     &             fact2*(0.25d0*a(1)**2 +
     &             3.0d0*a(2)**2))
c
      DF2 = jac(i,j)
c
      return
      end
c
      double precision function DF3(i,j,a,p,k)
c=================================================================
      implicit     none
      integer      i,j
      real*8       jac(3,3),a(3),p,k,
     &             pi,fact1,fact2,fact3
c
      pi     = 4.0d0*dATAN(1.0d0)
c
      fact1  = (2.0d0*p*k) / (1.0d0+2.0d0*k)
      fact2  = 1.0d0 / (1.0d0+2.0d0*k)
      fact3  = 1.0d0 + ( k / (1.0d0+2.0d0*k))
c
      jac(1,1) =   pi**4/96.0d0*((1.0d0-p) +
     &             fact2*(3.0d0/4.0d0*a(1)**2 +
     &             a(2)**2 + 9.0d0/4.0d0*a(3)**2))
      jac(1,2) =   pi**4/96.0d0*(fact2*2.0d0*a(1)*a(2))
      jac(1,3) =   pi**4/96.0d0*(fact2*9.0d0/2.0d0*a(1)*a(3))
c
      jac(2,1) =   pi**4/24.0d0*(0.5d0*fact2*a(1)*a(2))
      jac(2,2) =   pi**4/24.0d0*((4.0d0-p) +
     &             fact2*(0.25d0*a(1)**2 +
     &             3.0d0*a(2)**2 + 9.0d0/4.0d0*a(3)**2))
      jac(2,3) =   pi**4/24.0d0*(fact2*9.0d0/2.0d0*a(2)*a(3))
c
      jac(3,1) =   9.0d0*pi**4/96.0d0*(0.5*fact2*a(1)*a(3))
      jac(3,2) =   9.0d0*pi**4/96.0d0*(fact2*2.0d0*a(2)*a(3))
      jac(3,3) =   9.0d0*pi**4/96.0d0*((9.0d0-p) +
     &             fact2*(0.25d0*a(1)**2 +
     &             a(2)**2 + 3.0d0*9.0d0/4.0d0*a(3)**2))
c
      DF3 = jac(i,j)
c
      return
      end
c
      subroutine   MVNE(n,x0,x,k,p,force,xsi,eps)
c=================================================================
c     Function:    This subroutine computes the root vector of a system of
c                  equation F(i,x)=0 ,i = 1,...,n  using the multivariate
```

```
c                    Newton method
c
c     Usage:         Call Sequence: call MVNE(n,x0,x,k,p,force,xsi,eps)
c     Calls to:      Subroutine GAUS1(n,m,nd,a,delt)
c                    Function   F(i,x,force,p,xsi,k)
c                    Function   DF(i,j,x0,p,k)
c     Parameters:
c       Input:
c                n   Number of simultaneous linear equations (less than 30)
c               x0   n by 1 array of initial approximate root vector values
c              eps   Error bound (tolerance)
c       Output:
c                x   n by 1 array of approximate roots
c
c     Reference:     An Introduction to Numerical Computations
c                    S Yakowitz, F Szidarovszky
c=====================================================================
c
      implicit       none
      integer        l,m,n,i,j,nd
      real*8         p,force,xsi,k,
     &               a(30,31), x0(n), x(n),
     &               delt,eps,
     &               F1,F2,F3,DF1,DF2,DF3

c
c---  initialization
      l      = 1
c
c---  compute vector x as the root
      do while(l .le. n)
         do i = 1, n
            do j = 1, n
               if (n .eq. 1) then
                  a(i,j) = DF1(i,j,x0,p,k)
               else if (n .eq. 2) then
                  a(i,j) = DF2(i,j,x0,p,k)
               else if (n .eq. 3) then
                  a(i,j) = DF3(i,j,x0,p,k)
               end if
            end do
            if (n .eq. 1) then
               a(i,n+1) = -F1(i,x0,force,p,xsi,k)
            else if (n .eq. 2) then
               a(i,n+1) = -F2(i,x0,force,p,xsi,k)
            else if (n .eq. 3) then
               a(i,n+1) = -F3(i,x0,force,p,xsi,k)
            end if
         end do
```

```
c
c---  perform gaussian elimination
         m     = 1
         nd    = 30
         delt = 1.3877787807814457d-17
c
         call GAUS1(n,m,nd,a,delt)
c
         do i = 1, n
            x(i) = x0(i) + a(i,n+1)
         end do
c
c---  if solution change is small then stop
         l = 1
         do while (ABS( x(l)-x0(l) ) .lt. eps .and. l .le. n)
            l = l + 1
         end do
         if (l .le. n) then
            do i = 1, n
               x0(i) = x(i)
            end do
         end if
      end do
c
      return
      end
c
      subroutine     GAUS1(n,m,nd,a,delt)
c=====================================================================
c     Function:      This subroutine computes the solutions for m systems with
c                    n equations and n unknowns using Gaussian elimination
c
c     Usage:         Call Sequence: call GAUS1(n,m,nd,a,delt)
c
c     Parameters:
c       Input:
c                n   Number of equations and unknowns
c                m   Number of systems (right hand side vectors)
c               nd   Upper bound to the linear equation order
c                a   n by m+n (usually, m=1) array of coefficients
c                    augmented with each right side vector
c             delt   estimate of error bound (machine epsilon)
c       Output:
c                    a(1,n+j),...,a(n,n+j)
c                    Solution of the j-th system (j = 1,...,m)
c
c     Referance:     An Introduction to Numerical Computations
c                    S Yakowitz, F Szidarovszky
c=====================================================================
```

```
c
      implicit      none
      integer       n,m,nd,k,kk,in,i,ie,ix,j
      real*8        a(nd,nd+m),piv,x,delt
c
      if (n .gt. 1) then
         do k = 1, n-1
            piv = ABS(a(k,k))
            kk  = k + 1
            in  = k
c
c---  search for index in of maximum pivot value
            do i = kk, n
               if (ABS(a(i,k)) .gt. piv) then
                  piv = ABS(a(i,k))
                  in  = i
               end if
            end do
            if (k .ne. in) then
c
c---  interchange rows k and index in
               do j = k, m+n
                  x      = a(k,j)
                  a(k,j) = a(in,j)
                  a(in,j) = x
               end do
            end if
c
c---  check if pivot too small
            if (piv .lt. delt) then
               write(6,4)
               return
            end if
c
c---  forward elimination step
            do i = kk, n
               do j = kk, m+n
                  a(i,j) = a(i,j) - a(i,k) * a(k,j) / a(k,k)
               end do
            end do
         end do
         if (ABS(a(n,n)) .lt. delt) then
            write(6,4)
            return
         end if
c
c---  back substitution
         do k = 1, m
            a(n,k+n) = a(n,k+n)/a(n,n)
```

```
            do ie = 1, n-1
               i  = n - ie
               ix = i + 1
               do j = ix, n
                  a(i,k+n) = a(i,k+n) - a(j,k+n) * a(i,j)
               end do
               a(i,k+n) = a(i,k+n) / a(i,i)
            end do
         end do
         return
      else if (ABS(a(1,1)) .lt. delt) then
         write(6,4)
         return
      end if
      do j = 1, m
         a(1,n+j) = a(1,n+j) / a(1,1)
      end do
c
4     format(2x,'The matrix is singular. Gaussian'
     &           ' elimination cannot be performed.')
c
      return
      end
```

APPENDIX E: MSc COURSEWORK

The following courses were completed in partial fulfilment of the degree of Master of Science in Engineering. The degree requirements are 20 credits coursework and a half thesis.

COURSE		YEAR	CREDITS
END 520Z	Applied Mechanics A	1989	3
END 521Z	Applied Mechanics B	1989	3
END 522Z	An Introduction to Finite Elements	1989	3
END 523Z	Finite Element Analysis	1989	4
END 524Z	Engineering Software Design and Development	1989	3
AMA 363F	Numerical Analysis	1989	3
AMA 367F	Continuum Mechanics	1989	3
		TOTAL:	22

E.1 DESCRIPTION OF INDIVIDUAL COURSES

END 520Z APPLIED MECHANICS A *(3 credits)*

Concepts of stress, strain, compatibility. Equilibrium equations and constitutive relationships. Applications to beams, rods, plates and two dimensional elasticity. Solutions of simple boundary value problems in plane stress/strain and plates. Energy concepts in mechanics.

END 521Z APPLIED MECHANICS B *(3 credits)*

Topics in nonlinear mechanics: Limit analysis, shakedown. Behaviour of elastic-plastic solids. Elastic-plastic constitutive relations. Practical aspects of computational plasticity. Viscoplasticity and creep.

END 522Z AN INTRODUCTION TO FINITE ELEMENTS *(3 credits)*

The use of the finite element method in various engineering disciplines. Finite elements available in 1-D and 2-D applications. Approach to problem solving techniques using finite elements. The use of finite element packages. Topics include stress analysis, heat transfer, seepage flow and fluid flow.

END 523Z FINITE ELEMENT ANALYSIS *(4 credits)*

Generalized displacement method of analysis. Formulation of finite element equations. Approximation and interpolation of functions. Isoparametric formulation of elements for 1-D, 2-D and 3-D applications. Structure of finite element programs and implementation of elements. Some advanced topics in finite element analysis.

END 524Z ENGINEERING SOFTWARE DESIGN AND DEVELOPMENT *(3 credits)*

Microcomputer hardware components, DOS operating system, software design methodologies, modularity and information hiding, login and decision tables, data abstraction and file handling. Testing and debugging. Man-machine interface and computer graphics. Project management and documentation. Software tools and packages. Numerical representation and accuracy.

AMA 363F NUMERICAL ANALYSIS *(3 credits)*

Numerical methods of solution of ordinary differential equations. Approximation to functions. Eigenvalue methods. Modelling examples.

AMA 367F CONTINUUM MECHANICS *(3 credits)*

Tensor algebra and analysis, fluid and solid mechanics, Navier-Stokes equations, the partial differential equations of elasticity, examples.